UNIVERSITEIT VAN PRETORIA
UNIVERSITY OF PRETORIA
YUNIBESITHI YA PRETORIA

Reduction of rolling contact fatigue through the control of the wheel wear shape

by

Ulrich Spangenberg

Submitted in the partial fulfilment of the requirements for the degree

Philosophiae Doctor (Mechanical Engineering)

In the Faculty of Engineering, Built Environment and Information Technology

University of Pretoria

Pretoria

2016

Reduction of rolling contact fatigue through the control of the wheel wear shape

by

Ulrich Spangenberg

Supervisor: Prof. P.S. Els
Co-Supervisor: Dr. R.D. Fröhling
Department: Mechanical and Aeronautical Engineering
Degree: Philosophiae Doctor

Summary

Heavy haul railway operations permit the transport of huge volumes at lower cost than other modes of transport. The low cost can only be sustained if the maintenance costs associated with such railway operations are minimised. The maintenance costs are mainly driven by wheel and rail damage in the form of wear and rolling contact fatigue (RCF). Low wear rates in the wheel-rail interface have resulted in an increase in the prevalence of rail RCF, thereby increasing rail maintenance costs.

The aim of this study is to develop an approach to reduce rail RCF on South Africa's iron ore export line by managing the worn wheel shape. This approach is developed by evaluating wheel and rail profile shapes that contribute the most to RCF initiation, studying the influence of suspension stiffness and rail profile changes as well as a redesign of the wheel profile.

The influence of wheel and rail profile shape features on the initiation of rolling contact fatigue (RCF) cracks was evaluated based on the results of multibody vehicle dynamics simulations. The damage index and surface fatigue index were used as two damage parameters to assess the influence of the different features. The damage parameters showed good agreement to one another and to in-field observations. The wheel and rail profile shape features showed a correlation to the predicted RCF damage. The RCF damage proved to be most sensitive to the position of hollow wear and thus bogie tracking. RCF initiation and crack growth can be reduced by eliminating unwanted shape features through maintenance and design and by improving bogie tracking.

Two potential mitigation measures had been adapted from those published in literature to reduce RCF. The mitigation measures involved changes in suspension stiffness to spread wheel wear across the tread and the use of gauge corner relief rail profiles. These mitigation measures were evaluated by means of multibody dynamics and wear

simulations to determine their efficiency as a RCF management strategy to minimise maintenance costs. These mitigation measures, however, did not prove to be successful in reducing RCF initiation while maintaining a low wheel wear rate. The current operating conditions on South Africa's iron ore line, although still not optimal overall, were found to be better in terms of their wear and RCF performance than the two proposed RCF mitigation measures.

Based on the finding of the study on two RCF mitigation measures it was recommended that a conformal wheel profile be developed to spread the wheel wear across the tread to reduce the occurrence and propagation of RCF cracks, while still maintaining low wheel wear rates. A comparative study of this new wheel profile design and the current wheel profile design was therefore performed using multibody dynamics simulation together with numerical wheel wear and RCF predictions. The advantages of the conformal wheel profile design were illustrated by evaluating the worn shape and resulting kinematic behaviour of the conformal design. The conformal design had a steadier equivalent conicity progression and a smaller conicity range compared with the current wheel profile design over the wheel's wear life. The combination of a conformal wheel profile design with 2 mm hollow wear and inadequate adherence to grinding tolerances often result in two-point contact, thereby increasing the probability of RCF initiation. The conformal wheel profile design was shown to have many wear and RCF benefits compared with the current wheel profile design. However, implementation of such a conformal wheel profile must be accompanied by improved rail grinding practices to ensure rail profile compliance.

Based on these findings an approach is proposed where the conformal wheel profile design together with improved compliance of the in-service rail profiles to the target rail profile are implemented. This has the potential to reduce RCF initiation on South Africa's iron ore export line.

Keywords:
Wheel-rail interaction, wheel-rail profiles, rolling contact fatigue, wear modelling, anti-head check profiles, conformal wheel-rail profiles, wheel profile design

Acknowledgements

I wish to express my sincere gratitude to:

The University of Pretoria, for providing the opportunity to complete my research.

Prof. Schalk Els, who provided his guidance and shared his knowledge and enthusiasm during my research. Thank you for your willingness to take on this challenge, your positivity and open-door policy.

Dr. Robert Fröhling, thanks for your encouragement and providing an environment for further personal and academic growth. Thanks for allowing me the opportunity to complete this study with support of Transnet Freight Rail's resources and time.

My parents, Dina and Izak Spangenberg, for your help, support and encouragement throughout my studies.

My wife, Melishé Spangenberg, thanks for your support and unwavering belief in my abilities.

My colleagues, for all those whom I could approach for help and your unconditional assistance.

Table of contents

List of Figures

List of Tables

Nomenclature List

Symbol	Description	Unit
English letter and Symbols		
A	Area	m^2
a	Length-wise semi-axis of the contact ellipse	m
b	Width-wise semi-axis of the contact ellipse	m
DI	Damage index	$10^{-6}/axle$
f	Proportionality factor or wear coefficient	g/Nm
FI	Fatigue index	
k	Material's yield strength	Pa
L	Load path length of a travelling particle in contact patch	m
l	Half distance between two contact points	m
N	Normal force	N
P	Frictional power of wear number	N
p	Contact pressure	Pa
R	Radius	m
r	Wheel radius	m
T	Tangential force or traction	N
v	Velocity	m/s
y	Lateral wheelset displacement	m
Greek letters		
α	Contact angle	rad
γ	Creepage	
δ	Wear depth	m
λ	Conicity of a wheel	
μ	Coefficient of friction or utilised traction	
ρ	Material density	kg/m^3
σ	Stress	Pa
τ	Shear stress	Pa
υ	Normalised vertical load	
Subscripts		
c	Value with respect to a curve	
d	Relating to the density of the variable	
e	Value with respect to the shear	
eq	Equivalent value	
$mild$	Value with respect to mild wear	
o	Nominal value	
r	Value with respect to the rail	
$severe$	Value with respect to severe wear	

Symbol	Description	Unit
Subscripts		
$surf$	Value with respect to the surface	
TP	Value with respect to the turning point	
ut	With respect to the ultimate tensile strength of the material	
w	Value with respect to the wheel	
x	Value with respect to the x-direction	
y	Value with respect to the y-direction	
y	With respect to the yield strength of the material	
z	Value with respect to the z-direction	

List of abbreviations

Abbreviation	Definition
CDF	Cumulative distribution function
DI	Damage index
HPF	High positive friction modifier
LCF	Low coefficient friction modifier
MGT	Million Gross Tons
PS	Primary suspension
PSD	Power spectral density
RCF	Rolling contact fatigue
RRD	Rolling radius difference
$T\gamma$	Wear number
VHPF	Very high positive friction modifier

Chapter 1: Introduction and literature review

1.1 Introduction

The wheel-rail interface is one of the most important interfaces in the railway system. This interface presents the only contact between the vehicle and the track. If this contact is maintained well and functioning optimally, the result is a system working in harmony with proper guidance, low frictional forces, low operational cost and satisfactory safety. Lundén and Paulsson (2009) mention that there is an increasing demand for railway transportation, because it provides an attractive alternative to other modes of transport from an ecological point of view. Further research is needed to improve the railway's efficiency, safety, reliability and economy of the transportation system to make it more attractive and competitive for customers. Six key areas that are deemed of major importance for research and implementation are listed by Lundén and Paulsson (2009). One that is mentioned in particular, is active control of the wheel-rail interface. Research in this area is aimed at finding new applications for improving vehicle dynamics, reducing noise levels and damage in the form of rolling contact fatigue (RCF) and wear.

Damage in the form of excessive wear and RCF may result when the wheel-rail interface is not controlled or maintained properly. The usable service lives of wheels and rails are governed by either wear or RCF. Damage at the interface is influenced by many sources such as vehicle dynamics, which effectively govern contact forces, track degradation, tribology and profiles of the mating surfaces. Many authors have studied the influence of vehicle behaviour and wheel-rail profiles on damage at the interface (Burstow, 2003; Burstow, 2004; Fröhling et al., 2008; Tunna and Urban, 2009; Fröhling et al., 2012; Karttunen et al., 2014a; Karttunen et al., 2014b).

A heavy haul iron ore export line is operated within South Africa and runs from the mines in Sishen to the port in Saldanha over a distance of 861 km. Surface-initiated RCF cracks are prevalent on the gauge corner of the high rails and on the field side of the low rails. The greatest concern is gauge corner RCF cracks on the high rail, since RCF cracks may grow, unite and branch across the railhead leading to spalling of the rail surface or even result in a rail break (Johnson, 1989). RCF cracking not only affects the safety of the railway system, but also affects its economy. Costs associated with rail replacement, track maintenance and rail grinding may be reduced, if the prevalence of RCF cracks is lowered or eliminated.

Scheffel (1974) designed a self-steering, high stability freight bogie in the pursuit of wear reduction. This type of freight bogie has been used on South Africa's iron ore export line since April 1976 (Scheffel, 1978). The reduction in wear achieved from the use of this bogie, together with straighter track, rail grinding and tighter gauge control, led to the concentration of wheel tread wear or concentrated hollow wear. The contact conditions

that prevail when hollow-worn wheels contact rails may lead to the development of surface- initiated RCF if the worn state of the wheel is not tightly controlled. A hollow wear limit was introduced within the South African railways to reduce the occurrence of unfavourable contact conditions and reduce the formation of RCF (Tournay and Mulder, 1996).

In 2001, the iron ore export line was upgraded to an axle load of 30 tons. This upgrade caused surface-initiated RCF on the gauge corner of the high rail and field side of the low rail to become prevalent. An investigation into the primary drivers of RCF on the line was performed by Fröhling et al. (2012). This investigation was limited to the calculation of wheelset kinematics and contact stresses at the wheel-rail interface. The need exists to extend this study of the primary drivers of RCF as they have a direct effect on the usable service life of wheels and rails as well as the safety of the system.

Both wear and RCF drive the cost of wheel and rail replacement and maintenance. Kalousek (2005) emphasised the reciprocity of damage within the wheel-rail interface, stating that improvements to the wheel will result in improvements of the rail and vice versa. Improvements in the wheel-rail system will have a positive effect on the cost of vehicle and track maintenance. If the primary drivers of RCF are identified and understood, these drivers can be either avoided or mitigated through improved design and maintenance of the wheels and/or rails. Design improvements can be made when the fundamentals of wear and RCF are understood. Recent developments in wear models and RCF initiation models together with computer software capable of describing vehicle behaviour facilitate the enhancement of the wheel-rail interface. Various authors have used mathematical optimisation to improve the wheel-rail interface by developing wheel profiles (Shevtsov et al., 2005; Shevtsov, 2008; Shevtsov et al., 2008) and/or rail profiles (Smallwood et al., 1991; Persson et al., 2010). Although optimal performance criteria differed from author to author, the greatest emphasis was placed on the reduction of wear and/or RCF in the wheel-rail interface.

The aim of this study is to develop an approach to reduce rail RCF on South Africa's iron ore export line, ultimately reducing maintenance costs. The review of the literature presented in paragraph 1.2 introduces fundamental concepts of wheel-rail interaction and addresses the models and prediction tools used to evaluate the main drivers of wheel and rail damage in the form of wear and RCF.

1.2 Literature review

1.2.1 Modelling of the wheel-rail interface and vehicle behaviour on track

The wheel-rail interface is governed by the transverse profiles of the two interacting bodies of the wheel and the rail. The general terminology used to describe the transverse profiles of wheels and rails is shown in Figure 1-1 and Figure 1-2 respectively. The different components of the profiles serve different functions. By studying their interaction, wheel and rail damage can be analysed, studied and understood. Many

mathematical models exist that describe the kinematic behaviour, the contact stresses and contact forces arising from wheel-rail interaction. These facilitate the study of wheel and/or rail damage analytically, reducing the need for a trial-and-error approach. The succeeding paragraphs describe the mathematical models that are used in analytical studies.

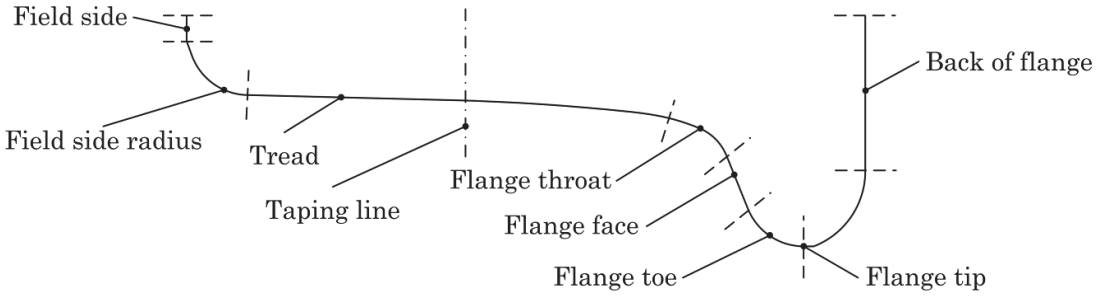

Figure 1-1: Wheel terminology

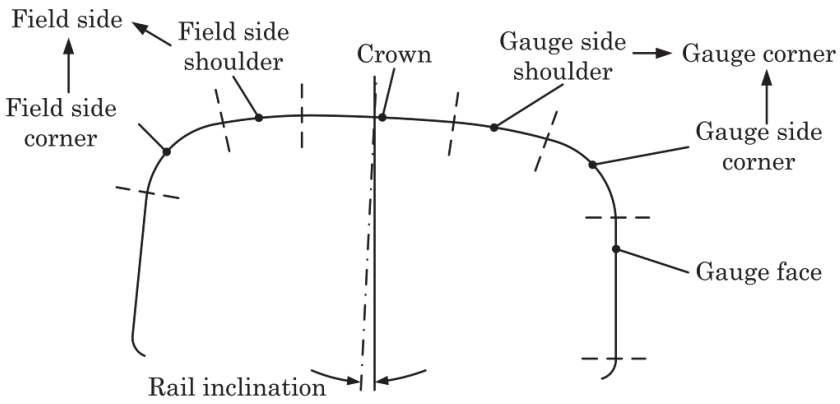

Figure 1-2: Rail terminology

1.2.1.1 General wheel-rail interaction

A railway wheelset consists of two wheels mounted on a common rigid axle. The railway wheelset has evolved over the centuries, but the general construction has remained the same. Iwnicki (2006) provides an historic overview of the evolution the railway wheelset. In the early days of railways, the greatest concerns of railway pioneers were the reduction of rolling resistance and wear while increasing strength. Coning of the wheel tread was introduced to reduce the rubbing of the wheel flanges on the gauge face of the rail and partly to reduce the rolling resistance in curves. When a coned wheel displaces laterally from its equilibrium position, a rolling radius difference is generated between the two wheels. This rolling radius difference aids in wheelset steering around a curve, but on tangent track it causes kinematic oscillations or instability. According to Iwnicki (2006), this kinematic oscillation was mathematically described by Klingel in 1883. This description was based on the geometry of the coned wheel contacting the rail.

It was noted that it is important that a wheelset radially aligns itself in a curve to sustain pure rolling. This was therefore followed by theoretical analysis of a coned

wheelset in a curve. This analysis was only based on geometrical relationships of an unconstrained wheelset negotiating a curve. It was established that the lateral displacement (y) required to sustain pure rolling is a function of the radius of the curve (R_c), the nominal radius of the wheelset (r_0), the distance between the two contact points ($2l$) and the conicity (λ) of the wheels as shown in equation (1-1) (Wickens, 2003; Iwnicki, 2006). This relationship shows that the ability of a wheelset to roll freely around a curve is dependent on the conicity of the wheelset.

$$y = \frac{r_0 l}{R_c \lambda} \tag{1-1}$$

Wheel profiles currently employed by the rail industry no longer have pure coned profiles. Wheel profiles evolved into shapes that reduce wear, increase stability on tangent track, allow for negotiation of curves without flange contact and lower contact stresses. Combinations of various radii and straight lines define the profiled shape of the wheels. These profiled wheel shapes can no longer be presented by a single cone angle or conicity. The conicity of a profiled wheelset at an instance of contact at a predefined lateral displacement can be described by a wheelset with a set cone angle that produces equivalent kinematic behaviour. The conicity obtained in this manner is known as the equivalent conicity of a profiled wheelset and is a function of the lateral displacement amplitude of the wheelset. It can be said that the conicity of the profiled wheel is made up of the conicity of various coned wheelsets at different lateral displacement amplitudes.

The concept of equivalent conicity becomes very important when stability and curving ability is considered. Tangent and curved tracks require conflicting behaviour of the wheelset. On a tangent track, stability is of greatest concern, whereas a certain degree of instability is required by a curved track to facilitate curving.

The equivalent conicity (λ_{eq}) of a wheelset can easily be related to the rolling radius difference (Δr) and the twice the lateral displacement ($2y$) through simple geometry. This relationship is given in equation (1-2) (Pearce, 1996; Shevtsov, 2008).

$$\lambda_{eq} = \frac{\Delta r}{2y} \tag{1-2}$$

For the calculation of the equivalent conicity, another relationship (equation (1-3)) exists, which depends on the transverse radii of the two contacting bodies (Magel and Kalousek, 2002). Equivalent conicity is a function of the transverse radii of the wheel (R_w) and the rail (R_r) as well as contact angle (α). The contact angle is given by the angle between the plane of contact and the track level. The equivalent conicity therefore depends on the shape of the wheel and rail profiles. The denominator of equation (1-3) shows that when $R_r \rightarrow R_w$, the equivalent conicity $\lambda_{eq} \rightarrow \infty$, and the wheelset will experience immense instability. Wheel profiles that tend to wear hollow will experience this increase in equivalent conicity and instability. This effect is well known and mentioned by many authors including Tournay and Mulder (1996), Fröhling et al. (2008), Shevtsov (2008), Bruni and Braghin (2009).

$$\lambda_{eq} = \frac{R_w}{R_w - R_r} \sin \alpha \quad \textbf{(1-3)}$$

Another approach to the calculation of the equivalent conicity is described by the International Union of Railways' UIC code 519 (2004). The calculation is based on the mean slope of the rolling radius difference graph. This approach is more practical when worn profiles are considered.

Pearce (1996) divided equivalent conicity into four categories based on their values. Low conicity was defined for values less than 0.15, medium conicity was defined between 0.15 and 0.3, high conicity was defined between 0.3 and 0.5 and very high conicity for values greater than 0.5. Parameters that may increase the conicity were discussed. These included tightening of the track gauge, flattening of the rail crown, reducing the rail inclination, thickening the wheel flange and the increase of hollow wear. Pearce (1996) examined the effects of wear on the conicity of a wheel-rail combination. The fundamentals of tread and flange guidance were addressed. Tread wear was examined in more detail to understand the effect it has on the conicity.

The rolling radius difference depends on the transverse wheel and rail profiles at the point of contact. It is a function of the wheelset lateral displacement and can be calculated from the Cartesian coordinates of the profiles (International Union of Railways, 2004). When equation (1-2) is substituted in equation (1-1), it results in equation (1-4). The rolling radius difference (Δr) required for pure rolling around a curve with radius R_c can be determined based on the geometrical constants of the wheelset (r_0 and l).

$$\Delta r = \frac{2 r_0 l}{R_c} \quad \textbf{(1-4)}$$

Shevtsov (2008) used the rolling radius difference function to optimise the transverse wheel profile. An inverse problem was solved by calculating the wheel profile shape based on the designed rolling radius difference function. The rolling radius difference function was designed by applying equation (1-4) to curve radii that the wheelset needed to traverse. The rolling radius difference and the equivalent conicity are important terms when evaluating wheelset kinematics.

The wheel and rail transverse profiles are of great importance when stability and curving are concerned. Different regions of the wheel and rail profiles interact and have different requirements. According to Tournay (2001), three functional regions of wheel-rail contact can be defined. They are shown in Figure 1-3.

Region A defines contact between the central region of the rail crown and wheel tread. Contact is usually made in this region when a vehicle negotiates tangent or mildly curved tracks. This contact is associated with low contact stresses, low lateral creep forces with more significant longitudinal creep forces. The conicities and radius differentials for contact in this area can be calculated using geometrical methods. They should be designed to provide stability and an adequate radius differential for mild curves. The conicity in this region should be as low as possible, within the requirements

for curving, to spread the contact occurrences across the wheel tread. The change in conicity from new to worn-wheels should be considered, as good tracking may lead to hollow-worn wheel profiles. The conicities of the hollow-worn profiles deviate from the design conicity and may cause vehicle instability.

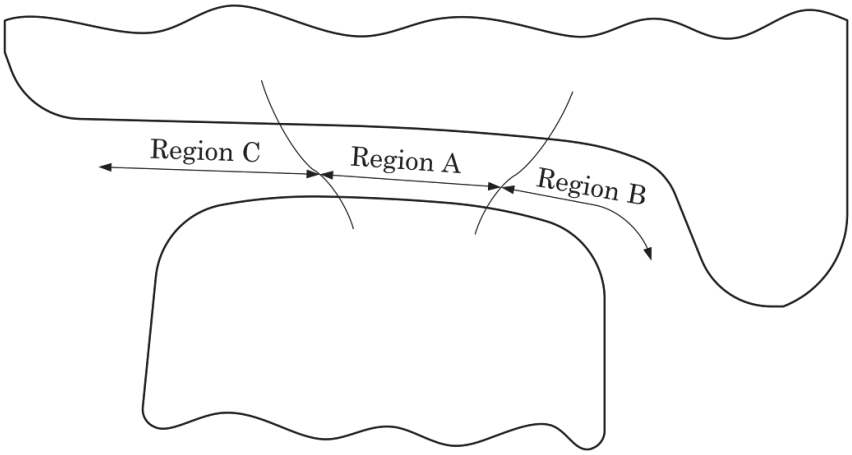

Figure 1-3: Three functional regions of wheel-rail contact

Region B defines contact between the gauge corner and the flange throat. High angles of attack are associated with contact in the gauge corner, resulting in high lateral creep forces. The contact patch size is small and the associated contact stresses are high. Contact in this region may be characterised by single-point, two-point and conformal contact.

Single-point contact of Figure 1-4(a) leads to high contact stresses, high longitudinal creepage and spin creepage. It is the most damaging to wheel and track with respect to the different types of contact in region B. Single-point contact produces gauge corner RCF cracking and may lead to vehicle instability in the form of hunting due to the large longitudinal creep forces. Single-point contact may result from inappropriate wheel and rail profile design, due to flattening of the railhead or due to hollow-worn wheels. The bump formed at either side of a hollow-worn wheel profile is known as false flanges. The gauge side false flange occurring on hollow-worn wheels produces an unwanted contact condition due to severe single-point contact (Figure 1-4(a)).

A vehicle that is unable to steer through a curve without making flange contact produces flange forces and lateral creep forces, which are associated with two-point contact (Figure 1-4(b)). Large slippage and wear is associated with two-point contact due to these forces and lead to accelerated flange wear until the wheel flange conforms to the rail profile as shown in Figure 1-4(c). According to Tournay (2001), the lubrication film applied to the gauge face or flange face may become negated by excessive flange forces leading to excessive wear. Two-point contact is occasionally preferred by profile designers. Here rail profiles are designed or ground with gauge corner relief to avoid fatigue damage associated with gauge corner contact (Burstow, 2004; Shevtsov et al., 2008; Persson et al., 2010) at the expense of two-point contact. This type of contact does limit the amount of radius differential that can be established and therefore the steering ability of the

wheelset and/or vehicle. According to Tournay (2001) this may eventually lead to more damaging single-point contact if the wheels are left to wear to the shape of the gauge corner relief rail profile.

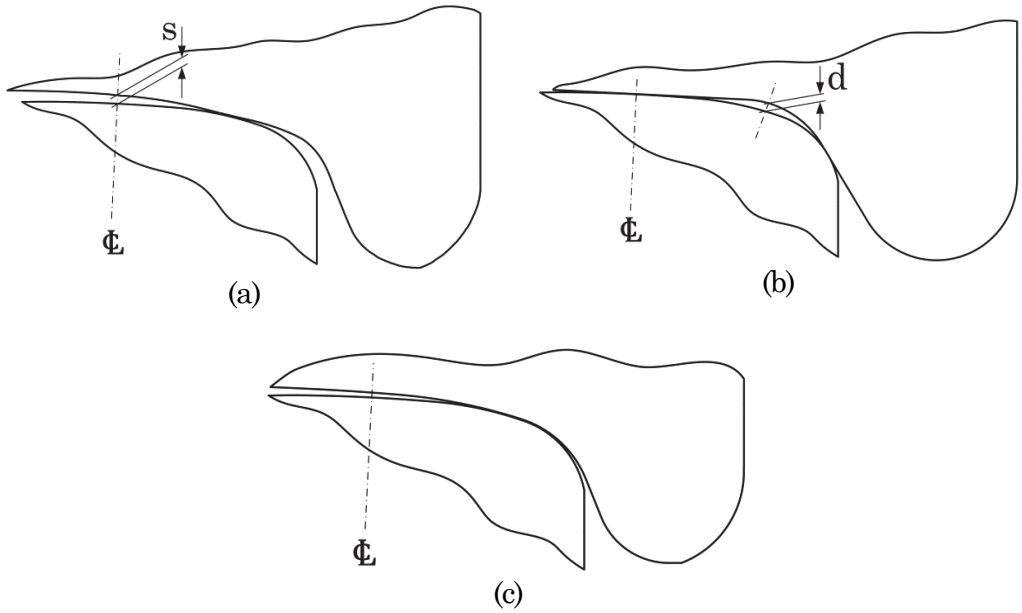

Figure 1-4: Three types of gauge corner contact: (a) single-point, (b) two-point and (c) conformal contact (adapted from Tournay, 2001 and Magel and Kalousek, 2002)

Two-point contact increases wheel flange wear. A wheel subjected to a large amount of flange wear requires that more material is removed to restore the shape of the design profile (Figure 1-5(a)). Wheels that are only exposed to tread wear require less material removed to restore the design profile (Figure 1-5(b)). The number of times that wheels with flange wear can be reprofiled is far less than that of wheels with no flange wear. The serviceable lifetime of a wheel can therefore be extended by reducing the development of flange wear.

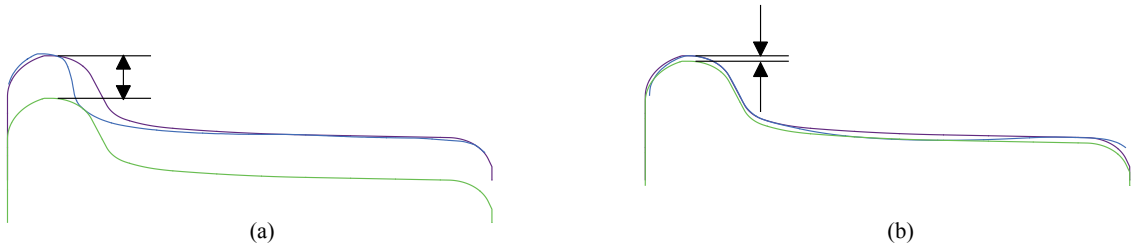

Figure 1-5: Required material removal to restore the design profile in green for (a) flange wear and (b) tread or hollow wear shown in blue

The preferred contact type in region B is the conformal contact as illustrated in Figure 1-4(c). It is preferred as it maintains the shape of the wheel, it performs successfully in terms of fatigue, the lubrication film is supported due to lower pressures and conicities are lower compared to single-point contact (Tournay, 2001). Design for conformal contact should be performed with care to avoid any two-point contact. A general criterion for

optimised wheel and rail profiles state that closely conformal contact should be avoided to reduce the probability of rail corrugation development. Closely conformal, conformal and non-conformal contact are classified as shown in Figure 1-4(a) and (b) as $\max(s,d) < 0.1$ mm, 0.1 mm $< \max(s,d) < 0.4$ mm and 0.4 mm $< \max(s,d)$ respectively (Magel and Kalousek, 2002).

Region C (Figure 1-3) is the third contact region described by contact between the field side of the rail and the outer tread towards the field side radius of the wheel. The contact in this region is very difficult to optimise. Contact in this region should still ensure low contact stresses to avoid metal flow on both wheel and rail as well as field side RCF damage on the rails. If contact in this region is not optimal, it could lead to the development of a false flange on the field side of the wheel tread, which can further lead to accelerated rail RCF damage. An optimised profile should ideally spread contact in this region as far as possible to the field side of the wheel without encouraging metal flow on the wheel or causing field side crushing.

One of the general criteria for optimising wheel and rail profiles listed by Magel and Kalousek (2002) addresses the distribution of contact points. It states that the optimisation process should ensure that the contact points are well distributed across the tread to have many contact points that will spread the wear. This criterion forms the basis of their pummelling model, which analyses the contact point distribution. Selective gauge widening and/or narrowing can be applied in such a manner as to spread the severity and frequency of contact to many different points on the running surfaces. This will ensure that favourable contact geometries are maintained and that the damage accumulation per contact point is reduced. When designing a wheel profile with the intent of optimising the contact condition, this central idea of the pummelling model becomes very critical. The wheel and/or rail profiles should be designed in such a manner that the contact points are spread over the tread of the wheel to maintain optimal contact conditions especially with contact in regions B and C.

The preceding discussion addresses the geometry and kinematics of a wheelset. In addition to the geometry and kinematics the forces acting at the wheel-rail interface becomes crucial when evaluating the dynamic behaviour of a vehicle and analysing damage at the wheel-rail interface.

Creep or creepage (γ) is one of the important quantities needed to calculate interacting forces in the wheel-rail interface. Creepage or creep is a term used to define the deviation of two bodies in rolling contact from the pure rolling state. In other words, creep describes the relative slip between the two bodies. Lateral and longitudinal creepages are non-dimensional, but spin creep has the dimension of length^{-1} (Garg and Dukkipati, 1984). Steering forces in the form of longitudinal and lateral force as well as wear are caused by this relative slip between the wheel and rail. The forces generated in the contact patch will be discussed in more detail in paragraph 1.2.1.2.

1.2.1.2 Modelling wheel-rail contact mechanics

The forces generated in the contact patch depend on the elastic interaction between the wheel and rail as well as the friction between the two bodies. These forces can be subdivided into normal contact and tangential traction forces. It is possible to calculate the normal contact patch size and contact pressure distribution accurately by means of the finite element (FE) method. This is, however, computationally expensive. A simplified approximation is required to calculate the contact conditions readily. The following three simplifying assumptions are made for such approximate algorithms (Braghin et al., 2009):

a) The contacting surfaces of the wheel and rail are assumed continuous and non-conforming. This implies that the dimensions of the contact area are much smaller than the dimensions of the wheel and rail.
b) The constitutive law of the wheel and rail materials is assumed linear elastic.
c) From a structural point of view, the two contacting bodies can be approximated by half-spaces.

The half-space assumption limits the solution to areas where the contact area is small relative to the typical dimensions of the contacting bodies. In the railway system, these dimensions are usually the diameter of the wheel and the minimum radius of curvature near the contact (Kalker, 1990). This assumption therefore may be violated, should the point of contact be conformal.

When these simplifications are applied to the normal contact solution, the half-space assumption may lead to large deviations from the true contact conditions. When tangential contact stresses are added to the problem, there is no suitable alternative to the elastic half-space assumption.

To solve the normal problem, the position, shape and size of the contact patch and the distribution of the normal contact stresses are calculated from the local geometry of the two contacting profiles and the normal force acting between the two bodies. To solve the tangential problem, the tangential contact stresses and slippages are defined inside the contact patch and are calculated from the normal pressures and the creepage components.

Based on the listed simplifying assumptions and the assumption that the wheel and rail materials have similar Young's modulus and Poisson's ratio, the quasi-identity applies. The implication of the quasi-identity is that the tangential stresses will not affect the distribution of the normal pressures, which means that the normal and tangential problems are decoupled and can be solved separately (Kalker, 1990).

The normal problem is commonly solved by applying Hertz's theory. Here two contacting bodies are assumed to have constant curvature over a region that is wide enough to include the entire contact patch. By applying this condition and retaining the listed assumptions, it is possible to calculate an elliptic contact area and a semi-ellipsoidal pressure distribution.

The size and shape of the contact patch are described in terms of the length (a) and the width (b) of the semi-axis of the contact ellipse. The maximum contact pressure is a function of the curvature of the two contacting bodies and the normal force acting between the two bodies. The contact patch size and pressure distribution are described by analytical formulae based on elliptical integrals, which make the solution of the normal problem by means of the Hertzian model, computationally efficient.

If some or all the aforementioned assumptions are violated, the contact condition results in what is known as non-Hertzian contact. The assumption that the contacting bodies are continuous and non-conforming may, for example, become violated due to the contact position as well as wear causing the two contacting surfaces to become conformal. To solve the normal problem, strategies that are more complex have to be implemented. One strategy is to approximate the undeformed distance function by piecewise constant curvature polynomials and then to apply Hertzian theory to each, separately. This procedure is known as "multi-Hertzian" solution and the actual non-elliptical contact patch is approximated by the superposition of more than one Hertzian ellipse. The two simplifying assumptions that are made by many algorithms to solve the non-Hertzian contact condition are:

- The contact patch is estimated by the footprint obtained as the rigid wheel and rail surfaces are interpenetrated by a given amount.
- The normal stresses have a semi-elliptical distribution in the longitudinal direction.

Kalker (1990) presented a more accurate way of modelling the normal problem. This model is applied in his CONTACT algorithm and is often referred to as the exact solution. Here the simplifying assumptions made for algorithms approximating contact conditions (listed in points a) to c)) are still valid with the addition that the contacting bodies may have a generic transverse profile.

The solution to the normal contact problem is the first step in solving the interaction between wheel and rail. The solution of this interaction is completed by solving the tangential problem. The tangential problem is solved by calculating the tangential creep forces in the contact patch based on the normal pressure distribution and creepages. These tangential creep forces are further subdivided into longitudinal and lateral creep forces. The longitudinal creep forces are a function of the longitudinal creepages generated by the lateral displacement of the wheelset as well as traction and braking. Lateral creep forces are a function of the lateral as well as spin creepages. Lateral creepages are caused by wheelset yaw, and spin creepages are caused by the relative angular motion between the wheel and rail about the normal to the contact patch (Wickens, 2003).

Coulomb's friction law is shown in equation (1-5) and shows that the traction force (T) is function of the maximum friction coefficient (μ) and the normal force (N). Rolling contact theories describing exact nonlinear three-dimensional contact in terms of longitudinal, lateral and spin creepages, are based on the principle that the tangential traction satisfies Coulomb's friction law (Garg and Dukkipati, 1984). Thus, the traction cannot exceed the available traction limit defined by the friction coefficient multiplied by the

normal force as indicated in equation (1-5). Olofsson et al. (2013) discussed the factors affecting the friction coefficient and mentioned that it is a system property rather than a material property, as it depends not only on the mating materials, but also on factors such as temperature and humidity. The friction coefficient can have a significant influence on the wheel-rail interface. If it is too low, the maximum braking force of the vehicle is reduced leading to safety issues, and if it is too high, it can lead to higher wheel and rail wear.

$$\left|\vec{T}\right| \leq \mu N \tag{1-5}$$

The tangential problem is commonly solved by simplification of the problem to obtain computationally inexpensive solutions. One such an algorithm, which provides an approximate but fast solution to the tangential problem, was proposed by Kalker (1990). This algorithm is known as the FASTSIM algorithm and is based on Kalker's simplified theory. Braghin et al. (2009) described the solution process of the FASTSIM algorithm as follows. The FASTSIM algorithm was originally developed to be applicable over elliptical Hertzian contact patches. The FASTSIM algorithm divides the contact patch into longitudinal strips and computes a constant gradient of deformation within each strip based on the creepage components. The algorithm then proceeds to solve the tangential contact forces at discrete positions along each strip. This is accomplished by assuming that each force component is proportional to the corresponding component of wheel-rail deformation in the same point through constant flexibility coefficients. The tangential forces are then saturated to the traction bound that equals the product of the local normal pressure and the friction coefficient. The slip is calculated based on the difference between the saturated and unsaturated tangential forces, using the flexibility coefficients. The earlier constraint of having the algorithm function over Hertzian contact patches, allows the flexibility coefficients to be chosen to match the analytical expression of the linearised creep force – creepage graph. If the FASTSIM algorithm is extended to include non-elliptical contact, the identification of appropriate flexibility coefficients becomes difficult.

A more general and accurate numerical solution to the tangential problem has been proposed by Kalker (1990) under the name CONTACT. This solution is referred to as the exact solution. The solution is used in combination with the solution of the normal problem produced by the CONTACT algorithm. With this solution, there is no need to assume or approximate the contact with an elliptical contact patch, although the simplifying assumptions made for algorithms approximating contact conditions (listed earlier under points a) to c)) are still valid. The method used in the CONTACT algorithm is computationally expensive and therefore it is not often used and applied in simulation packages. It, however, provides a very good approximation of the real contact condition. The algorithm is often used as a reference to which the solution of simplified and faster algorithms can be compared (Braghin et al., 2009).

The creep forces present in the wheel-rail interface have a direct effect on the dynamic response of the vehicle and vice versa. Tangential creep forces are influenced by the contact area and contact pressure between the wheel and the rail. The geometries of the wheel and rail profiles are significant as they determine the size and shape of the contact

patch. This has direct influences on the pressure distributions which relate to the local adhesion, creep and wear characteristics of the contact occurrence.

1.2.1.3 Vehicle dynamics modelling

With advances in digital computing and numerical methods, the solution of the dynamics problem by means of computer algorithms has received great attention. Various textbooks are available describing railway vehicle dynamics. These textbooks often start with the fundamental description and solution of single and multi-degree of freedom dynamic systems. The modelling of wheel-rail contact theories and the fundamental differential equations required to solve railway vehicle dynamics are introduced. The descriptions of the underlying differential equations start at the equations of motion of an unconstrained wheelset. The complexities present in the models increase from single wheelsets to bogie models and finally models addressing many degrees of freedom. These degrees of freedom include the longitudinal, lateral, vertical translational responses and roll, yaw and pitch rotational responses. These texts include good modelling practices and some provide examples of modelling complex subsystems such as coupler interaction or modelling of suspension elements (see Garg and Dukkipati, 1984; Wickens, 2003).

The models described by Garg and Dukkipati (1984) are special-purpose models and are solved by algorithms developed specifically for these models. Further developments in this field resulted in the development of general computational multibody system algorithms that are capable of solving differential and algebraic equations in general. Shabana et al. (2008) described the basic equations used in such algorithms.

There are many commercial codes available to solve multibody dynamic systems or more specifically train vehicle dynamics. These software packages include Vampire, Gensys, Simpack, VI-Rail (previously known as Adams/Rail) and Nucars. Iwnicki (1999) compared the responses predicted by each of these packages to a set of predefined benchmark cases. In general, all the simulation packages showed good agreement.

The wheel-rail contact algorithms have been extended to include the use of measured wheel and/or rail profiles during simulations. This allows further analysis of various combinations of influencing factors, as the behaviour of worn profiles might deviate significantly from the behaviour of new profiles.

Simulations performed with such computer packages are used to study the performance of vehicles. The performance metrics are often related to vehicle stability, passenger comfort and the likelihood of derailment. According to Bruni and Braghin (2009), the two most important geometrical features of wheel-rail contact that influence vehicle dynamics are:

a) The variation of the rolling radius difference between two wheels on an axle as the wheelset is displaced laterally. This governs the equivalent conicity of the wheel-rail contact and therefore stability.
b) The resistance of the vehicle against derailment is affected by the contact angle or the inclination of the tangent to wheel-rail contact.

The field of study and application of these codes have grown significantly. In recent years, these codes have been used in the study of wheel and rail damage in the form of wear and rolling contact fatigue (RCF). With more knowledge of these damage mechanisms, it is possible to predict the worn shape of wheels (Iwnicki, 2009; Dirks and Enblom, 2011) and to predict the initiation of surface-initiated RCF (Burstow, 2003; Burstow, 2004; Tunna and Urban, 2009; Wu et al., 2010; Dirks and Enblom, 2011).

The complexity of the analysis may be further increased by including the effects of track irregularities. This complexity allows the researcher to perform a simulation over a track that represents deviations that are more realistic. Karttunen et al. (2014a) applied lateral irregularities to study their effects on the initiation of RCF. Berggren et al. (2008) have shown that vertical track irregularities with wavelengths shorter than 2 m produce high dynamic wheel-rail interaction forces.

VI-grade (2014) has recently included elements that can be used in modelling three-piece bogie components in their software VI-Rail (2014). These elements can be used to model friction wedges, side bearers and the centre plate interface between the wagon body and bolster. The formulations of these elements allow the inclusion of the frictional damping of these components. These elements increase the complexity of the model, but at the same time provide better estimation of the actual friction forces, damping and overall vehicle behaviour.

The aforementioned computer packages facilitate the modelling of railway vehicles. These packages do not guarantee accurate results when inaccurate modelling and/or incorrect properties of elements such as the springs and dampers are used. These models therefore have to be validated against highly accurate experimental data. Cole (1998) mentioned three approaches to simulation model validation, namely visual, distortion and statistical comparisons. The visual approach is self-explanatory. The distortion approach relies on the premise that any model can be forced to fit any transient or system output if it is given enough distortion. Therefore, the model requiring the least amount of distortion is the best model. The statistical comparison approach was described in more detail and many statistical parameters were introduced to assist in realising an objective validation measure. These parameters included the mean square error; the root mean square error, the standard deviation, the mean error, the correlation coefficient and the cross-correlation function. The use and applicability of these parameters have been discussed based on the comparison of measured and simulated data.

Cole (1998) discussed the usage of validated multibody dynamics simulation models to describe normal and extreme running conditions accurately. The results from two simulation models at extreme operating conditions were compared to one another. Both models were validated against measured values and it was shown that the results could differ quite significantly. It was suggested that validation data under more extreme conditions were needed to have more confidence in the simulation model used for analysis of such extreme conditions.

1.2.2 Rolling contact fatigue

In heavy haul railway operations, high axle loads and high tangential loading prevail at the wheel-rail interface. These contact conditions may result in the growth of surface- or subsurface-initiated fatigue cracks. These cracks are widely known as rolling contact fatigue (RCF) cracks. This type of fatigue crack differs from fatigue cracks observed in the majority of engineering components because they initiate and grow under compressive and not tensile loads (Fletcher et al., 2009). Ekberg and Kabo (2002) and Ekberg et al. (2014) provided an overview of the various mechanisms behind RCF cracks, means of prediction and modelling, the parameters influencing the initiation and growth of these cracks and possible means of correction and prevention. A more recent review on wear and RCF has been presented by Tunna et al. (2007). Grassie (2015) presented a broad overview of wear and rolling contact fatigue from practical experiences with such rail damage. Ekberg et al. (2014) also discussed the prevention of RCF from a practical perspective. Good maintenance practices that enable the reduction of surface-initiated RCF were addressed.

RCF failures are usually confined to the gauge corner of the high rail or the field side of the low rail in curves. Here plastic deformation and crack initiation are caused by high contact stresses and tractive cornering forces. These fatigue cracks may grow and unite with other fatigue cracks to cause shelling of material. These cracks can branch across the railhead, finally causing a complete fracture of the rail (Johnson, 1989). For this reason, RCF cracks have a significant impact on the safety, reliability and availability of track and rolling stock. Uncontrolled growth of RCF cracks that leads to broken rails or wheels has a direct influence on safety and reliability of the railway system. The occurrences of fatigue cracks in rails and wheels increase their maintenance demand. The availability of track and rolling stock is therefore influenced by the increased maintenance demand. The safety, reliability, availability and maintenance cost associated with a railway system can be positively influenced by reducing the occurrence and severity of RCF cracks.

Surface-initiated RCF cracks occur in a thin surface layer of the material and are shallow. These surface-initiated cracks may eventually grow deep into the rail increasing the potential of a catastrophic rail failure. Subsurface cracks will initiate at non-metallic inclusions or at microstructural inhomogeneities. Fatigue cracks grow rapidly parallel to the surface and propagate at the depth of the highest shear stress caused by normal and tangential loading. Assuming elasticity the highest shear stress will occur just below the surface for traction coefficients above ~0.3. The deformations shift to the surface layer when this boundary is exceeded (Johnson, 1989; Bower and Johnson, 1991). Tunna et al. (2007) stated that the tangential forces generated during curving are considerably larger than the tangential forces generated during traction or braking. The most severe contact condition arises during curving whilst braking with high creepage since these tangential forces superimpose.

Fletcher et al. (2009) and Lewis and Olofsson (2009) divided the life of a surface-initiated RCF crack into three phases. During the first phase, the rail is either crack-free or a small crack, in the order of hundreds of microns, has initiated. Crack initiation is caused

by repeated contact loading, resulting in an accumulation of plastic strain increments. This process is known as ratchetting. This accumulation eventually exhausts the ductility of the surface material at which point a crack initiates (Lewis and Olofsson, 2009). These cracks are formed in the near-surface, plastically deformed layer of the rail. The transition into and growth of the second phase is characterised by shear-driven crack growth. This mechanism is attributed to the cyclic shear stress that the rail material experiences with each passing wheel or each wheel accumulates as it runs over the rails. The third phase is dominated by crack growth to rapid catastrophic failure. This rapid failure is caused by bulk stresses in the wheel or rail.

The predictive models used to describe the initiation of a surface fatigue crack during the first phase of crack growth are discussed in more detail in paragraph 1.2.2.1. The propagation of an initiated crack, and thus the second phase of crack growth, is attributed to shear and can be described by a mode II fracture mechanism. According to Johnson (1989), there are many objections to this statement. The following two situations were cited that oppose this theory. Firstly, fluid entering the crack can pry the crack open, which facilitates the propagation. Secondly, mode II crack propagation actually propagates as mode I branch cracks. The cracks branch out, alternating in direction. The general direction of the growth is in the direction of the plane of maximum shear.

According to Tunna et al. (2007), it is important to consider the tangential and normal forces, the contact pressure, creepage and the presence of lubrication when analysing the contact conditions and their effect on wear and RCF. It is widely accepted that fluid contaminants entering the crack often accelerate the second phase of crack growth (Ekberg and Kabo, 2002). Due to the incompressible nature of these contaminants, they will cause pressurisation once they become trapped as a wheel passes over the crack and accelerate the growth rate. In the presence of fluid contaminants, the failure mode becomes a tensile failure mode and can be described by an mode I fracture mechanism. Although fluid entrapment can accelerate crack growth, it is not a prerequisite for crack growth. Kimura et al. (2002) argued that similar RCF behaviour has been observed on lubricated, marginally lubricated and unlubricated systems. There appears to be a finite number of cycles to failure, irrespective of whether the contact surface is regarded as a driver or a follower. However, the number of cycles to failure of the driver is higher than that of the follower. This can be attributed to the crack opening mechanism and wear on the driver.

The third and final phase advances rapidly as the cracks in the material become large and bulk stresses drive the material to failure. Bulk stresses are associated with bending stresses and tensile residual stresses in rails as well as thermal loading (Fletcher et al., 2009).

The current study will focus on the initiation of surface RCF cracks, the way in which the initiation of these cracks is modelled and the treatment of such cracks.

1.2.2.1 Predictive models for RCF

1.2.2.1.1 Shakedown-related models

Materials subjected to rolling contact can respond in one of four ways, namely perfectly elastic, elastic shakedown, cyclic plastic and incremental collapse or ratchetting (Johnson, 1989). If the load on any one of the contacting materials remains below the yield strength of either, the behaviour will remain perfectly elastic (response 1 of Figure 1-6). An effective increase in the yield strength of the material is caused by work hardening when the first application of the load exceeds the yield limit of the material. The material will experience elastic shakedown if the steady cyclic state remains below this increased yield strength. This process eventually leads to fully elastic behaviour (response 2 of Figure 1-6). If the steady state loading cycle exceeds the yield strength of the material regularly, but the cycle remains within a closed plastic stress-strain loop without the net accumulation of unidirectional plastic strain, the material responds in a state of plastic shakedown (response 3 of Figure 1-6). Incremental collapse or ratchetting is closely related to plastic shakedown. In this case, however, the plastic cycle is an open loop and there is an accumulation of unidirectional plastic strain.

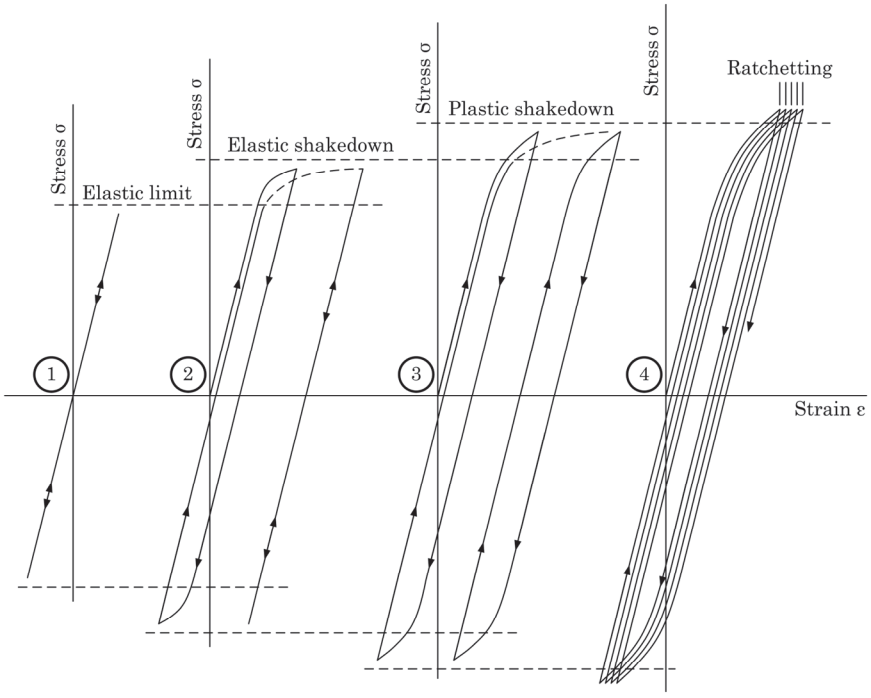

Figure 1-6: Four types of material responses to rolling contact (Adapted from Johnson, 1989)

There are mechanisms that cause a change in the material and geometry of the contacting bodies to lessen the effect of subsequent cycles and aid in the shakedown process. Kimura et al. (2002), for example, have shown that the magnitude of plastic flow has a non-linearly diminishing relationship to the number of times the surfaces make contact. This is mainly due to strain hardening that suppresses the material flow as the

number of contact incidents increase. These mechanisms take place between the first load application and the steady cyclic state. According to Johnson (1989) they are:

a) Plastic deformation during the early cycles causes residual stresses in the material. These residual stresses are protective and have to be overcome before subsequent plastic deformation can take place, thus they decrease the likelihood of subsequent plastic deformation.
b) Strain hardening during the early cycles reduces subsequent plastic deformation of the material.
c) Plastic deformation causes the two contacting bodies to become more conformal, thus increasing the area of contact and reducing the contact stress for a given load.

Johnson (1989) produced the well-known shakedown diagram. The shakedown diagram represents the four possible ways in which a metal can respond to rolling contact based on the normal and tangential contact loading (Figure 1-7). The y-axis of the diagram is a non-dimensional load factor defined as the maximum Hertzian contact pressure (shown in equation (1-6) (Johnson, 1985)), divided by the yield strength in cyclic shear (k_e) of the softer material. It is assumed that the contact pressure is given by Hertz, implying elastic behaviour, although plastic deformation is present in the shakedown process. The contact stress for surface loading is well defined and known (Johnson, 1985). The x-axis of the diagram represents the utilised traction coefficient (μ) calculated as the traction force divided by the normal force (T/N) (as shown in equation (1-7)). The utilised traction coefficient is non-dimensional.

$$p_0 = \frac{3N}{2\pi ab} \tag{1-6}$$

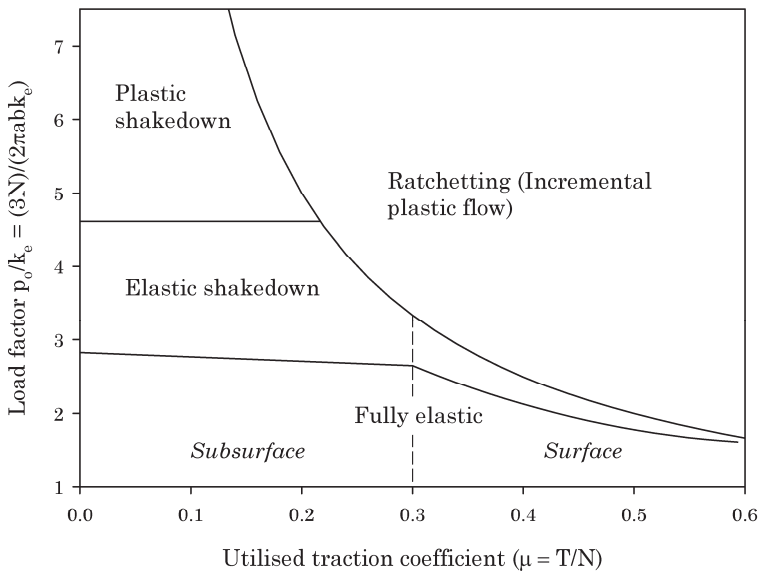

Figure 1-7: Shakedown diagram (Adapted from Johnson, 1987)

$$\mu = \frac{\sqrt{T_x^2 + T_y^2}}{N} \tag{1-7}$$

The yield strength in cyclic shear (k_e) of the material is usually not specified. This value can be estimated from the tensile yield strength (σ_y), depending on the applicable yield criterion. According to the von Mises criterion (Johnson, 1985; Tunna et al., 2007), the yield strength in cyclic shear can be calculated from equation (1-8). According to the Tresca criterion, equation (1-9) should be applied (Johnson, 1985). Furthermore, Tunna et al. (2007) indicated that the tensile yield strength can be estimated from the ultimate tensile strength (σ_{ut}) as shown in equation (1-10). Equations (1-8) to (1-10) facilitate the calculation of the materials yield strength in cyclic shear based on the ultimate tensile strength of the material.

$$k_{e_{von\ Mises}} = \frac{\sigma_y}{\sqrt{3}} \tag{1-8}$$

$$k_{e\ Tresca} = \frac{\sigma_y}{2} \tag{1-9}$$

$$\sigma_y = \frac{\sigma_{ut}}{\sqrt{3}} \tag{1-10}$$

For smaller values of the traction coefficient (below approximately 0.3), yield occurs on first loading at a point beneath the surface. For traction coefficient values above this limit yielding occurs at all points of the contact interface. Johnson (1989) showed that the load factor (the y-axis) is inversely proportionate to the utilised traction coefficient (the x-axis) of the shakedown diagram, when yielding occurs at the interface of the two bodies according to equation (1-11). This relationship is often used as the shakedown limit line.

$$\frac{p_0}{k_e} = \frac{1}{\mu} \tag{1-11}$$

Johnson (1985) described Melan's theorem that defines shakedown in the following way: if there exists any time-independent residual stresses distribution that, in combination with the elastic stresses due to the applied load, results in a system of stresses that remain below the elastic limit, the system will shakedown. In contrast in any system in which no such distribution of residual stresses can be found will not allow the system to shakedown, but rather plastically deform with every passage of the load.

A two-dimensional case was used and it was shown that a distribution of residual stresses can be chosen in such a way that shakedown limit is governed by the shear stress τ_{zx} (in-plane shear stress) according to the Tresca criterion. The system will shakedown if the maximum of this shear stress remains below the yield shear stress value k_e. Johnson (1985) calculated the shakedown limit for an elastic cylinder contacting an elastic perfectly plastic half-space according to the Tresca criterion. The shakedown limit was calculated at a value of $p_0/k_e = 4$. This shakedown limit was applied by Wu et al. (2010). Johnson (1985) proceeded to calculate the shakedown limit for a ball rolling on an elastic-plastic half-space. This is an example of three-dimensional

rolling contact and the values for first yield and the shakedown limit were calculated at $p_0/k_e = 2.8$ and $p_0/k_e = 4.7$, respectively. These two values correspond more closely to the elastic and shakedown limit of Figure 1-7. It should be noted that these limits were all calculated under full slip conditions at no tangential loading.

Melan's theorem defines the necessity of determining the residual stresses to calculate the shakedown limit. Bower and Johnson (1991) described a simple non-linear kinematic hardening law. This law can be used to predict the response of rail steel to sliding contact. The hardening law was used to study the deformation under high tractive loads. This type of deformation is the most common form of deformation leading to wear and RCF on railway track. Bower and Johnson (1991) proceeded with calculating the shakedown limits under the condition of full slip for four types of contact. These included point and line contact under longitudinal or lateral traction loads. It was shown that the shakedown limits for line contact lie below the limit line defined by the inverse of the utilised traction coefficient ($1/\mu$). The shakedown limits for the two-point contact types exceeded this line. The shakedown limits for line contact under partial slip conditions proved that, as the available traction coefficient is increased, the associated shakedown limit reduces and moves away from the line defined by the inverse of the utilised traction coefficient. It follows from the approximate solution of the stress locus that the damaging effect of partial slip in point contact will not be as severe as that of in line contact. Therefore, the full slip assumption is widely used to assess the initiation and growth of RCF cracks (Bower and Johnson, 1991).

It is common practice to apply the shakedown limit defined by the inverse of the utilised traction coefficient ($1/\mu$) that was derived under full slip conditions to study RCF crack initiation and growth (Ekberg et al., 2002; Fröhling et al., 2008; Iwnicki, 2009; Wu et al., 2010). The condition of full slip is not always met but partial slip shakedown diagrams are not used under partial slip conditions. This is one of the limitations when applying the shakedown diagram to RCF problems.

An engineering model that predicts surface-initiated fatigue, subsurface-initiated fatigue and fatigue that originates at deep material defects in railway wheels was developed by Ekberg et al. (2002) and was discussed by Ekberg (2009). Surface-initiated fatigue failures result in small pieces of tread material becoming detached. Subsurface-initiated fatigue may result in very large sections of rim material becoming detached and may even lead to a catastrophic failure. Fatigue that initiates deep in the material is caused by large local stresses at material defects within the wheel material. Cracks may form due to these large stresses and propagate causing catastrophic failure of the wheel.

The maximum Hertzian contact pressure for an elliptical contact patch can be calculated according to equation (1-6) (Johnson, 1985) and can be substituted to expand the equation of the load factor or y-axis of the shakedown diagram (p_0/k_e shown in Figure 1-7). The model that Ekberg et al. (2002) used to predict surface-initiated fatigue was based on the shakedown diagram and was called the surface fatigue index (FI_{surf}) (equation (1-12)). This equation is based on the horizontal projection of the distance from the working point (defined by the μ and p_0/k_e values of the contact condition on the shakedown diagram) to the shakedown limit approximated by $1/\mu$. It is noted that this value approximates the true distance and therefore is less accurate at very high traction

values and low values of the load factor. Under conditions of very high tractions and low load factor values wear is expected to dominate. Surface-initiated fatigue is predicted to occur when equation (1-13) holds true.

$$FI_{surf} = \mu - \frac{k_e}{p_0} = \mu - \frac{2\pi abk_e}{3N} \quad \textbf{(1-12)}$$

$$FI_{surf} > 0 \quad \textbf{(1-13)}$$

Ekberg et al. (2014) extended the use of the FI_{surf} and showed how it can be applied to predict the fatigue life of wheels and rails. The FI_{surf} values can be used to calculate the incremental damage per wheel revolution or passage on a rail. This incremental damage can be applied to variable amplitude loading and accumulated to provide an indication of a surface RCF crack initiation. Furthermore, an application of FI_{surf} under more general slip conditions is discussed.

The surface-initiated fatigue index (FI_{surf}) proposed by Ekberg et al, (2002) has found widespread application in work related to the study of surface-initiated RCF (Shevtsov et al., 2008; Persson et al., 2010; Dirks and Enblom, 2011; Karttunen et al., 2014a; Karttunen et al., 2014b; Ekberg et al., 2014).

The engineering model of Ekberg et al. (2002) can predict subsurface-initiated fatigue cracks based on the Van Dang multi-axial fatigue criterion. Cracks that initiate at a depth between 3 mm and 10 mm are considered as subsurface-initiated cracks. The boundary between subsurface-initiated fatigue and fatigue initiated at deep defects is not always very clear. However, the fatigue initiated at deep defects was considered as a function of high vertical load and relatively large material inclusions. If the vertical load exceeds a threshold value, fatigue at deep defects are predicted. These fatigue cracks are less dependent on lateral load and initiate at a depth around 10 to 25 mm. The engineering model was applied to multibody dynamics simulations to compare the values of the three fatigue index parameters of four wheels within a bogie. It was noted that this model is ideal for a comparative design where the results from an existing state can be compared to those from a projected state. No fatigue limits are needed for such a comparison as only the fatigue performance is compared.

1.2.2.1.2 Models based on the dissipation of energy in the contact patch

Burstow (2003) investigated the use and application of different damage parameters to predict the location of surface-initiated RCF cracks. Damage parameters were based on the shakedown diagram, a squat damage parameter and the wear number ($T\gamma$). Burstow (2003) determined correlation between the location predicted by the damage parameters and the location of RCF cracking measured at two test sites. It was found that the damage parameter that provided the best correlation for the two test sites was the parameter derived from the wear number. The reasoning behind the wear number ($T\gamma$) damage parameter is that it was not possible to derive a meaningful damage parameter

from the shakedown diagram and the fact that the shakedown diagram does not take the amount of creepage in the wheel-rail interface into account (Burstow, 2004). The shakedown diagram, however, indicates when ratchetting is taking place.

According to Burstow (2003), the wear number is calculated as the product of the tangential loading forces (T_x, T_y) and the creepage (γ_x, γ_y) as shown in equation (1-14). This damage parameter is simple and can be readily calculated from the output of vehicle dynamics simulations. The wear number itself is a description of the amount of energy dissipated in the contact patch and was thought to indicate the amount of energy which would be available for crack initiation. This energy term was earlier correlated with wear (Pearce and Sherratt, 1991) and it was thought that this term could describe the competition between wear and RCF. This competition will be examined in paragraph 1.2.4. According to Wu et al. (2010), the wear number not only allows for the prediction of the wear rate and risk of RCF damage, but also shows the effect on the rolling resistance as it provides an indication of the energy dissipated in the wheel-rail interface.

$$\text{Wear number} = T\gamma = T_x\gamma_x + T_y\gamma_y \quad \textbf{(1-14)}$$

A damage function (Figure 1-8) was defined and further refined by Burstow (2004). The damage function is material specific and a function of the ductility of the material. A method for calculating the damage function based on the strength of the material, contact area and predefined creepage values is used to verify the shape of the damage function. This computation has been applied by Wu et al. (2010) to examine the change in the shape of the damage function when the material properties or the contact area is altered. The operation of the damage function was described by Burstow (2004) and Iwnicki (2009) as follows:

a) A $T\gamma$ in the region between 0 and 15 N indicates that insufficient energy is available for crack initiation and thus no RCF or wear is predicted in this region.
b) A $T\gamma$ between 15 and 65 N indicates that the energy available for RCF initiation is growing to a maximum value at 65 N. Only RCF initiation is predicted in this region.
c) A $T\gamma$ between 65 and 175 N indicates an increase in the energy to encourage wear. The RCF and wear compete in this region until the energy available balances the wear and RCF initiation at 175 N.
d) With a further increase in the $T\gamma$ value to more than 175 N, the dominant damage form is wear and no RCF is initiated. The damage function values are negative as the action of wear actually reduces the damage caused by RCF.

The damage function is intended to describe the incremental damage that occurs with each passing wheel. The values for the damage per wheel passage can be summed to indicate the initiation of a crack when the value reaches unity. The reciprocal of the damage function gives the number of cycles to failure at each $T\gamma$ value. In a manner similar to Miner's damage rule, the number of cycles that a wheel or rail experiences at each $T\gamma$ value, divided by the number of cycles to failure at each $T\gamma$ value can be added. A crack is said to initiate when this value reaches unity. The total number of cycles to failure can be calculated in this way.

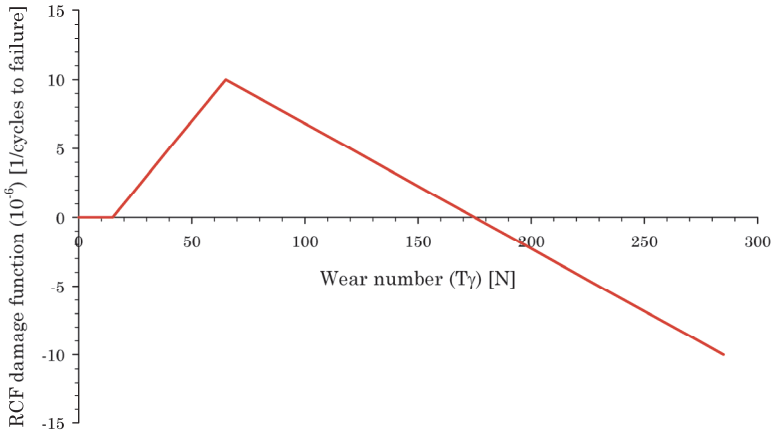

Figure 1-8: Damage function used together with the wear number (Adapted from Burstow, 2004)

Burstow (2004) applied this damage parameter and damage function to investigations at four sites to validate the damage function. These applications proved that this parameter provides the best prediction of the occurrence of RCF. The wear number could predict the location and the size of the surface-initiated cracks by summing the incremental damage of each passing wheel. The one drawback of this approach is that it does not explicitly account for the normal contact stress term. It is known to be an important term in shakedown and ratchetting theory and therefore plays a part in the formation of RCF cracks (Burstow, 2003). Since the development of the wear number, many authors have applied it to their work (Tunna and Urban, 2009; Wu et al., 2010; Dirks and Enblom, 2011; Karttunen et al., 2014a).

1.2.2.1.3 Comparison of RCF predictive models

Dirks and Enblom (2011) investigated similarities and differences between models used to predict the initiation of surface-initiated RCF crack. The performance of the FI_{surf} and $T\gamma$ RCF models was compared. This was accomplished by a study of parameters influencing the behaviour of the two models. The parameters that were studied included curve radius, worn wheel and rail profiles, the coefficient of friction, primary suspension stiffness, track irregularities and cant deficiency. The correlation between the models showed good agreement for the curve radius. However, when worn wheel and rail profiles were used, the models started to deviate significantly. It was shown that the two models differed significantly for the coefficient of friction. With a higher primary suspension value, both models indicated an increase in the probability of RCF initiation. The effect of cant deficiency proved to be more pronounced on the outer wheel. This was attributed that the fact that the load on the outer wheel increases due to an increase in cant deficiency.

Dirks and Enblom (2011) proposed two variations to the two models. The FI_{surf} value was calculated in a local and global manner and spin creep was included in the calculation of the wear number. Both alterations are thought to have a significant influence on the prediction of fatigue initiation. In wider curves (radius > 1500 m), the

influence of including the spin creep in the wear number calculation was reduced because the location of the contact patch resulted in a lower spin creep value.

The two models outlined in paragraph 1.2.2.1 both have their limitations. The advantages and disadvantages of using the shakedown diagram or the wear number to predict surface-initiated RCF crack are summarised in Table 1-1.

Table 1-1: Shakedown diagram and wear number advantages and disadvantages

	Shakedown diagram		
	Advantages		**Disadvantages**
1.	Considers the tangential and normal forces.	1.	Was developed under the assumption of full slip.
2.	Considers the contact pressure.	2.	Uses the maximum Hertzian contact pressure and therefore Hertzian assumptions should still hold true.
3.	Can readily be calculated from the output of vehicle dynamics simulations.	3.	Does not include the effect of creepage.
	Wear number		
	Advantages		**Disadvantages**
1.	Considers the tangential loads and creepage.	1.	It does not include the effect of the normal load or contact pressure.
2.	Can readily be calculated from the output of vehicle dynamics simulations.	2.	No distinction can be made between the likelihood of surface or sub-surface initiated cracks.
		3.	It requires more parameters to estimate the damage curve leading to greater uncertainty.

1.2.2.2 The influence of track parameters on RCF initiation

Since RCF occurs in the wheel-rail interface, it is affected by both the wheel (and thus the vehicle) and the rail (and thus the track structure and track layout). It is known that RCF initiation is related to curve radius (Evans and Iwnicki, 2002; Fröhling, 2002; Tunna and Urban, 2009; Dirks and Enblom, 2011; Karttunen et al., 2014a; Grassie, 2015), because higher steering forces arise in sharper curves. The influence of cant deficiency was studied by Evans and Iwnicki (2002), Dirks and Enblom (2011) and Stow et al. (2011). Evans and Iwnicki (2002) showed that cant deficiency is neutral with regard to RCF initiation. Stow et al. (2011) found similar results and proposed that a change in cant deficiency will yield the greatest results in curves with radii between 1000 and 1800 m. Grassie (2015), on the other hand, stressed that cant excess leads to higher tangential forces and should be avoided to reduce rail RCF damage. The consensus seems to be that cant deficiency is either neutral or beneficial to the reduction of RCF.

In addition to the influence of curve radius and cant, Evans and Iwnicki (2002), Burstow (2003) and Tunna and Urban (2009) found that RCF initiation can be linked to track quality. Karttunen et al. (2014a) furthered the investigation of the influence of track geometry on RCF initiation. The influence that irregularities will have on RCF

development was studied. A single lateral track irregularity and lateral track irregularities generated from a power spectral density (PSD) were considered in the study. This study was performed by evaluating the FI_{surf} and $T\gamma$ values obtained from the simulated response of a vehicle fitted with Y25-TTV bogies.

Karttunen et al. (2014a) showed that large wheelset oscillations on straight track were caused by the single lateral irregularity. The wheelset may then make contact with both the left and right gauge corner and, correspondingly, the wheel flange throats. This causes high longitudinal creep forces due to the large rolling radius difference and promotes RCF crack initiation. The influence of lateral track irregularities generated from a PSD was studied within circular curves. The length of rail that is influenced by RCF depended on the curve radius and the level of lateral irregularities. For curves with a radius less than 1250 m, the length of the high rail affected by RCF reduced with irregularities of a higher level. This was due to the irregularities forcing the wheelset away from the gauge corner and flange throat. For curves with a radius greater than 1250 m, the length of track affected by RCF increased with irregularities of a higher level. Lateral track irregularity wavelengths between 10 and 50 m caused the greatest RCF damage on curves with a radius greater than 1250 m. It is, therefore, very important to maintain track quality to high standards as it will lower the propensity to RCF crack initiation.

Karttunen et al. (2014b) suggested that vertical irregularities would only influence vertical wheel forces. Longer irregularity wavelengths (> 2 m) have only a minor influence on the value of FI_{surf}. This means that for shorter irregularity wavelengths there will be a localised increase in vertical wheel load, which should increase the load factor (y-axis) of the shakedown diagram. Vertical irregularities should therefore rather be avoided, in parametric studies, as the load factor may be influenced more by the vertical irregularity than the parameter being studied.

The influence of track layout and quality was addressed from a practical standpoint by Wu et al. (2010), who noted that high energy in the wheel-rail contact patch leading to RCF initiation or wear is generally caused by:

- Poor track alignment and rail fastening,
- Poor gauge face and/or wheel lubrication,
- Poor top of rail friction control,
- Poor wheel-rail contact conditions resulting from high contact stresses and/or two-point contact,
- Poor vehicle curving performance.

The first three points illustrate the importance of track layout and quality on the initiation of RCF. The last two points refer more to the influence of the wheel and rail profile shape and vehicle dynamics on RCF initiation.

1.2.2.3 Influence of wheel-rail profiles and vehicle dynamics on RCF initiation

The influence of the track on RCF initiation has been introduced in paragraph 1.2.2.2. The influence that the wheel and rail profiles have on RCF initiation will be dealt with in more detail. The profiles of the wheels and rails affect the contacting forces at the interface. These profiles therefore have a definite influence on the running behaviour of vehicles. It is thus obvious that the shape of the wheel and rail profiles will have an influence on the probability of RCF initiation.

The wheel and rail profile combination should provide adequate stability in tangent track and facilitate steering in curved track. Due to the wear of these profiles, the straight-line stability and steering ability will change because of the change in equivalent conicity (Pearce, 1996). Pearce (1996) examined the worn shape of three different wheel profiles. In particular, a hollow-worn profile was produced by a vehicle with soft lateral suspension that ran over a relatively straight track. The increase in conformity between the hollow-worn wheel and the rail increased the conicity of the wheel in the high to very high region.

Burstow (2003) studied the effect of very high equivalent conicity on the initiation of RCF. Based on the results from vehicle dynamics simulations of one site, it was determined that the RCF is caused by the worn state of some of the wheels. The wheel profiles became highly conformal with the rail profile causing a very high degree of equivalent conicity, resulting in vehicle instability. Due to the instability and the sharp changes in contact position, very high forces resulted in the contact patch. Such high forces would lead to an increase in the risk of RCF. This was proven by removing conformal wheel profiles from the analysis resulting in a reduction in the risk of RCF.

An increase in the equivalent conicity is caused by hollow-worn wheel profiles (Tournay and Mulder, 1996). This higher conicity causes larger lateral wheelset displacements and thus the wheel contact point to move laterally beyond the hollow wear band. It is known from Karttunen et al. (2014a) that lateral track irregularities have a significant impact on RCF initiation linked to larger lateral wheelset displacements. Tunna and Urban (2009) proved that conicity has a significant influence on the development of RCF damage on curves with radii larger than 1500 m. According to Evans and Iwnicki (2002), a low conicity wheel profile is more favourable from an RCF perspective, but it will produce more flange wear.

Large lateral displacements, causing the wheel contact point to move beyond the hollow wear band, together with the instability of hollow-worn wheel profiles, will be aggravated by lateral irregularities. Large lateral displacements often result in the false flanges at both the flange and the field side of the wheel contacting the gauge corner and field side of the rail, respectively. This causes extremely small contact areas and often results in high longitudinal creepages due to the large radius differential generated by the wheelsets. According to the shakedown diagram and $T\gamma$ RCF damage model, the increase in normal pressure and tangential loads will inevitably result in a greater

probability of RCF initiation. RCF resulting from false flange contact is shown in Figure 1-9.

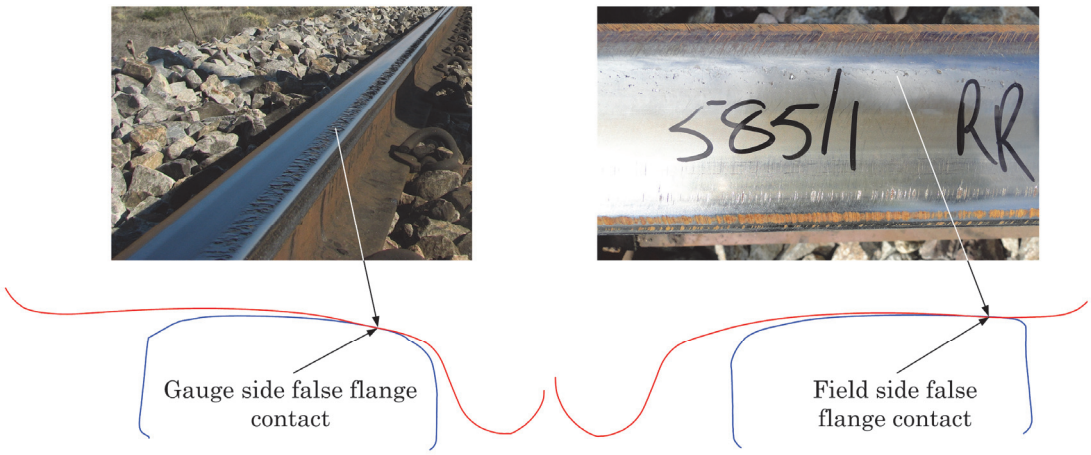

Figure 1-9: Gauge side and field side false flange contact damage

Fröhling et al. (2008) examined the risk of initiating surface RCF due to hollow-worn wheel profiles. High lateral forces and a narrow contact patch are associated with a high propensity to develop RCF. It was shown that high fatigue impact occurrences correlate strongly with high frictional forces and less with high normal forces. It was suggested that the impact of false flange contact should be restricted by limiting the amount and controlling the shape of the hollow wear.

Fröhling et al. (2008) described the negative properties of hollow-worn wheels as:

- False flange damage to the rail surface and special track work such as turnouts,
- Increased lateral forces in curved track,
- An increased risk of hunting (instability due to conformal contact) or other unsound running behaviour on tangent track,
- Poor steering with steering forces toward the outside of the curve.

The effect of the shape of hollow-worn wheel profiles on the initiation of RCF was further investigated by Fröhling et al. (2012) and Karttunen et al. (2014b). Fröhling et al. (2012) determined that the 2 mm hollow wear limit proposed by Tournay and Mulder (1996) was still valid. It was further shown that the initiation of gauge corner RCF cracks was sensitive to the gradient of the false flange on the flange side of the wheel.

Karttunen et al. (2014b) developed a method to parameterise a worn wheel profile. Meta-models were used to study the relative influence of the various worn wheel parameters to identify those with the greatest influence on the RCF and wear. Initiation of RCF indicated sensitivity to the rail inclination of a standard UIC60 rail profile, showing the importance of the rail profile shape in RCF initiation. The two most influential parameters for both the inner and outer wheel were the parameters defining the minor axis of an ellipse fitted to the hollow wear (in other words the hollow wear depth) and angle of that ellipse. Therefore, if these two parameters are reduced or changed it should have a positive effect on both the outer and inner wheels.

The influence that a vehicle has on RCF initiation was studied by Evans and Iwnicki (2002) as well as Tunna and Urban (2009). It was found that the wheelbase of the bogie and primary yaw suspension stiffness influence RCF crack initiation. A lower bogie yaw stiffness or a soft primary suspension stiffness reduce the tendency to develop RCF cracks on small radius curves. Iwnicki (2009) illustrated the effect the stiffness of the primary suspension has on the shape of an optimised rail profile. The optimisation was aimed at reducing RCF and wear. The influence of the primary suspension stiffness therefore has to be carefully considered when attempting to reduce RCF initiation and growth. The steering ability and therefore tangential curving forces of the vehicle are influenced by the wheel and rail profile shapes as well the primary suspension stiffness.

The prevention of RCF can be achieved by suppressing the most damaging operational conditions (Ekberg et al., 2014). The most damaging operating conditions can be suppressed by managing the rail profile shape, applying lubrication, maintaining track geometry, joints, switches and crossings, mitigating corrugations, etc. One of the ways in which many railways try to suppress RCF is by grinding a so-called anti-head check or rail shoulder relief type rail profile (see Evans and Iwnicki, 2002; Iwnicki, 2009; Persson, et al., 2010; Stow et al., 2011; Schöch, 2011). The rail profile can be ground to provide gauge shoulder relief, which reduces the chance of gauge corner contact and therefore crack initiation. Evans and Iwnicki (2002) discussed how the target rail profile in the UK was rotated to 3.4° rather than the usual 2.86° and the tolerance for grinding was set to +0/-0.6 mm to ensure more gauge shoulder relief. This resulted in a reduction in conicity and the steering ability of the wheels. Gauge shoulder relief should be accompanied by lubrication to reduce wear of the gauge face and wheel flange due to this reduction in steering ability.

The track, wheel-rail profiles and vehicle dynamics have a significant impact on the initiation and propagation of RCF cracks. These features influence the forces generated in the contact patch at the wheel-rail interface. Both the FI_{surf} value, based on the contacting forces at the contact patch, and the wear number ($T\gamma$) describing the energy dissipated in the contact patch, have been proven to indicate the probability of RCF initiation. It follows that RCF formation can be effectively controlled and reduced by managing the contacting forces and thus the dissipated energy at wheel-rail interface. To be able to manage the contacting forces effectively, the influence of the current system parameters need to be understood. In the current study, the influence of the track is of lesser concern, but the wheel-rail profiles and suspension design are of greater importance.

1.2.3 Wear in the wheel-rail interface

Wear of the wheel and rail is an inevitable consequence of the rolling-sliding action at the contact patch when the two bodies move relative to one another. Wear is a significant damage mechanism that influences the service life of wheels and rails. Maintenance costs of wheels include reprofiling of a wheelset or renewal of the wheels once the wheelset has reached specified wear limits. According to Fröhling (2002), railway wheels must ideally be managed to change as little as possible during their lifetime resulting in reduced wheel maintenance costs. Maintenance costs of rails include rail replacement

once the rail wear has reached its specified wear limits. The cost of operating and maintaining a railway system is directly linked to the wear of the wheel-rail system. The potential to save on maintenance costs can be directly influenced by the wheel and rail wear rates. The wear rates can be preserved or minimised through the intelligent design and maintenance of the vehicle-track system, which includes the track, interacting wheel and rail profiles, bogies and vehicles.

Not only does the vehicle-track system have an influence on the wear rates, but the wear caused by the system may also have a feedback that negatively influences its performance and safety. The performance of the system as it pertains to wheelset guidance, equivalent conicity, wheel wear, RCF and safety was considered by Scheffel (1976), Pearce (1996), Bruni and Braghin (2009) and Nia et al. (2015).

Braghin et al. (2009) showed that some wheel profiles, when new, exhibit elliptical contact with high normal pressures. The wheel profile changes its shape due to wear. The contact then becomes more conformal, which leads to a wider contact patch. This contact patch is no longer elliptical, and normal pressures are lower. The worn profile with conformal contact has a lower sensitivity to wear as the normal pressure inside the contact patch and the frictional power density (given by $T\gamma/A$) has reduced. Scheffel (1974, 1976) recognised this advantage of conformal wheel profiles and developed a bogie that is capable of stable running with such conformal wheel profiles. This bogie facilitates control and limitation of wheel wear. This allows the worn shape and equivalent conicity of the wheelset to be maintained over longer distances.

Tread and flange wear are often considered separately, since the mechanisms driving these types of wear differ. Tread wear is caused by any curving forces that act on the wheel tread and by forces generated while the vehicle negotiates track irregularities. Tread wear is also influenced by traction and braking. The effect of braking will not be considered in the following studies reported on in the thesis, although tread wear is influenced by braking and even more so by tread braking. Flange wear is mainly caused by curving when the flange contacts the gauge face of the high rail (Pearce, 1996). The actual profile wear that is experienced, is a function of the vehicle type and the route characteristics, since these characteristics determine whether tread or flange wear will dominate.

Chudzikiewicz et al. (1998) reported that Archard proposed a classification of the wear regime as either mild or severe. This classification, together with a catastrophic regime, is often used when dealing with wheel-rail wear (Pombo et al., 2011; Olofsson et al., 2013). Tunna et al. (2007) reported that the two predominant types of wear in wheel-rail contact are adhesive and delamination wear. Adhesive wear is considered mild, with thin flakes produced during wheel-rail contact. With mild wear, the interacting surfaces become polished and the wear rate is low. Tread wear is associated with mild wear. Delamination wear is more severe, with thin cracks initiating at the surface. These cracks propagate under the surface, until they branch up to the surface, which causes a metal flake to become dislodged. The severe wear regime is associated with such surface damage and the wear rate is high. With the catastrophic wear regime, the wear rate increases far beyond the severe wear regime. Flange wear is associated with either the severe or catastrophic wear regimes.

Management strategies to limit and control wheel wear were discussed by Fröhling (2002) and were based on both a scientific and practical approach. The scientific analysis was used to understand the influence factors such as speed, curve radius, track gauge and bogie design have on the angles of attack of the wheelsets and wheel wear distribution. It was concluded that in terms of wear, steering bogies showed the greatest advantage. The practical strategies mentioned by Fröhling (2002) included limiting hollow-wheel wear, lubrication on the gauge corner of the high rails, optimising the wheel profile, pummelling, rail grinding, gauge control in curves and bogie design and maintenance.

(a)

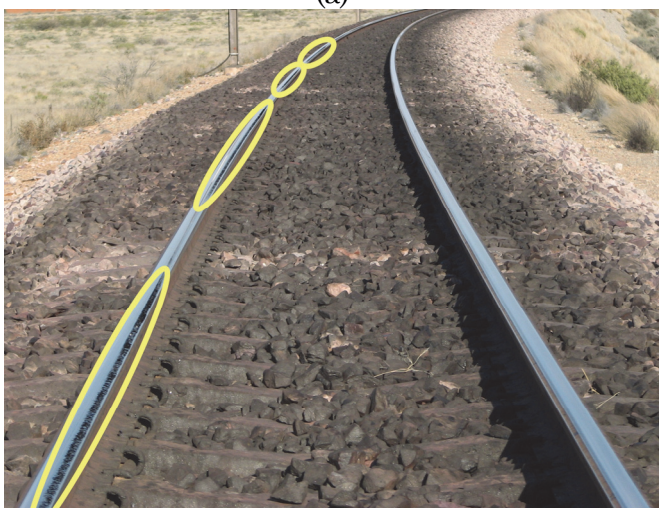

(b)

Figure 1-10: Alternating RCF damage on (a) straight and (b) high rail of a curve

By limiting the hollow wheel wear, it is possible to reduce wheel and rail RCF damage and reduce the probability of vehicle instability caused by an excessive equivalent conicity. Optimisation of the wheel profile can be used to reduce the wheel wear rate. It is suggested that the optimisation should focus on conformal contact between the wheel flange and the rail gauge corner. Conformal contact in this region will produce larger contact areas and lower the contact stresses, resulting in lower wear rates and support of the lubrication film. In addition, the optimised wheel profile should spread the wear across the wheel tread. Bogie designs such as Scheffel's self-steering bogie could be used to reduce the angle of attack of the wheelset and subsequently reduce the wear rates.

Scheffel (1974) compared the wheel wear resulting from the use of a self-steering suspension design to the wheel wear resulting from wheels in a conventional three-piece bogie, as well as a standard UIC bogie. The wear results proved that the self-steering design can reduce both tread and flange wear to a greater extent than the other two bogie designs.

The trade-off between greater conformity between wheels and rails and its effect on the equivalent conicity should be carefully considered. If the predominant wear pattern is concentrated hollow wear, then the increase in conformity may lead to increased equivalent conicity and vehicle instability, leading to alternating RCF cracks on tangent track and sinusoidal appearance on the high leg in curves (Figure 1-10). However, if the wear is spread across the wheel tread, this greater conformity may be beneficial in terms of the wear rate.

1.2.3.1 Modelling wear during wheel-rail contact

The natural progression from mathematical modelling of vehicle dynamics and contact mechanics is the modelling of damage mechanisms such as wear and RCF. The wear problem is therefore often solved in conjunction with the vehicle dynamics problem. This is done to gain a better understanding of the influence of the railway system on wear rates, the shapes of the worn profiles and its subsequent performance concerning its safety and tendency to RCF formation.

The railway industry works hard at remaining competitive with other modes of transport. Competitiveness can be driven by the economics of the railway industry, which is directly affected by wear and RCF damage to wheels and rails. It has therefore become imperative to simulate such damage and study factors influencing its severity. Such studies can be used to reduce maintenance costs, prolong service lives of wheels and rails and increase profits.

Braghin et al. (2009) provided an overview of the calculation of worn wheel profiles by means of multibody dynamic simulations. An iterative procedure is followed where the contacting forces are used to calculate wheel wear. The wheel wear is scaled, based on the original profile and an updating strategy. This is achieved by updating the profile after a predetermined distance has been traversed, or a predetermined wear depth has been reached. The process can be repeated to obtain worn profiles after traversing several kilometres of simulated track.

A schematic overview of the wheel wear process presented by Braghin et al. (2009) is reproduced in Figure 1-11. The various influencing processes are evident, as well as the coupling between the algorithms or models used to calculate the contact mechanics and wear. The output of the contact model is used as input of the wear model, predicting the amount of material to be removed from the original wheel profile. The influence of the worn or updated profile has a significant influence on the vehicle dynamics, resulting in a change in contact forces, creepages and contact positions, ultimately changing the contact mechanics and wear amounts.

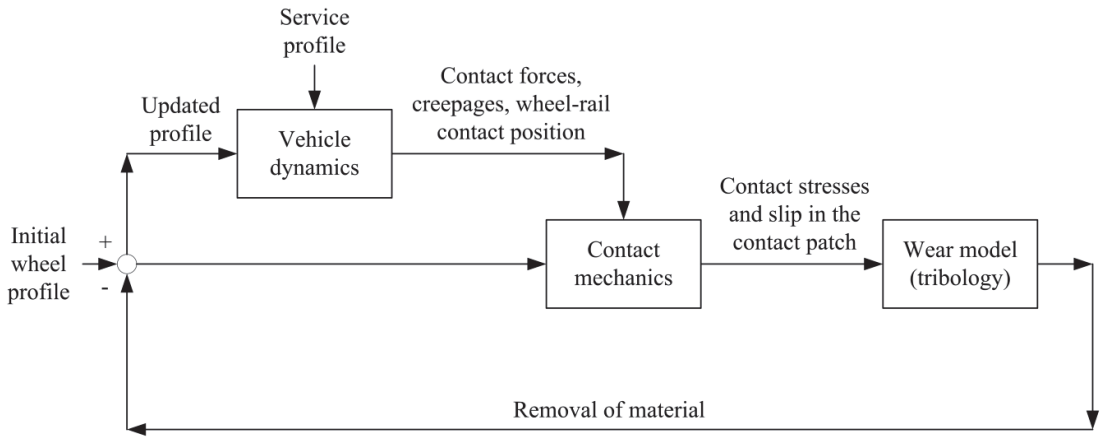

Figure 1-11: Schematic representation of the wheel wear process (Adapted from Braghin et al., 2009)

According to Zobory (1997), various models have been developed over the years to predict wear in the wheel-rail interface. In earlier studies, the wear algorithm was applied separately to the solution of the vehicle dynamics and was based on probabilistic methods predicting the contact area, size and location. This research was focussed on the prediction of wear based on contact mechanics and the full non-linear theory of contact. These initial methods have further evolved into methods that run concurrently with vehicle dynamics simulations or by post-processing the simulation results. This method usually applies approximations when treating contact mechanics.

Chudzikiewicz et al. (1998) discussed the solution of the wheel-rail contact problem, as its accuracy and output are required to solve the wear problem. It was stressed that the realistic calculation of wear requires an accurate and reliable contact algorithm. A contact algorithm that is able of solving non-elliptical contact had been proposed for this purpose. This algorithm allows the calculation of contact areas of any shape at multiple contact locations. Currently employed wear algorithms were highlighted and discussed by Chudzikiewicz et al. (1998). Tunna et al. (2007) and Enblom (2009) reviewed wheel wear mechanisms and wear prediction models. Although not the focus of the paper, Enblom (2009) included a section related to wheel polygonisation or out-of-round wear and rail corrugation development, since these are wear-related phenomena.

Enblom (2009) mentioned that two predictive wear models are currently applied in the railway context. The first assumes that material loss is proportional to frictional energy dissipated during contact (equation (1-14)). The second is based on Archard's wear model, which assumes that material loss is proportional to the product of normal force and sliding distance and inversely proportional to the material hardness. Both Tunna et al. (2007) and Pombo et al. (2011) compared energy dissipation wear models to Archard's wear model. Good agreement was found between the different models for the studied contact conditions. Enblom and Berg (2005) argued that the energy dissipation model could easily be calculated from computer simulation outputs. It therefore provides a good first approximation of gross wheel wear. Pombo et al. (2011) evaluated the manner in which these wear models can be applied both locally and globally on the results of the

contact algorithm. Similar results were obtained with global and local wear functions and it was recommended that the global wear formulation should be applied since the accuracy is not compromised, but the solution time is drastically reduced.

The proportionality between the amount of worn material and the frictional energy dissipation is often used for relative comparisons when evaluating the effect of contacting profiles, track layout or changing vehicle parameters on wear (see Fröhling, 2002; Shevtsov et al., 2005; Karttunen et al., 2014b). This assumption of proportionality is applied by many researchers in an attempt to evaluate and predict wear (see Kalker, 1991; Pearce and Sherratt, 1991; Zobory, 1997; Chudzikiewicz et al., 1998; Pombo et al., 2011; Ignesti et al., 2012).

Archard's wear model is commonly used in the tribology community to model sliding wear (Jendel, 2002). The use of Archard's wear model has become more and more prevalent (see Jendel, 2002; Jendel and Berg, 2002; Enblom and Berg, 2005; Johansson and Andersson, 2005; Chang et al., 2010; Pombo et al, 2011, Dirks and Enblom, 2011; Bevan et al., 2013; Nia et al., 2015). Chang et al. (2010) extended the application of Archard's wear model from its application in faster approximate contact algorithms to an application in a three-dimensional, non-linear, finite element model, increasing its accuracy. According to Enblom (2009), the wear models applied during the time of the review were dominated by the proportionality between the wear amount and the dissipated energy or frictional power. Archard's approach was deemed to have greater potential with respect to its generality and accuracy.

1.2.3.1.1 Wear algorithms based on energy dissipated in the contact patch

Kalker (1991) presented a method to estimate wheel profile wear with the FASTSIM algorithm by assuming that the wear amount is proportional to the frictional work and applying a fixed proportionality constant. Only tread wear was considered during the analysis. The predicted worn wheel profile was compared to a measured wheel profile and reasonable correlation was obtained. The frictional work per unit area was calculated from the integral of the tangential force times the relative velocity with respect to time. This was further simplified and it was shown that this integral is equivalent to the integral of the tangential force times the creepage with respect to distance. This form is similar to the $T\gamma$-approach where only the values of the tangential force and creepage are considered together with a metal removal rate (Pearce and Sherratt, 1991).

Pearce and Sherratt (1991) proposed a wear algorithm to calculate the loss of area from a radial section of a profile based on the wear number. A material loss value is calculated based on the wear number value and the type of wear regime of the prevailing contact conditions. The algorithm was applied to the P8 and P11 wheel profiles. The evolution of the equivalent conicity caused by a change in wear was compared to the change in equivalent conicity of measured worn wheel profiles. The algorithm achieved reasonable correlation with measured results.

Zobory (1997) discussed the prediction of wheel and rail profile wear. A simplified-combined wear hypothesis was formulated based on the combination of the dissipated energy wear hypothesis and the normal traction-based wear hypothesis. Here, the energy dissipated in the contact patch was calculated from the product of the creep forces and creepages including the product of the spin moment and spin creepage. The wear experienced on the tread and flange was treated as two separate processes with a slightly different definition.

Ignesti et al. (2012) developed a wear prediction tool based on the energy dissipated in the contact patch. The wear prediction tool is applied by performing a multibody dynamics analysis. A customised algorithm developed by the authors was applied in the calculation of the global contact parameters. The global contact parameters were post-processed with FASTSIM to obtain the local distribution of tangential creep forces and creepages, which were used in the wear prediction step. The wear prediction tool was developed to predict the wear on both the wheel and the rail and was validated for both. During the validation, it was shown that the wear is concentrated on the flange due to the winding line being considered.

1.2.3.1.2 Wear algorithms based on Archard's wear model

Jendel (2002) developed a tool capable of predicting wheel profile wear based on Archard's wear model. The methodology used by the tool was based on a load collective concept. The load collective concept tries to emulate the true operating conditions based on a limited description of the track and operating conditions. Time-domain simulations are carried out on this load collective and the results are post-processed with the wear algorithm embedded in the FASTSIM algorithm. The wear prediction tool was applied to a vehicle operating on the commuter rail network in Stockholm. The wheel profiles and four scalar wear measures were compared and the agreements between these were very good.

Enblom and Berg (2005) proposed an improvement to the contact model used by Jendel (2002). The method applied by Enblom and Berg (2005) included the elastic contribution to the creep calculation, which was neglected by Jendel (2002). It was proven that its inclusion is essential to calculate correct sliding velocity distributions. This is especially true in the case of large spin and partial slip contact conditions.

Enblom and Berg (2005) investigated the effects of including disc braking and lubrication on the wheel-rail contact conditions and wear depth. It was noted that the influence of braking becomes important, because it is large at the wheel tread on tangent track and on the field side of the inner wheel on curved track. The flange wear at the outer wheel is reduced when braking is applied within a curve. The relative influence of braking on the tread wear is similar irrespective of the curve radius.

The evolution of the application of Archard's wear model is ongoing. Chang et al. (2010) developed a tool to predict wheel profile wear based on Archard's wear model within a three-dimensional, non-linear, finite element model (FEM). This FEM is not subjected to the half-space and linear elasticity assumption of contact algorithms such as FASTSIM and CONTACT. Steady-state wheel-rail contact is assumed and the finite element model

is used to calculate the contact patch, contact pressure distribution, tangential forces and slip velocities. The results from the FEM are further processed to determine the wear depth at the various interaction nodes based on Archard's wear model. The tool was applied to predict the wheel wear of a heavy haul freight wagon; though no comparison to measured wheel wear had been made.

The evolution of Archard's wear model is not only limited to the improvement of the accuracy of the model, but it can further be extended to model other phenomena such as polygonal wheel wear (Johansson and Andersson, 2005). The studied polygonal wear included wavelengths in the order of 1 to 20 around the wheel circumference. This tool uses the time domain output of vehicle-track interaction model and predicts longer-term wheel wear. The predicted wheel wear is not assumed constant over the circumference of the wheel, but rather at the current contacting position of the wheel. This allows the wheel to wear to a polygonal shape, since irregular wear is simulated.

As an example, the tool was applied to a bogie of a subway train travelling on a straight track. In this example, the greatest increase in the out-of-round amplitude was observed in the orders 14 to 20. The prediction of polygonal wheel wear is not only limited to wear models based on the Archard's formulation. Zobory (1997) discretised wheel and rail profiles in such a manner that it allows the algorithm to accumulate wear discretely along the circumference of the wheel profile, which allows the simulation of the irregular wheel wear around the circumference. This should allow the algorithm to treat the prediction of out-of-round wear although this was not discussed by Zobory (1997).

1.2.3.1.3 Uncertainty related to the wear coefficients

Ramalho (2015) explained that the dependency of the wear coefficient on the local contact conditions is the main source of inaccuracy when applying Archard's wear model in numerical calculations. Ramalho (2015) proposed the use of weighting factors related to the contact pressure, sliding speed and creep ratio to determine the wear coefficient of the Archard wear model. However, these weighting factors are only valid for the materials that were tested and new relationships should be determined from tests for other materials.

Wear coefficients used in the wear algorithm are often dependent on the material properties of the interacting wheels and rails. Zobory (1997) noted that, similar to other wear prediction algorithms, the wear coefficient applied in his study depended on the material properties as well as the value of the energy density flow. The energy density flow was used to distinguish between mild and severe wear and to adjust the wear coefficient accordingly. Pombo et al. (2011) noted that wear functions of both the British Rail Research (BRR) and the University of Sheffield (USFD) are limited to the materials used to develop them. Jendel (2002) proposed the use of a wear map that defines the value of the wear coefficient as a function of the contact pressure and the slip velocity. According to Pombo et al. (2011), this wear function is independent of the material and therefore more general, but introduces approximations in the method. Extensive material testing is required to determine the wear coefficients needed for accurate wear predictions. The test data pertaining to wear coefficients are not freely available and are quite limited, since not all varieties of wheel and rail materials have been tested.

1.2.3.2 Load collective design considerations

Fröhling (2002) discussed the importance of defining a representative load collective during wheel wear analysis. According to Fröhling (2002), the load collective generally includes a representation of the track layout, traffic conditions, wheel-rail profiles, coefficient of friction, track irregularities, as well as vehicle braking and traction.

The load collective defined by Fröhling (2002) had a track layout representing the South African coal and iron ore line as well as the Swedish iron ore line. The traffic conditions were simplified since the wagons were ring-fenced, thus there was no need to consider different routes. The wheel and rail profiles considered in this load collective had designs developed in South Africa. The coefficient of friction was constant and equal to 0.4. Track irregularities of a single representative section of track were used. Track symmetry was assumed and thus only curves in one direction could be used during simulation. In a similar approach, Nia et al. (2015) assumed symmetry in the wear of the inner and outer wheel within a curve. It was assumed that due to symmetry the wheel wear on the inner and outer wheel would be the same and the same amount and location of wear was accumulated on both these wheel profiles within a curve.

Jendel (2002) addressed the design of the load collective in detail. Key concepts implemented during the load collective design were mentioned. The load collective discussed by Jendel (2002) included macro track geometry, track irregularities, measured rail profiles and the coefficient of friction. Data for the wear calculation were sampled every two to three metres. An average coefficient of friction was used. The track geometry was described by a discretisation of the curves in radius intervals. A representative curve with constant radius and super-elevation was used to present the geometry of all the curves within an interval. Curves with a radius above 3000 m were considered as straight track. Track irregularities were applied to spread the wear. Various measured rail profiles were included to account for their contributions, with more than one measured rail profile used for curve radii below 800 to 1000 m. Jendel and Berg (2002) stressed the importance of using worn rail profiles representative of the actual network during wear simulations.

The coefficient of friction is always an important consideration when predicting wheel and rail wear because it will influence the wear amount. Jendel and Berg (2002) used a constant coefficient of friction of 0.3 and it was noted that it is better to model lubrication by changing the wear coefficient. Enblom and Berg (2005) proposed how disc braking and lubrication can be included in wheel wear simulations based on the work of Jendel (2002).

The accurate design of the load collective is extremely important for wheel wear predictions. Nevertheless, there are many simplifying assumptions that can be made during the load collective design to ensure faster solutions times while maintaining accurate wear predictions.

1.2.3.3 VI-Rail's wear model

The algorithm used by the VI-Rail's (2014) wear toolkit to predict wheel and rail wear is based on the proportionality between the worn material and the energy dissipated during contact. The equation applied to calculate the wear depth (δ) is presented in equation (1-15) (VI-grade, 2014).

$$\delta = \frac{f\left(T_x\gamma_x + T_y\gamma_y\right)L}{A\rho} \tag{1-15}$$

This algorithm only distinguishes between mild and severe wear. The wear coefficient (f) is based on work performed by Linder (Chudzikiewicz et al., 1998). It is defined as either 4.5×10^{-7} g/Nm for mild or 1.25×10^{-6} g/Nm for severe wear. These values were originally tuned by Linder to fit polygonal wheel wear predictions. The wear coefficients are therefore specific to the material and analysis of Linder and may not be applicable in general. The transition from the mild to the severe wear regime is made when equation (1-16) exceeds 4×10^{6} W/m^2 (VI-grade, 2014).

$$P_d = \frac{\left(T_x\gamma_x + T_y\gamma_y\right)v_o}{A} \tag{1-16}$$

The current study focusses on wheel wear to understand the progression of wheel wear and factors influencing concentrated hollow wear. Thus, with the wear toolkit within VI-Rail and a load collective definition, it is possible to predict wear for a certain wagon type, running over a specified track until a wear limit or a predefined running distance has been reached. There are some uncertainties regarding the wear coefficients, because they were tuned for the study performed by Linder. Their generality is questioned and thus only a relative, quantitative comparison of wear can be made.

1.2.4 The complex relationship and trade-off between wear and RCF initiation

There is a strong relationship between RCF crack growth and wear on the rail. Rail life can be influenced by either of these damage mechanisms. Ekberg et al. (2014) discussed the interaction between wear and RCF. Excessive wear will cause premature rail replacement, whereas RCF cracks may branch and unite with one another, leading to a rail break. In rail life optimisation there is thus a trade-off between low material removal leading to more fatigue crack growth and excessive material removal reducing the rail life due to wear.

Kimura et al. (2002) analysed and discussed the elemental process that affects wear and RCF during rolling contact. The wear process is treated in more detail and it is shown that wear depends on the creep between the two surfaces. It is shown that the wear rate is a function of the normal load and creep, and generally increases as both these variables increase. According to the shakedown theory of Johnson (1989), RCF crack initiation and growth is dependent on the normal load and the utilised traction

coefficient. The utilised traction coefficient can be related to creep and it is evident that the elemental processes causing wear and RCF are similar.

According to Ekberg (2009), wear and surface-initiated RCF can be seen as the manifestation of the same phenomenon. Both these damage mechanisms are caused by high frictional stresses in the wheel-rail interface. Tunna et al. (2007) discussed the similarity between the mechanisms causing RCF initiation and delamination wear. In both mechanisms, micro-cracks between the ferrite lamellae are caused by repeated plastic deformation in the surface and subsurface layers of the driven surface. This shows that as one damage mechanism dominates, the other is suppressed.

Johnson (1989) stated that when pure rolling is present, the wear rates are very low. Wear on tangent track is very low and the most significant wear occurs on the high leg of sharp curves due to flange contact. When the contact condition changes to high-friction, the wear rate increases and enough surface material is worn away not to cause any fatigue crack growth. If, however, the wear is controlled by lubrication, the surface layer is not removed regularly and it is possible to cause pitting fatigue. Fletcher et al. (2009) elaborated on this trade-off between wear and fatigue crack growth. It was shown that for small cracks the wheel is able to wear the rail fast enough, resulting in a negative net crack growth rate. This means that a crack will reduce in size and no sustained crack growth occurs. However, for larger cracks the opposite is true.

Dikshit et al. (1991) carried out a site trial to study the development of RCF cracks in head-hardened rails within a curve. Samples were taken from the rail at various stages of its life to study the development of these cracks. The maximum crack depth and crack density were studied from different samples. The rail samples showed that RCF cracks were present very early in the life of the rail. It was noted that the number of short cracks reduced, while the number of long cracks increased as more traffic passed over the rails. It was suggested that some of the short cracks are worn away and the other short cracks continued to propagate and form long cracks. The long cracks will continue their propagation. Should the depth of the long cracks exceed the depth of material removed by grinding, it could lead to spalling of the rail surface. This observation was affirmed by Fletcher et al. (2009) who presented the growth rate for larger cracks as a non-linear increasing relationship to the crack size. This relationship established that when a crack becomes large enough to sustain crack growth, the growth rate will increase and a small crack can quickly become larger.

The $T\gamma$ damage model proposed by Burstow (2003 and 2004) considered the interaction between RCF and wear in a single damage model. Bevan et al. (2013) developed a tool that is capable of predicting the deterioration rates of the wheel tread with respect to wear and RCF. This model included a reduction in the predicted RCF damage due to wear and therefore tried to model the interaction between the two competing damage mechanisms. In a similar approach, Nia et al. (2015) reduced the effect of RCF initiation by considering the fact that high dissipation of energy in the contact patch (high $T\gamma$ values) will wear the initiated cracks away.

The wear and RCF relationship has two facets of note. Firstly, should wear be the dominant damage mechanism, the RCF cracks will be truncated and reduce in length.

Thus, the likelihood of RCF initiation and sustained crack growth is reduced. However, maintenance and replacements of wheels and rails will increase due to wear. Secondly, wear changes the wheel-rail contact positions and areas, which can further lead to increased normal and tangential stresses. This effect was mentioned by Ekberg (2009) and was linked to the wheel not wearing uniformly. The progression of non-uniform wear has a significant impact on the dynamic response of the vehicle and prevailing contact conditions, which can lead to acceleration in crack growth. During the trials performed by Dikshit et al. (1991) it was noted that adverse worn wheel profile contact with new or as-ground rail profiles are prolonged due to the higher wear resistance of head-hardened rails. The rails retain their profile shape much longer due to their higher wear resistance. Wheel wear causing adverse contact conditions together with the high wear resistance of head-hardened rails have the potential to worsen rail RCF.

The complex interaction and relationship between wear and RCF gave rise to the concept of a "magic wear rate". Zarembski (2005) discussed the magic wear rate and the relationship between wear and RCF. When the magic wear rate is achieved, wear will balance the growth of RCF cracks and no net crack growth will occur. This balance is usually achieved through rail grinding to increase the rail wear rate. Enblom (2009) discussed the effect of lubrication on the wear rate and mentions that lubrication may be applied to tune the wear rate and reduce RCF through controlled wear. Olofsson et al. (2013) discussed the application of various types of lubrication or friction controls, including slip control, low coefficient friction (LCF), high positive friction (HPF) and very high positive friction (VHPF) modifiers. These measures can be applied to manage and balance wear and RCF.

Rail grinding is one method that can be applied to reduce the growth and severity of RCF by managing the wear rate to approach the magic wear rate. Alternative rail steels are being developed that are RCF and/or wear resistant (Tunna et al., 2007; Olofsson et al., 2013). Although new rail steels are pursued to reduce the initiation and growth of RCF cracks, rail grinding is still one of the best remedies to treat cracks once they have initiated.

1.2.4.1 Rail grinding

The use of rail grinding to remove defects from the surface of the railhead was introduced in the early 20th century (Zarembski, 2005). Since the late 1930s, rail grinding was primarily used to eliminate rail surface defects such as corrugations, engine burns and batter at the rail ends. The removal of surface defects was applied for over 50 years and helped to avoid costly rail replacements. In the 1970s and 1980s, the use of rail grinding was extended to control the transverse rail profile and thus manage the contact conditions between the wheel and the rail. This concept found its origins in the mining railroads of Western Australia. This type of grinding was known as profile grinding, which developed into the modern concept of preventative rail grinding. The use of preventative rail grinding has numerous advantages. It improves the wheel-rail dynamic interaction and reduces the wheel-rail forces in both the horizontal and vertical planes. This in turn improves the rail life as it reduces damage to both the track and the rolling stock and lowers noise levels. Zarembski (2005) provided an overview of rail grinding and discussed its application.

Rail grinding is widely used and is one of the most effective treatment methods of surface-initiated RCF. Rail grinding is also used to reduce wear and plastic flow, which widens the contact band (Grassie, 2009). Rail grinding is a safety-critical maintenance activity, since rail breaks can develop from RCF cracks (Grassie, 2009). Fletcher et al. (2009) mentioned that rail grinding aims at managing the crack size to sustain lower crack growth rates or even maintain the crack size to sustain shear fracture mode II crack growth (linear elastic fracture mechanics mode II). Thus, the crack will remain in the initiation or plastic deformation phase.

The three different types of rail profile grinding strategies have been defined by Zarembski (2005). These strategies are used to control of gauge wear and lateral forces, control of corrugations and control of gauge corner fatigue. Additionally many railways apply grinding to control rolling noise, especially on commuter networks. Unfortunately, grinding to control wear, and grinding to control fatigue have contradictory requirements. When the profile is ground to control wear, the gauge corner is ground to improve steering of the wheelsets. This lessens the chances of flange contact and resulting side wear. However, when the profile is ground to control fatigue, relief is ground on the gauge corner (ground lower than the target profile) to shift the contact point more towards the centre of the railhead. This decreases the steering ability of wheelsets and leads to a two-point contact situation. With two-point contact, flange contact is predominant and more side wear is present.

Stow et al. (2011) examined the effectiveness of controlling the rail shape through grinding and lubrication to reduce RCF. They suggested that greater gauge shoulder relief could be ground to increase the gap between the gauge corner and the wheel. The aim of this grinding action is to reduce gauge corner contact. An anti-RCF wheel profile, such as the P12 wheel profile, which increases the gap to the rail gauge corner further reduces the probability of gauge corner contact. Such wheel profiles could be applied in addition to rail gauge corner relief.

Zarembski (2005), on the other hand, mentioned that another possible solution to the contradictory requirements of wear and fatigue control is to use conformal contacting profiles. These profiles have the added advantage that they promote steering in curves and are able to reduce the wheel-rail contact forces in the high stress environments.

Zarembski (2005) stated that more emphasis is placed on preventative grinding than on corrective grinding. With preventative grinding, the intervals between grinding interventions are shorter and most of the defects are removed, although only a small amount of material is removed. With corrective grinding, however, the intervals between interventions are long and heavy metal removal is required to obtain the required profile.

The intervals between grinding are one of the focus areas explored to achieve the magic wear rate. Guidelines that have been successfully used by many heavy haul railways are given by the International Heavy Haul Association (2001). Magel and Kalousek (2002) mentioned that preventive grinding in heavy haul operations is typically applied in intervals between 10 and 17 MGT.

Evans and Iwnicki (2002) remarked that grinding is a costly exercise and excessive grinding may lead to short rail lives. Magel and Kalousek (2002) stated that although grinding can provide many benefits, it does not provide a cure for all track damage. It should be applied in conjunction with good maintenance practices on both the track and rolling stock. For this reason, other means of addressing the RCF problem should be sought for a more cost-effective long-term solution. The trade-off between wear and RCF will be one of the focus areas of this study to change the worn shape of the wheel and to reduce the initiation of RCF. This change in the worn shape of the wheel and reduction in RCF initiation will influence the magic wear rate. This could reduce the need for excessive grinding, ultimately reducing rail maintenance costs and replacements.

1.2.5 Wheel-rail interface optimisation to combat RCF and/or wear

Damage in the wheel-rail interface, in the form of wear and RCF, has been discussed and the effect such damage has on the economics of railways has been shown to be significant. Enblom (2009) argued that the cost of maintaining the wheel-rail interface accounts for a major share of the railway's maintenance cost. Greater cost saving can be made should the prediction models of the deterioration mechanisms produce better estimates. Such models can be applied in the optimisation of the wheel-rail system. The predictive models for wear and RCF have been covered in paragraphs 1.2.2 and 1.2.3. The following discussion will deal with the optimisation of the wheel-rail interface to reduce these damage mechanisms and thus reduce wheel-rail related maintenance costs.

Braghin et al. (2009) mainly discussed wear, but since the elemental processes governing both wear and rolling contact fatigue are similar (Kimura et al., 2002), their discussion can be extended to include RCF. The amount of wheel and/or rail damage in the form of wear and RCF is influenced by vehicle dynamics, contact mechanics and tribology within the wheel-rail interface as shown in Figure 1-11. The damage within the wheel-rail interface can be reduced by influencing or changing any one of these interacting sub-processes. Magel and Kalousek (2002) listed and discussed six performance criteria that the optimisation of the wheel-rail interface should cover. Damage can further be influenced by changing the dynamic response of the vehicle and therefore altering the contact forces, creepages, wheel-rail contact positions and increasing stability. The influence of contact mechanics on wear and RCF is determined by the local contact conditions (contact patch size, contact angle, contact position, etc.) and the normal and tangential stresses. In their discussion of wear, Magel and Kalousek (2002) mentioned that the optimisation of the interface could be accomplished by reducing traction by means of friction control. This involves measures in the form of slip control, low coefficient friction (LCF), high positive friction (HPF) and very high positive friction (VHPF) modifiers. These friction modifiers, together with their area of application, were discussed by Olofsson et al. (2013). RCF can further be limited, if the amplitude and frequency of contact at a certain point on the wheel or rail profile can be limited (Magel and Kalousek, 2002).

One of the ways in which RCF and wear can be countered from a material's perspective is using RCF- and/or wear-resistant materials. Banitic steels provide an alternative to

pearlitic steels and they have a lower carbon content. A ductile material is produced through rapid cooling that is said to be more resistant to RCF and shelling, but due to the lower carbon content, it is expected to have higher wear rates than pearlitic steels (Tunna et al., 2007). Rail hardness has a definite influence on the wear rate. Increasing the hardness can reduce the wear rate (Olofsson et al., 2013). The probability of initiating RCF cracks can be reduced by increasing the resistance of the material to yielding (yield strength of the material in shear or k_e), controlling the contact geometry (the size of the Hertzian contact patch) by means of rail grinding, surface coating, rim quenching and compressive residual stresses within the material (Ekberg and Kabo, 2002).

A model called pummelling was created by Magel and Kalousek (2002) to evaluate the performance of rail profiles when loaded by a large number of new and worn wheel profiles. This model was developed to optimise the contacting wheel and rail profiles to reduce wear and increase the resistance to RCF. This optimisation strategy should be applied in addition to the usage of lubrication, improved materials and new bogie types to realise a greater resistance to damage within the wheel-rail interface. The pummelling model can be used to study and change the contact point distributions to spread the severity and frequency of contact to many different locations on the running surfaces. This will ensure that favourable contact geometries are maintained and that the damage accumulation per contact point is reduced. Pummelling can be applied through selective gauge widening and/or narrowing.

Although these measures could all be applied to optimise the wheel-rail interface, the aim of the current study is focussed on the optimisation of the wheel profile, rail profile and/or vehicle suspension design to minimise damage.

1.2.5.1 Wheel and/or rail profile optimisations

The optimisation of wheel and/or rail profiles has been the interest of railway engineers since the dawn of railways. Flanges were used to steer the wheels through a curve. Coning was later introduced to reduce flange contact and improve steering of the wheelset around a curve. Coning led to hunting and vehicle instability, which railway engineers were trying to reduce through bogie designs. Iwnicki (2006) discussed the development of the wheelset, the accompanying kinematics and dynamics and the development of bogies leading to the analysis of vehicle-track interaction. Fröhling (2003) provided an overview of the bogie development and wheel-rail interaction experience gained from two South African export lines. This overview was followed by a discussion of wheel profile development in South Africa. The design of wheel and/or rail profiles to optimise their interaction is illustrated by describing the evolution of the wheel profile. The wheel profile used in South Africa started from coned profiles, moved to geometries that are more complex and ended at a conformal wheel profile design. Pearce (1996) described that the design of new wheel profiles had been a black art where a lot of engineering experience was applied in the design and lengthy trials were used to evaluate the performance of the new design. The prediction of wheel profile wear has provided an aid in the design of new profiles, which allows the evaluation of their performance over a shorter period.
There are many reasons that drive railways to optimise the wheel-rail interface through redesign or maintenance. Some of the main reasons considered are maintaining a low to

medium equivalent conicity through the lifetime of the wheel, increasing safety against derailment, minimising wear and RCF initiation on either wheel or rail or both (Grassie, 2009). Jendel and Berg (2002) highlighted that a tool capable of predicting wheel profile can be used to design a wheel profile for specific purposes such as maintaining its equivalent conicity throughout its lifetime.

Pearce (1996) highlighted the necessity to optimise contacting profiles to maintain the equivalent conicity in the low to medium range (low conicity when $\lambda < 0.15$ and medium conicity when $0.15 < \lambda < 0.3$). It is difficult to design bogies that provide sufficient stability when the equivalent conicity becomes high. The equivalent conicity range of a worn wheel profile is dependent on the initial equivalent conicity of the wheel profile and the vehicle type. The contacting profiles should therefore be designed with an equivalent conicity value that is initially low or medium.

The minimum curve radius that a vehicle can negotiate without making flange contact is inversely proportionate to the equivalent conicity. This means that the higher the equivalent conicity becomes, the smaller the minimum curve radius will be that allows curving without flange contact. This trade-off between increased curving performance and stability should be considered carefully when designing wheel or rail profiles (Bruni and Braghin, 2009).

Conicity together with profile wear were discussed by Pearce (1996). It was shown that wear that is concentrated in the centre of the profile leads to high conicities. Once flange wear is initiated, the conicity drops. When the wear is spread across the profile, it results in more stable conicities. Sawley et al. (2005) investigated the influence of hollow-worn wheel profiles on the stability of vehicles on a straight track. This was done by means of simulations of a vehicle with varying levels of hollow-worn wheel profiles running on the same track. The lateral axle displacement and lateral car body acceleration were evaluated as measures of stability. The wheel profiles studied did not show conventional hunting behaviour and it was concluded that hollow wear is not the sole indicator of vehicle stability. However, the instability caused by the hollow-worn wheel profiles was significant and the lateral position of the wheel switched from the left most extreme to the right most extreme within a short distance.

The safety against derailment is another important factor to consider when designing a wheel profile. Pearce (1996) stated that new wheel profile designs can increase their safety against derailment by designing their flange angle between 68° and 70°. An improvement of safety against derailment was investigated by Shevtsov (2008) during the optimisation of a tram wheel profile. The safety against derailment was ensured by optimising the flange angle and allowing it to vary between 65° and 70°.

There are generally two schools of thought when designing or maintaining wheel and rail profiles to reduce RCF initiation. The first aims at eliminating contact at the locations where RCF is generally observed by removing material at these locations. This boils down to the fact that, should there be no material to contact, there should be no RCF initiation. This school of thought was mentioned by Stow et al. (2011) in the design of the P12 wheel profile and applied by Shevtsov (2008) and Shevtsov et al. (2008) to wheel profile design aimed at reducing RCF. Schöch (2011) suggested that many

railways apply this strategy to rail profile maintenance. So-called anti-head check rail profiles are becoming the norm in Europe. These profiles have gauge corner relief up to 0.6 mm below the original rail profile (Evans and Iwnicki, 2002; Schöch, 2011). Evans and Iwnicki (2002) suggested a larger rail inclination to ensure even more gauge corner relief. Such anti-head check rail and/or wheel profiles have been used in Sweden (Persson et al., 2010) and the United Kingdom (Evans and Iwnicki, 2002; Iwnicki, 2009; Stow et al., 2011). These studies showed that anti-head check profiles could effectively reduce RCF initiation and growth. Stow et al. (2011) found that RCF damage returned to sites with anti-head check rail profiles after a moderate amount of tonnage, which was less than the grinding interval. Worn wheel profiles were examined and it was found that all these profiles made contact with the designed and measured anti-head check profiles. Thus, the intention of avoiding contact at the gauge corner is negated.

The trade-off related to this strategy to reduce RCF, should be considered carefully. By applying such rail profiles, the RCF could possibly be reduced, but at the same time, it causes a reduction in conicity and wheelset steering. This reduction in conicity leads to the wheel steering by flanging, resulting in two-point contact (Figure 1-4(b)). It is well known that such anti-head check rail profiles result in two-point contact, with lubrication being applied to reduce the rail side wear and wheel flange wear (Evans and Iwnicki, 2002; Stow et al., 2011).

Wu (2006) investigated a redesign of a wheel profile that was promoting severe two-point contact. Worn wheel profiles indicated an increase in the flange root to rail gauge corner gap, thus becoming less conformal and promoting two-point contact. The lateral forces generated during curving were high due to the two-point contact conditions. Wu (2006) argued that such two-point contact would result in longitudinal forces at the two points of contact that would oppose one another. These forces reduce the steering moment and result in higher angles of attack and lateral forces. The lateral force and angle of attack substantially reduce when a single point of contact is present. A new wheel profile design was proposed to reduce two-point contact and reduce both wear and RCF. The negative impacts that two-point contact has on the steering of a bogie, the lateral forces and the rolling resistance are evident from the study performed by Wu (2006).

Wu's (2006) study introduces the second school of thought. Single point conformal contact could be used to increase the steering ability of a wheelset, lower lateral forces and reduce curving resistance. Although such contact conditions result in the lowest lateral forces and rolling resistance, it was noted that a wheel profile resulting in single point contact might promote RCF development or produce a high wear rate. Therein lies a second trade-off between increased curving performance with a reduction in lateral forces and potentially increasing wear and RCF.

A bogie such as Scheffel's self-steering bogie (1974, 1978), together with a wheel and rail profile promoting single point conformal contact, may avoid this trade-off. Enblom (2009) discussed profile design to reduce the wear of wheels and rails. It was reported that the aim of many such designs were single-point contact and increased conformity of the contacting profiles. Wu (2006) and Fröhling (2003) argued that conformal contact reduces the risk of RCF development.

The idea of using single-point conformal contacting wheel-rail pairs was confirmed by the case studies presented by Kalousek (2005). The concept of perfect curving of a bogie was discussed where the bogie exploits the steering ability of the wheel to reduce wheel flange and rail side wear. Under perfect curving conditions, the steering forces are minimised since the wheel is allowed to approach its pure rolling position. Kalousek (2005) mentioned that experience in the UK has shown that perfect curving of a bogie will result in the reduction of wear and RCF. A reduction in the concavity of worn wheels was suggested as one of the best ways of decreasing wheel-rail damage while improving curving, ride quality of bogies and the lifespans of wheel and rails. Kalousek (2005) listed the benefits of moving from a concave wear pattern to a semi-concave wear pattern. Three of the greatest benefits of the semi-concave wear pattern were highlighted as the reduction of wheel flange and rail side wear, a reduction in the spread in rolling radius difference across the wheel fleet and a reduction in the rate of rail profile change, which leads to an extension of the rail grinding intervals.

Polach (2011) mentioned that during the design of a new wheel profile, the contact point for nominal parameters, contact angle, the conformity of profiles, equivalent conicity and spreading of the contact, should be considered. Magel and Kalousek (2002) listed general criteria that could be applied to achieve optimised wheel and rail profiles. They are as follows:

- Design for low contact stresses and avoid contact stresses above 3 times the material's yield strength in cyclic shear.
- Avoid closely conformal contact where the transverse width of the contact patch is more than 20 mm.
- Design the rolling radius difference (Δr) of the profiles appropriately for the curves (see equation (1-4)).
- Ensure that the equivalent conicity is within the conicity envelope of the bogie.
- Ensure that the contact points are distributed well across the tread to have many contact points, which will spread the wear (reiterated by Shevtsov, 2008).

Zobory (1997) derived a formulation that can be used to optimise wheel profiles. This formulation is aimed at wear on the profile, reproducing the original profile. It was also mentioned that the optimum wear of the profile could be achieved by manipulating the wear coefficients at different locations along the profile to increase wear resistance in critical areas. The change in wear coefficients can be achieved by heat treatment and alloying. The wear experienced by such a profile will once again maintain the shape of the original profile. These optimisations are aimed at maximising the service life or expected mileage of wheels.

Leary et al. (1991) designed wheel profiles based on two approaches. The first was an averaging of measured worn wheel profiles and the second was based on the expansion of the rail profile to ensure single-point contact. The main aims were to produce a wheel profile that would reduce wheel and rail wear, increase safety against derailment, maintain stable performance at normal train speeds and have reasonable contact stresses. The wheel profile produced by averaging the worn wheel profile produced the best results and proved to reduce the initial flange wear rate. This profile also produced the lowest contact stresses of the candidate profiles due to its conformal shape.

Shevtsov (2008) described an optimisation method that can be applied to design new wheel and/or rail profiles using the rolling radius difference (RRD) function. This method is less expensive than optimising the wheel and/or rail profile using vehicle dynamics simulations. It was mentioned that design of new wheel and/or rail profiles could start with a similar method to obtain desired wheelset kinematics and contact conditions. This can be followed by fine-tuning the profiles with an optimisation using vehicle dynamics simulations. The disadvantages to this approach are that precise vehicle and track models are required as well as the fact that the method is extremely computationally expensive. The advantage, of course, is that excellent wheel and/or profiles are obtained that are designed specifically for the prevailing vehicle and track conditions.

Shevtsov (2008) described the procedure followed to optimise the wheel-rail interface in detail. The process is started by evaluating the wheel and/or rail profiles for any changes that may have occurred. In other words, the profiles are evaluated to ascertain whether the wheel or rail profiles changed due to new wheel profile designs or rail replacements. The current wheelset kinematics and wheel-rail contact positions are subsequently studied to determine the cause of the poor contact conditions, wear and/or RCF. Proposed changes are made to the RRD function to eliminate or reduce the poor contact conditions based on experience. This often involves a change in wheel profile and RRD function to allow a better spread of wheel-rail contact positions. A new target or limiting RRD function is defined. The area of the wheel profile that is most relevant for any improvements is chosen and the wheel is optimised until the target RRD function is obtained. The contact conditions and RRD function is then evaluated and the proposed change in wheel profile is studied using multibody dynamics simulations. The newly developed wheel profile is evaluated for its stability on straight track, curving ability as well as the wear number as it negotiates the curve. This check is performed to determine whether an improvement is achieved relative to the initial wheel profile. It is very important to note that the proposed design process allows for the design of new wheel profiles based on a priori defined contact properties. Therefore, some wheel-rail experience is still required to define new contact properties before optimising the wheel profile.

Shevtsov (2008) applied this procedure to the wheel profile design of tram (Shevtsov et al., 2005), metro train and passenger service train wheelsets (Shevtsov et al., 2008). According to Shevtsov et al. (2005), it is less complex and quite possible to obtain an optimal set of wheel and rail profiles when dealing with a closed or ring-fenced railway system. This type of railway system lends itself to optimisation as the bulk of the rolling stock carried by the railway line is of one type. This type of closed railway operation is usually seen in heavy haul operations.

In two of the three case studies presented by Kalousek (2005), a wheel profile change was used to spread the wheel wear across its tread, changing the concavity of the wheel wear resulting in an improvement of wheel flange and rail side wear and running stability. The wheel profile modifications were made to suit the track curvature and bogie suspension characteristics. In all three case studies, rail profile changes were suggested, with more than one rail profile design being ground on tangent track or over the complete track.

Polach (2011) developed a wheel profile design procedure intended to spread tread wear. The profiles generated with this procedure are suited to high power traction vehicles and vehicles running on relatively straight track. This procedure can be used to design a wheel profile based on a chosen contact distribution. It starts with a known rail profile shape and defining wheel contact points based on the wheelset's lateral displacement. These points are mapped to the rail profile. The gradient of the tangent to the wheel and rail should be the same at the contact point. This assumption is used to determine the vertical coordinate of the wheel profile at the various contact points on the one wheel. The rolling radius difference is employed to calculate the vertical coordinates of the opposite wheel. This procedure is repeated for the opposite wheel since symmetry applies. The design procedure was applied to a newly generated wheel profile. The wear performance of this newly designed wheel profile was compared to three other profiles. The new profile showed an increased contact area and a significant reduction in the maximum contact stress. A crude approximation to tread wear was used to evaluate the wear performance of the wheel profile. Based on this approximation, the new profile proved to spread the tread wear widely.

Nia et al. (2015) reported that the wheel life experienced on the locomotives operating on the Swedish iron ore line is very low due to RCF damage. The average running distance between reprofiling was around 40 000 km. The operator decided to change the wheel profile in an effort to reduce the creep forces, ultimately reducing the initiation of RCF. Two optimised wheel profiles had previously been generated through optimisation with a genetic algorithm. These optimised profiles had not been analysed for their long-term wear and RCF behaviour. Nia et al. (2015) analysed these wheel profiles to determine their long-term behaviour to ensure that the optimised profile will indeed maintain a low wear rate and reduced risk of RCF initiation.

Dede et al. (2015) described an optimal wheel profile design procedure. The procedure takes the layout of the track network, the longitudinal primary stiffness of the bogie, different loading scenarios, different friction conditions and gauge width into account. The design procedure is based on the calculation of an optimal rolling radius difference that produces the lowest wear rate. A wheel profile is designed to guarantee this optimal rolling radius difference while maintaining a single point of contact, which is spread across the wheel tread. The procedure tries to maintain a consistent pressure at the contact point across the wheel tread and avoids too large contact areas at the flange root. The optimal wheel profile design is finally checked for its running stability. This optimal design procedure produces a conformal wheel profile that is able to make contact close to the flange root. A case study was presented where the design procedure was applied to improve the wear behaviour experienced in-service.

Shevtsov (2008) mentioned that it is of more value to optimise the wheel profile to fit existing rail profiles as wheels are cheaper to replace than rails and they are reprofiled more often. Even so, it is not impossible to optimise the rail profile. To this end, Smallwood et al. (1991) and Persson et al. (2010) presented an optimisation applied to the rail profile. If the rail profile is optimised, the amount of material that will have to be removed in order to achieve a new rail profile must be considered (Smallwood et al.,

1991). Grinding will have to be used to achieve the optimised rail profile and will be less accurate than reprofiling a wheel.

Interestingly, the final optimised rail profile found by Persson et al. (2010) had a raised gauge corner with respect to the original target and the gauge corner relief profile. They originally recommended that a gauge corner relief profile should be ground to reduce RCF and then left to wear towards the optimised rail profile without further grinding to maintain the gauge corner relief profile.

1.2.5.2 Vehicle suspension design

Wheel and/or rail damage, in the form of wear and RCF, are influenced by vehicle dynamics as illustrated in Figure 1-11. Bogie design is one of the main contributors to the dynamic response of the vehicle. The conventional three-piece freight bogie design had been discussed by Orlova and Boronenko (see Iwnicki, 2006). This three-piece bogie consists of two wheelsets, two side frames and a bolster. These components are connected through bearings, spring nests and friction wedges, providing the necessary damping. These bogie types are known for their warping or losenging in curves. Wheelsets within such a bogie cannot adopt a radial position in a curve and large angles of attack are generated. Scheffel (1974) mentioned that the flange force increases with wheel load and angle of attack. The angle of attack can be influenced by improving the steering ability of the wheelsets within a bogie. This can be achieved by allowing pure rolling of the wheelset in curved track through unconstrained yaw of the wheelset.

Enblom (2009) mentioned that changes in bogie suspension received great attention during the 1980s. These changes were made to take advantage of the steering ability of an unconstrained wheelset resulting in better curving and improved wear performance. Bogie development was initiated within South Africa during the 1970s in an effort to maintain the worn shape and equivalent conicity of a wheelset over longer distances (Fröhling, 2002). This newly designed bogie can reduce the need for flange steering, minimises lateral creep and improves hunting stability. This ultimately results in reduced tread and flange wear, which increases the interval between wheel reprofilings. Fröhling (2003) provided an overview over the history of the development of the self-steering three-piece bogie.

Scheffel (1976) identified the need to improve freight bogies to optimise the wear performance within the wheel-rail interface. Scheffel (1976) analysed the effect that wheel wear had on the effective or equivalent conicity. It was noted that conventional bogies do not allow wheels to follow curved or misaligned track, but must creep and slip to remain on track. Conventional three-piece bogies lead to hollow wear and cause the wheel profile to wear conformal to the rail. This conformity is essentially a match between the wheel and rail radius, which increases the effective conicity (see equation (1-3)). The increase in effective conicity has an adverse effect on the hunting stability of the conventional three-piece bogie. Sawley et al. (2005) investigated such hunting instabilities and defined limits through which it can be detected.

It could be argued that a bogie design that could remain stable with conformal wheel profiles would reduce contact stresses and will have a positive effect on the wheel wear

rate. Conformal wheel profiles allow the wheel contact point to move over a wider band, spreading the wear over the tread surface. Wear-induced wheel profile change is reduced by spreading the wear across the tread. Scheffel (1976) argued that the hunting stability could be maintained for longer distances if the profile does not change much due to wear. This was seen as the solution to the hunting problem.

Scheffel (1976) showed that conventional bogie designs with conformal-worn profiled treads still resulted in high wheel tread and flange wear. This high wear rate eventually led to unacceptable hunting oscillations above 68 km/h. This was considered as proof that the suspension of the bogie needed to be changed to allow improved curving ability to better retain the original wheel profile shape and reduce hunting instability even with worn wheels.

Scheffel (1974) discussed two types of vehicle suspensions that are capable of resolving the conflicting requirements between hunting stability and curving ability in an uncompromising manner. Scheffel (1974) focused on the performance of the diagonally stabilised suspension arrangement. This diagonally stabilised bogie allowed better curving, but still maintained high stability on straight track. This was achieved by allowing low bending stiffness for adequate curving ability and a high shear stiffness for stability within the bogie (Fröhling, 2003). Rubber sandwiches with very low shear stiffness ensured a soft wheelset suspension both laterally and in yaw. The wheelsets remained slightly understeered in the curves but curving was entirely achieved by creep forces while maintaining hunting stability (Scheffel, 1974). A conventional three-piece bogie design was adopted as the basic design. This conventional design allows for low manufacturing costs, low weight and good load equalisation.

Test results of this suspension arrangement at different speeds and wagonloads were evaluated by Scheffel (1974). It was shown that the vehicle remains stable at various speeds and loading conditions. Comparisons were made to the stability of a conventional three-piece bogie and improved stability was proven. The effect of wheelset conicity change on the stability of the bogie design was examined and it was shown that a change in conicity, whether by design or due to natural wheel wear, had a significant effect on hunting stability of the new design bogie. Scheffel (1974) described that relatively high stiffness of the diagonal members coupling the wheelsets was required to suppress the hunting instability caused by the rotational oscillation of the bogie frame. This diagonal stiffness had been tuned to obtain optimal stability. This tuning is lost when there are considerable changes in the wheel tread conicity. Both an increase and decrease in the equivalent conicity of the wheelset will cause a loss of this tuning. The new bogie design should therefore be tuned to optimise stability at a specific conicity. This conicity should ideally be maintained throughout the life of the wheel to maintain hunting stability.

In addition to the increased stability provided by the diagonally stabilised suspension arrangement or self-steering design, the bogie offers a flexible yaw constraint to the wheelsets. This flexible yaw constraint allows the wheelsets to approach a pure rolling position in curved track. Scheffel (1974) stated that an unconstrained wheelset with a profiled wheel tread is never free from forces in the position required for pure rolling on a curved track. The gravitational suspension stiffness becomes significant and exerts a force on the wheelset due to the profiled nature of the tread. Therefore, pure rolling is

impossible when profiled wheels are used due to the influence of the gravitational suspension stiffness. Although the Scheffel design takes advantage of the steering ability of an unconstrained wheelset, the forces present due to the gravitational suspension stiffness will inevitably lead to wheel tread wear. However, Fröhling (2003) noted that flange wear was virtually eliminated by the self-steering bogie.

Enblom (2009) reported that Specht (1987) had investigated the wear performance of the Y25, Deutsche Bahn (DB) steering design and the Scheffel design bogies. The two steering designs indicated similar wear rates. Scheffel (1978) made a comparison between the self-steering bogie, a radial axle bogie and a rigid frame bogie. The self-steering bogie proved to have superior curving ability with reduced flange forces and energy dissipated by slip or creep. This shows that the wear performance of the self-steering design is unrivalled.

The curving performances of four different bogie designs were evaluated and compared by Garcia et al. (2000). The evaluated bogie types included a conventional bogie and three self-steering bogie designs. These designs were applied to three different passenger services including High Speed, Regional and Mass Transit. The curving performance was evaluated based on the stability, lateral wheelset forces in curved track and wear indices of the different designs. For the passenger services considered, it was found that the self-steering bogies did not provide a significant improvement over the conventional bogie design.

The services that were considered by Garcia et al. (2000) were all passenger services. The primary suspension stiffness applied to obtain stability for the self-steering bogies was in the order of five to seven times larger than the primary stiffness currently used on the self-steering bogies operating in South Africa. The wheelset steering ability is severely influenced since a self-steering bogie with primary suspension that is five times stiffer performs similar to a conventional three-piece bogie in terms of lateral forces and wear. Thus, all the good performance characteristics of the self-steering bogie are lost when the primary suspension stiffness is too high. The very high primary suspension stiffness used by Garcia et al. (2000) could therefore be a contributor to the result that the self-steering bogies did not provide a significant improvement over the conventional bogie design.

1.2.5.2.1 The use of Scheffel's self-steering bogie in South Africa

The heavy haul export line that carries iron ore from the mines in Sishen (Northern Cape province of South Africa) to the port at Saldanha (Western Cape province of South Africa), is a relatively straight railway line, with the sharpest curve radius equal to 1 000 m. Scheffel (1978) discussed the design of a 30 ton per axle bogie intended for the iron ore export line. The iron ore export line started operation during April 1976. The service experience gained with this bogie operating on this line was also discussed. The wheels used in these bogies experienced increased tread wear. The contributing factor was identified as the profile shape of the railhead. The crown of the railhead became

more pronounced and caused a reduction in the contact area resulting in higher contact pressures and wear.

The pattern of wear is influenced by the vehicle suspension or vehicle type and the route it travels. A stiff yaw suspension or a route with many tight curves will lead to flange wear. An optimised yaw suspension for good curving and a straighter route generate less flange wear and more tread wear. Concentrated tread wear can, however, lead to an increase in the equivalent conicity and result in instability even at relatively low speeds (Iwnicki, 2009).

The wheel and rail profile combination used on the iron ore export line together with the Scheffel's self-steering bogie (1974, 1976, 1978) currently result in concentrated hollow wheel wear. Fröhling (2003) described measures that are employed to monitor the condition and health of rolling stock and wheelsets on two export lines within South Africa. Various strategies were followed to prolong wheel life and the hollow wear in 2003 on the iron ore line. The hollow wear rate was in the order of 167 000 km/mm of hollow wear. Pummelling, proposed by Magel and Kalousek (2002), is one of the strategies that is used to reduce pronounced field side false flanges as well as the hollow wear rate.

The self-steering bogies have low steering forces but the concentrated hollow wear of the line produces an increase in the equivalent conicity. This increases the instability of the wheelset resulting in adverse contact conditions at the gauge corner and field side of the rail when the wheel is forces to contact beyond the hollow wear band. The development of Scheffel's self-steering bogie was based on the premise that the wheel profile designs are conformal to the rail profile. This allows spreading of the wheel contact positions across the tread to maintain the original wheel profile shape. This will allow low wear rates of both the tread and the flange and will maintain straight-line stability. The full potential of a conformal wheel-rail combination that spreads wear across the tread together with the low steering forces of the self-steering bogie can currently not be realised on the iron ore line since the main wheel wear mode is concentrated hollow wear. In-depth studies of the design of such a conformal wheel-rail combination and the subsequent wear life and potential to initiate RCF are required to prove this potential.

The heavy haul export line presents a unique challenge due to the topography of the line, but provides an excellent opportunity to optimise the wheel-rail system, since the wagons are ring-fenced. Lundén and Paulsson (2009) noted that such an optimisation should be performed with a thorough understanding of the complex mechanisms that drive wear, corrugation, RCF, etc. These concepts have been introduced in paragraphs 1.2.2 and 1.2.3.

1.3 Scope of work

On the export iron ore line the self-steering bogie together with reduced wear rates, straighter track and tight gauge control causes concentrated hollow wheel wear. This concentrated hollow wheel wear is characterised by gauge side and field side false flanges. This hollow wear caused changes in the wheel-rail interface, which have

resulted in an increase in the prevalence of rail RCF, ultimately increasing rail maintenance costs. The complex relationship between wear and RCF forms the basis of the current investigation. The focus is to determine whether the wheel wear shape can be controlled in such a manner as to reduce adverse contact conditions while maintaining low wheel and rail wear rates. If RCF initiation and growth can be reduced, savings on rail maintenance related to rail replacement and grinding maintenance will be incurred together with an increase in safety.

1.3.1 Aim

The aim of the study is to reduce rail RCF on South Africa's iron ore export line by managing the worn wheel shape.

1.3.2 Proposed approach

A numerical approach was used during the study of the reduction of RCF damage. A numerical model of the main wagon type running on the iron ore line was built and thoroughly validated against on-track measurements. The model was proven to represent the physical behaviour of this vehicle. The various RCF studies were performed with this validated model to explore the various contacting profiles and changes in suspension.

1.3.3 Outline of the study's progression

RCF damage was explored by identifying the wheel and/or rail profile shapes that have the largest effect on rail RCF. Long-term wear and RCF performance of potential RCF mitigation measures were investigated. Based on the findings of these studies, a new wheel design was proposed. A wheel profile was designed to allow conformal contact with rail to lower associated contact stresses. Since the elemental processes of wear and RCF are similar, it follows that, should the contact stresses be reduced, the wear and RCF on wheel and rail will be reduced.

1.4 Dissertation overview

The dissertation is organised into six chapters. The content of each chapter is discussed and the objective of each chapter is provided.

- Chapter 1:

  The main problem and motive for investigation is introduced. The relevant literature on relevant topics is reviewed.

- Chapter 2:

The numerical model and its validation are discussed. The numerical model is validated against on-track measurements and the results are critically discussed.

- Chapter 3:

The analysis of wheel and rail profile shapes that contribute to RCF initiation and growth is described and discussed. The results of this analysis are used to propose RCF mitigation measures.

- Chapter 4:

The analysis of two RCF mitigation measures is described and discussed. The long-term wear and RCF performance of these measures are critically evaluated. The results of this analysis are further applied to optimise the wheel-rail interface to maintain low wear rates and reduce RCF initiation and growth.

- Chapter 5:

A new wheel profile design that is able to reduce the initiation and growth of RCF cracks is proposed and discussed. The wheel profile is designed based on the results presented in chapters 3 and 4.

- Chapter 6:

The work is critically evaluated and concluded.

Chapter 2: Numerical model

2.1 Introduction

The MkV bogie mainly operates on South Africa's two heavy haul lines, the coal export line and iron ore export line. A CR-13 wagon was chosen for this study because it is the main wagon type operating on the iron ore export line. This wagon runs exclusively on this line and is thus ring-fenced. The CR-13 iron ore wagon consists of a CR-13 wagon body and two MkV self-steering bogies. The layout and running behaviour of the MkV self-steering bogie are discussed by Scheffel (1974, 1976, 1978).

2.2 Vehicle model construction

A multibody dynamics model of this wagon was built in VI-Rail (2014) and it included non-linear friction elements commonly found in three-piece bogies. The friction elements included the centre bowl interface, the side friction wedges and the side bearers. The characteristics of each of these friction elements as well as those of the primary suspension rubber were determined from test data. These characteristic values together with the mass, inertia, stiffness and damping of the other components of the MkV bogie and the CR-13 wagon were used to define the bogie model (Figure 2-1). The connections between the various rigid bodies are graphically depicted in Figure 2-2.

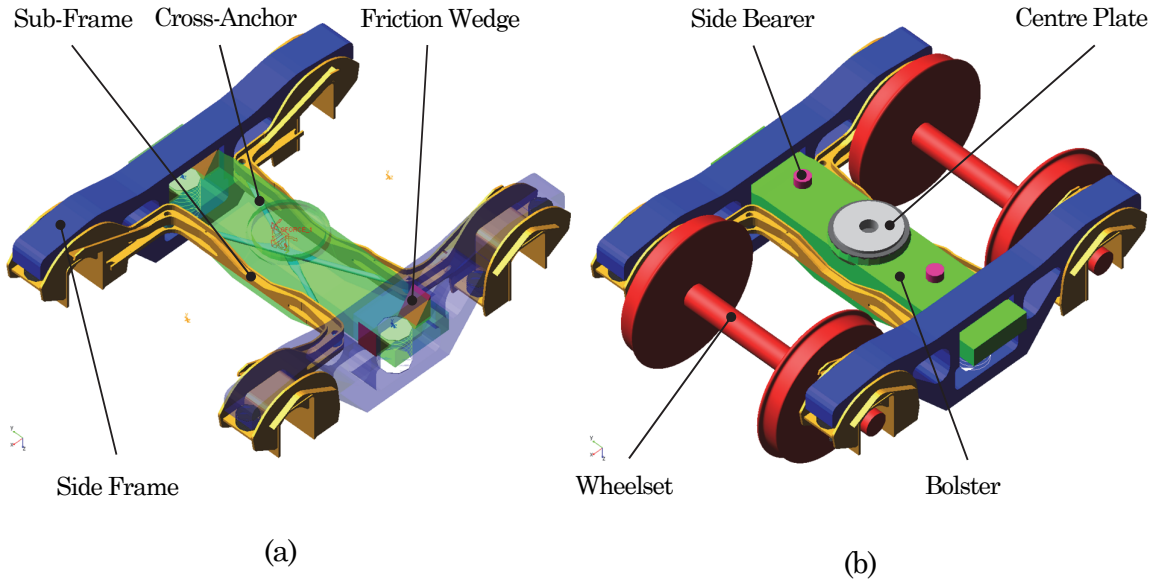

Figure 2-1: Model of the MkV bogie illustrating (a) the hidden components and (b) the assembled bogie

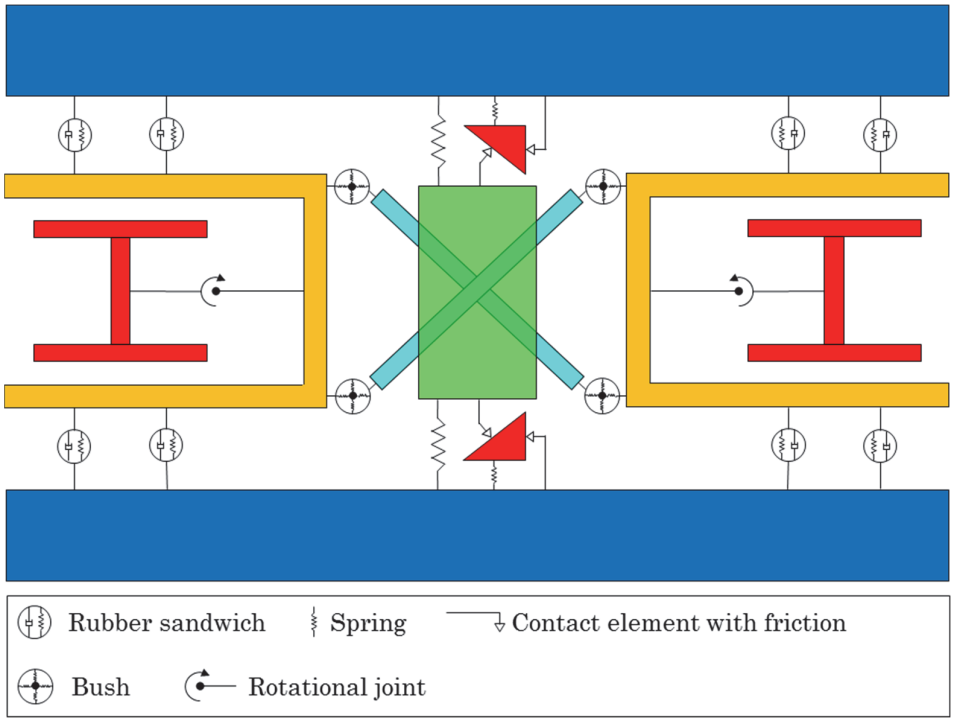

Figure 2-2: Graphical depiction of the connections between bodies of the MkV bogie model

The primary suspension was modelled with a rubber sandwich element in VI-Rail (2014). The connection was made between the sub-frame and the side frame. A suspension element with linear stiffness in all six directions of freedom was used. During characterisation tests it was noted that the linear stiffness assumption is valid, but the damping of the rubber is non-linear. A general force element was implemented to provide a damping force based on the velocity between the ends of the primary suspension element. This force-velocity relationship approximated the damping provided by the rubber. This model is not a physics based model and could be improved by implementing a more realistic model. The secondary suspension was modelled with a linear spring with stiffness in the six directions of freedom. The secondary suspension connects the bolster to the side frame. The cross-anchors connected to the sub-frames through bushing elements. These bushing elements were modelled with linear stiffness values. The damping of the bushing was set to a constant percentage of these linear stiffness values. A rotational joint was implemented between the sub-frame and the wheelset. This joint allows only for rotation about the lateral direction to allow the wheels to rotate. The revolute joint presents a stiff connection between the axle boxes of the wheelset and the sub-frame. Thus no additional freedom of movement is allowed between the axle boxes and the sub-frames. A friction wedge element was implemented between the side frame and bolster. This element modelled the non-linear damping of the friction wedges by producing friction at its interfaces with the side frame and bolster. The non-linear damping is provided by a contact model that includes friction provided by a modified Masing/Kolsch model (VI-Grade, 2014). VI-Grade (2014) explained that the classical Masing model is often used to model elasto-plastic behaviour. The model consists of a spring element connected in parallel to a combination of a spring and dry friction element connected in series. When the force in the series spring exceeds the hold

force in the dry friction element, the friction part starts to slide and a friction force is generated opposite to the direction of travel.

The fully assembled wagon is shown in Figure 2-3 and a graphical depiction of the elements connecting the body to the two MkV bogies is shown in Figure 2-4. The bogie models were connected to the wagon body through centre plate elements. The centre plate elements element is used to located the bogies relative to the wagon body and allow rotation between the bogies and the wagon body. The centre plate element provides resistance and non-linear damping to the translations and rotations of the wagon body relative to the bolster. The bogie model included side bearer elements with action between the bolster and the wagon body. The side bearer implementation used in this model is a single spring with a gap between the two bodies. Thus, the side bearers will only allow non-linear damping once the wagon body closes this defined gap and contacts the side bearer. The non-linear damping of the centre plate element and side bearers is produced by a contact model that includes friction provided by a modified Masing/Kolsch model (VI-Grade, 2014). The WRGEN wheel-rail contact element is used to model the interaction between the wheel and the rail. This contact model allows the use of general or measured wheel and rail profiles and calculates the actual contact kinematics at each simulation step. This model allows the solution of multiple contact points, evaluating the local contact parameters based on the geometry and material properties. The FASTSIM algorithm (Kalker, 1990) was used in conjunction with this contact element to solve the wheel-rail contact problem. It should be noted from Figure 2-4 that the couplers and subsequently the coupler forces were not included in the CR-13 wagon model.

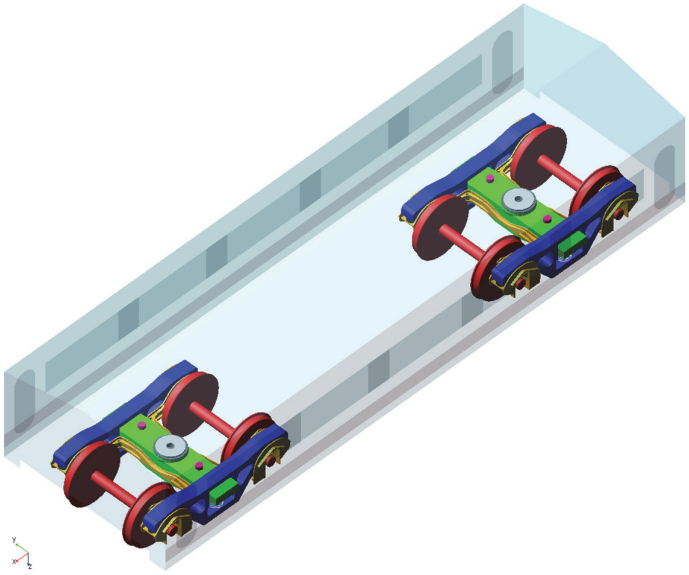

Figure 2-3: Assembled CR-13 wagon with two MkV self-steering bogies

Figure 2-1 to Figure 2-4 show that the CR-13 wagon model has 27 rigid bodies connected through various elements. These 27 rigid bodies amount to 162 degrees of freedom. Only four rotational joints were used in total, removing only 20 degrees of freedom leaving 142 unconstrained degrees of freedom. These unconstrained degrees of freedom were only restricted by means of stiffness, damping and contacts with friction. Once the model was

created, the performance of the model needed to be verified. This is required to ensure the validity and accuracy of the model with respect to the forces and displacements. The model verification was performed against on-track measured data. The following chapter discusses the simulations that were performed as well as the validation of the simulated responses against measured data.

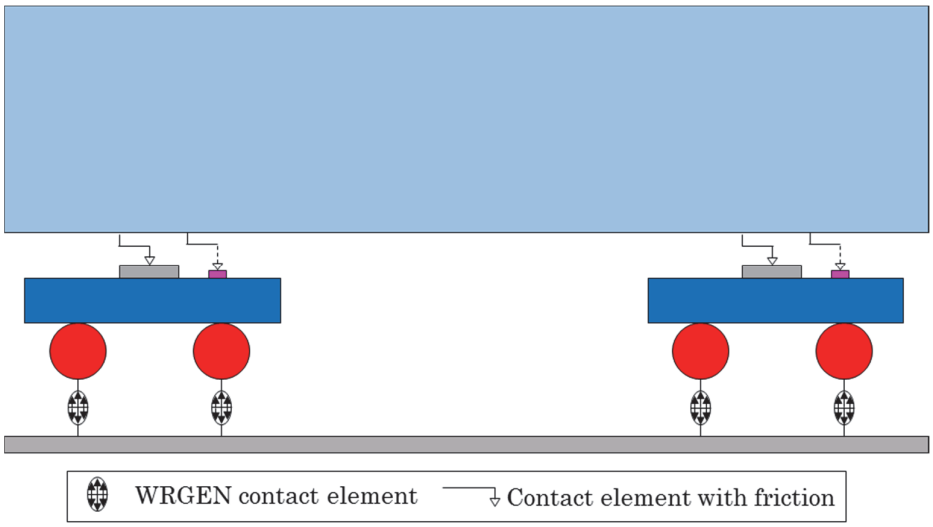

Figure 2-4: Graphical depiction of connections between the wagon body and the two MkV bogie models

2.3 On-track measurement of vehicle responses

It would have been ideal to test this vehicle on the track where it regularly operates. Such a test, unfortunately, has many limitations. One of which is the logistics associated with the setup, transport and test of the vehicle on the line. The second limitation relates to the physical track features. The iron ore export line is mainly a straight line with many large radius curves. The minimum curve radius on the line is equal to 1 000 m. This minimum curve radius does not require the wheelsets to steer with large creep forces and will not cause large rotations and displacements of the suspension elements. Thus, the signal to noise ratio of the data may be too low to permit any meaningful correlation. To increase the wheel-rail forces and allow for greater rotations and displacements, the wagon was tested on a winding section of track near Belfast, Mpumalanga, South Africa. A CR-13 wagon fitted with two of Scheffel's MkV self-steering bogies were instrumented at the Railway Testing and Development Centre at Koedoespoort, South Africa for these on-track tests.

2.3.1 MkV bogie instrumentation

The MkV bogie was instrumented to measure the response of the major components within the bogie. These components included the wheel forces, primary suspension displacements, secondary suspension displacements, side bearer clearances and centre bowl or bogie rotation. Instrumented wheelsets were used to measure the wheel-rail

forces as well as the contact position on the wheel. These wheelsets were placed at the leading and trailing position within the front bogie (Figure 2-5).

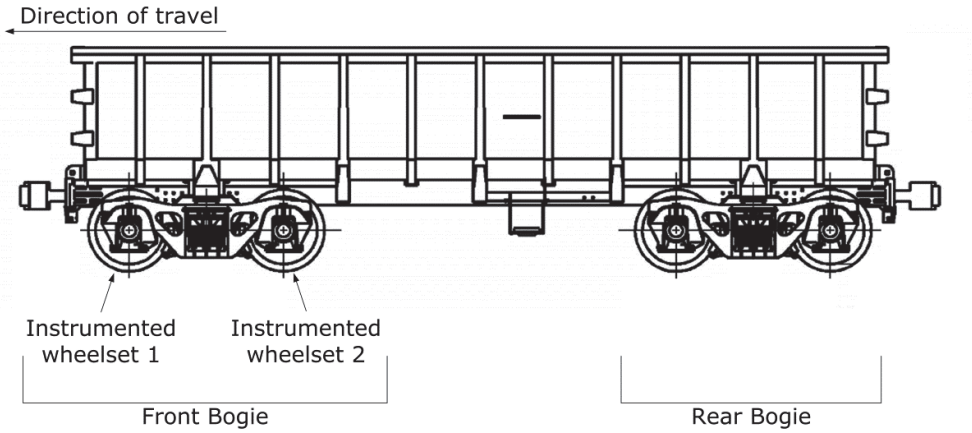

Figure 2-5: Position of instrumented wheelsets on front bogie

The secondary suspension displacement was measured with a rope displacement transducer. The displacement was measured between the side frame and bolster. This arrangement is shown in Figure 2-6.

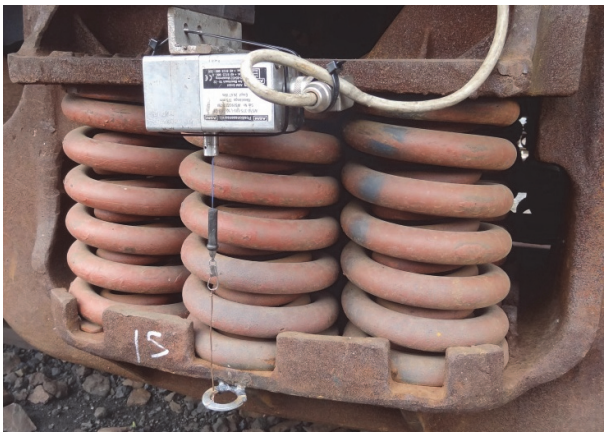

Figure 2-6: Measurement of secondary suspension displacement

The bogie rotation or the angle of the wagon body relative to the bolster was measured with laser displacement transducers. The displacement was measured from the wagon body relative to the bolster. This is effectively the rotation experienced at the centre bowl interface. This measurement arrangement is shown in Figure 2-7(a). The displacement of the wagon body relative to the side frame was measured by means of rope displacement transducers, in addition to the laser measurements. The rope displacement measurement was used as a verification of the displacements measured with the laser transducer. The measurement arrangement is shown in Figure 2-7(b).

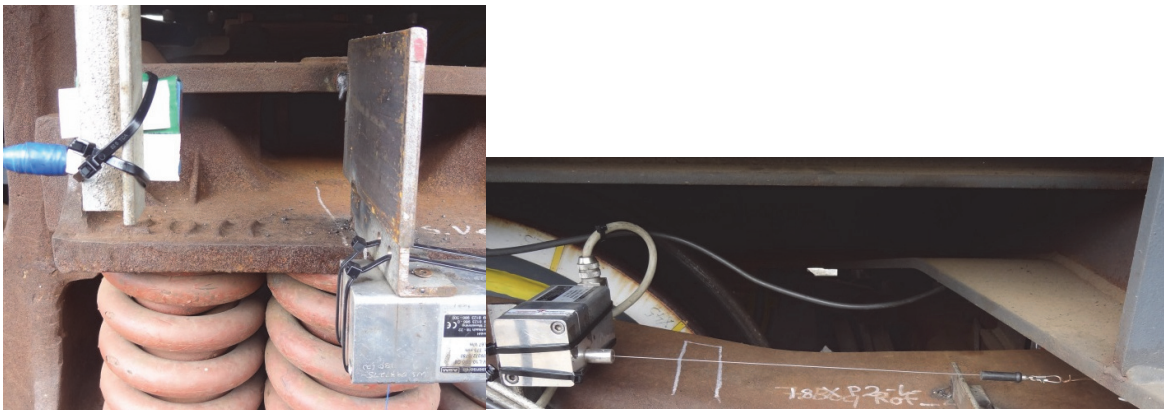

(a) (b)

Figure 2-7: Measurement of bogie rotation relative to the wagon body (a) with a laser and (b) with a rope displacement transducer

The longitudinal and lateral displacements of the primary suspension rubber were measured by means of rope displacement transducers as well as a stereo vision camera setup. The longitudinal displacement was measured from the side frame to the centre of the sub-frame as shown in Figure 2-8. The lateral displacement was measured from the end of the sub-frame to the opposite end of the side frame as shown in Figure 2-9. The vertical, lateral and longitudinal displacements of the primary suspension were measured by means of the stereo vision camera system as shown in Figure 2-10.

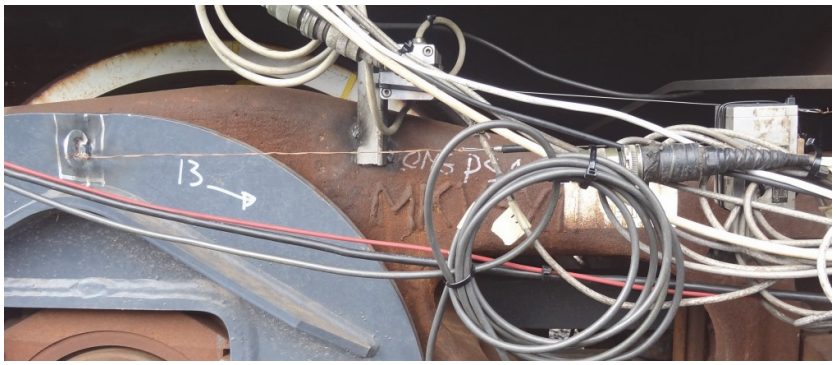

Figure 2-8: Measurement of longitudinal displacement of the primary suspension

The displacement of the wagon body relative to the bolster was measured with a laser displacement transducer. This displacement measurement delivers the side bearer clearance. The relative displacement was measured from the wagon body to the bolster and the transducer was placed next to the side bearer as shown in Figure 2-11.

The roll and yaw responses of the wagon body were measured with an inertial measurement unit (IMU). The IMU was mounted more or less on the centre line of the wagon body at the rear of the wagon. The IMU attachment location is shown in Figure 2-12.

Figure 2-9: Measurement of lateral displacement of the primary suspension

Figure 2-10: Stereo vision cameras mount to measure primary suspension displacements

Figure 2-11: Measurement of body displacement relative to the bolster

Figure 2-12: Location of the IMU measuring body responses

A load measuring wheelset was used to measure the resulting wheel-rail forces. The load measuring wheelset uses strain gauges stuck around the circumference of the wheelset. The strain gauge measurements are processed with a calibration matrix to obtain the resulting forces and moment. The load measuring wheelsets do not allow continuous force measurement, since the strain gauges are stuck at discrete intervals around the circumference of the wheel. The strain gauge data is filtered with a low-pass filter at 40 Hz to eliminate higher order dynamic responses and noise. The instrumentation therefore functions more accurately and approximates continuous signals once the wheel travels faster than 20 km/h. The load measuring wheelset is not suited to low speed measurements.

2.3.2 Test train layout

A test train was assembled consisting of three 18E locomotives, two CR-13 wagons and one test coach. The arrangement is shown diagrammatically in Figure 2-13 and the physical layout is shown in Figure 2-14. The instrumented bogie was positioned at the second leading position of the second wagon. This arrangement allows the measurement of the largest forces experienced by the wagon.

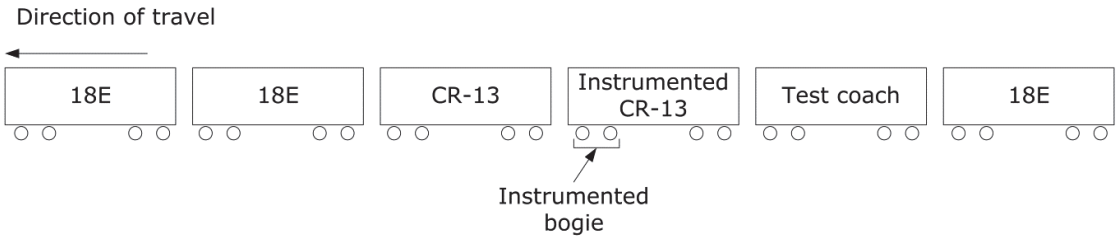

Figure 2-13: Schematic of test train layout

Figure 2-14: Physical test train layout

2.4 Definition of the representative track

A representation of the track layout, wheel-rail profiles, coefficient of friction, track irregularities and vehicle speed was defined for the test section as follows:

Track layout: The test track was the section of track between kilometres 91 and 96 just before Belfast station, which is shown in the small scale of Figure 2-15. The test section included three consecutive 400 m radius curves and a 600 m radius curve.

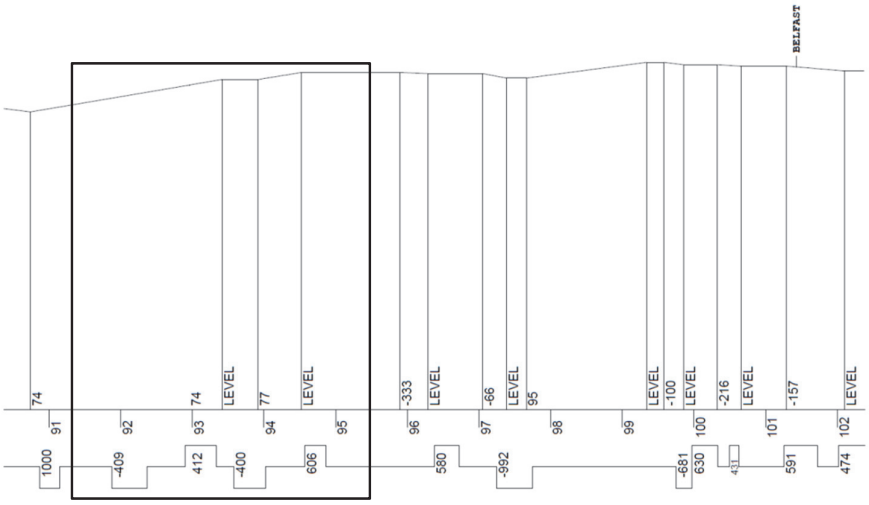

Figure 2-15: Small scale of test section

Super-elevation: The super-elevation (cant) was assumed constant within each curve and was determined from data collected with a track geometry measurement vehicle.

Track Gauge: The track gauge at the test section is nominally 1 065 mm. The track gauge was assumed constant within each curve and was determined from data collected with a track geometry measurement vehicle. The track layout, gauge and super-elevation values of the representative track are shown in Table 2-1.

Table 2-1: Track layout, gauge and super-elevation of the representative test track

Track layout	Direction	Length	Gauge	Super-elevation
		m	mm	mm
Tangent	-	100	1 065	0
409	Left	350	1 070	59
Tangent	-	565	1 065	0
412	Right	382	1 070	52
Tangent	-	403	1 065	0
400	Left	225	1 070	59
Tangent	-	678	1 065	0
606	Right	217	1 070	45
Tangent	-	480	1 065	0

Traffic conditions: A single CR-13 wagon was used during the simulations. The influence of the other wagon, test coach and locomotives were disregarded. Thus, no other external forces, such as coupler forces, were applied to the wagon.

Wheel profiles: The vehicle model included wheel profiles measured on the instrumented wagon.

Rail profiles: Rail profiles measured at each of the curves were used in the track definition. A constant rail profile was used in each curve section.

Coefficient of friction: A constant coefficient of friction of 0.4 was used on both rails.

Track irregularities: Track irregularities of the test section measured with a geometry measurement car were used during the simulations. The space curve output of the geometry car was used and thus vertical and lateral spatial location of the left and right rails were used.

Vehicle speed and braking: The initial velocity was approximately 65.5 km/h. A proportional-derivative (PD) controller was used to follow a velocity profile. The velocity profile is shown in Figure 2-16.

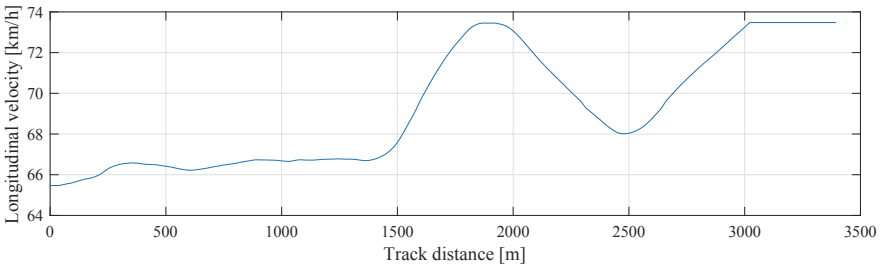

Figure 2-16: Wagon's velocity profile

Contact algorithm: The FASTSIM contact algorithm was used during the dynamic simulations with a Kalker factor of 0.5.

Wagon load: The CR-13 wagon used during the test was loaded with weights. These weights were distributed within the wagon to achieve a total body mass of 69 177 kg.

The inertia values were calculated from a computer-aided design (CAD) model of the CR-13 wagon loaded with the weights.

2.5 Comparison of on-track measurement and simulation results

The unfiltered longitudinal and lateral forces that were measured and simulated are compared in Figure 2-17. The results are noisy and comparisons of magnitudes are difficult. The comparison of steady-state behaviour is facilitated by filtering the data. However, the cut-off frequency of the filter should not filter out the steady-state response.

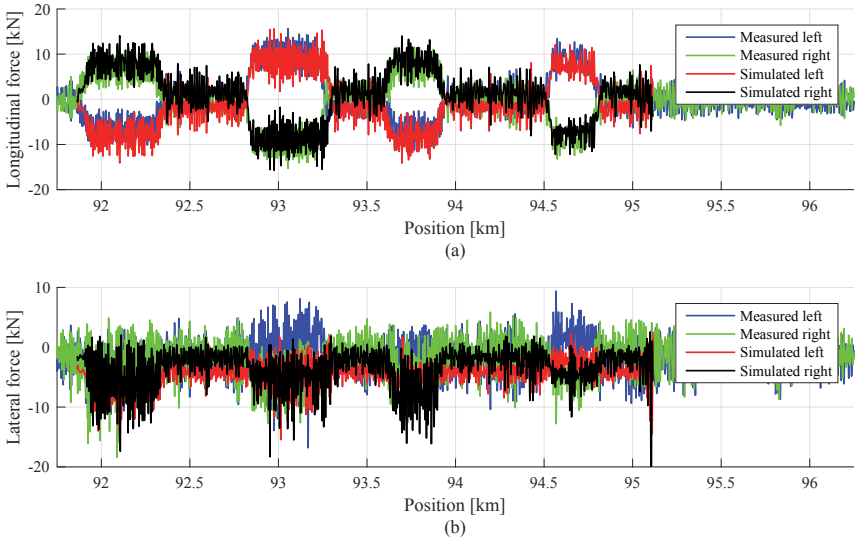

Figure 2-17: On-track and simulation data comparison with data low pass filtered at 10 Hz for the leading wheelset (a) longitudinal and (b) lateral forces

Similar frequency content is observed from the comparison of the Fast Fourier Transforms (FFTs) of both the measured and simulation data (see Figure 2-18). The largest amount of energy is present between 1 Hz and 2 Hz. It should be noted that the magnitudes of the FFTs were normalised with respect to the maximum value in this range. The energy is present in this range due to the response of the secondary suspension. The data can therefore be filtered below 1 Hz to eliminate any natural resonance mode of the secondary suspension, with the filtered data approximating the steady-state behaviour. The data presented in paragraph 2.5 is low pass filtered by means of a second order Butterworth filter with a cut-off frequency at 0.5 Hz.

The data obtained with the load-measuring wheelsets and transducers is compared to the simulation data in the following paragraphs. The following should be considered when these forces, rotations and displacements are compared:

a) The longitudinal wheelset forces measured with the load-measuring wheelset cannot be calibrated directly. The calibration value is estimated from the vertical calibration value. The longitudinal forces are much smaller than the vertical forces and therefore the sensitivity of the wheelset to longitudinal forces is lower.

b) The relative magnitude of the lateral forces measured at the leading wheelset compared to those of the trailing wheelset should be considered. The load-measuring wheelset measures the lateral force through wheel web bending. The sensitivity of the measurement technique is very low when small lateral forces are generated by the wheelset. Larger forces would produce larger web bending strains and the measurement of such forces becomes more accurate.
c) The initial condition of the test wagon as it reached the start of the test section is different to that of the simulation model starting at the same section. The simulation model assumes perfect starting conditions and the solution converges at each time step based on these initial conditions. The magnitudes of various forces and displacement responses may therefore be influenced by this difference.
d) The initial zeroing of channels may not have occurred at the perfect zero condition of the test wagon, which leads to an offset in measured values.
e) The gauge, cant and rail profiles vary throughout the test section, which will inevitably influence the forces on the test train. The simulation was performed under more ideal conditions.
f) The coefficients of friction on both rails are unknown. A constant coefficient of friction was used on both rails during the simulation phase. There may have been differences in the coefficients of friction between the left and right rails as well as variations along the track length, influencing the contacting forces.

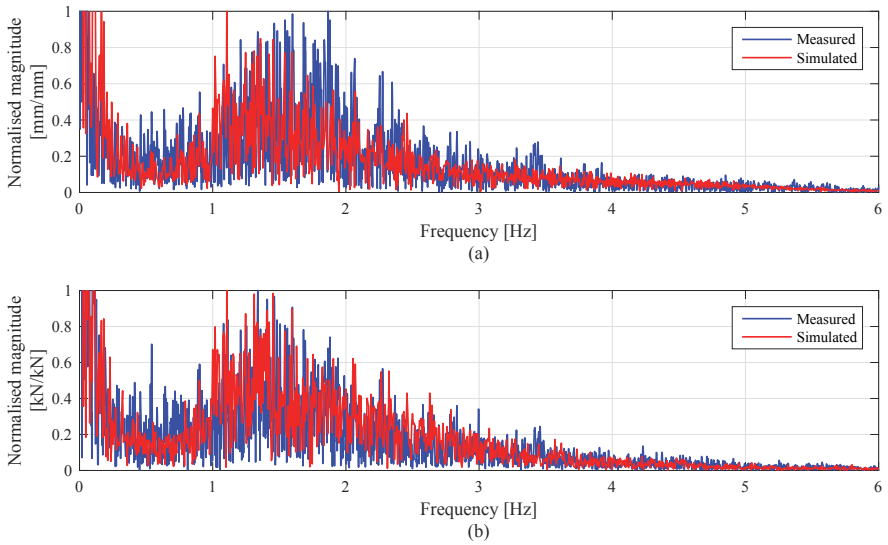

Figure 2-18: Comparison of the frequency content of the on-track and simulation data low pass filtered at 10 Hz (a) primary suspension longitudinal displacement and (b) longitudinal wheelset forces

2.5.1 Displacement data

The various displacements that were measured at the wagon body/bogie interface and the suspension components are compared and discussed in this paragraph. Most of the displacements were measured with rope displacement transducers. One of the disadvantages of using rope transducers is the measurement range compared with the maximum range of the transducer. The displacements that were measured were

relatively small compared to this maximum range. The displacements were in the order of ±5 mm, which is only 3.33 % of the maximum range of 300 mm. The sensitivity towards such small displacements is very low. This low sensitivity introduces measurement inaccuracies, which should be considered when evaluating the comparisons.

For the verification of the friction model of the centre bowl interface, the rotation angle of the wagon body relative to the bogie is very important. Friction is challenging to model properly, since the friction of in-service components may react differently to what was modelled. The measured and simulated results of the bogie rotation are compared in Figure 2-19 and it is clear that the bogie rotation is simulated well. Both the measured and simulated results show a slight rotational offset from zero once the wagon passed through the curve. The friction of the centre bowl causes this rotational offset. This offset is present since the forces present as the wagon exits the curve, are relatively small and are not enough to overcome this friction. This illustrates the detail and accuracy of the model.

A comparison of the measured and simulated lateral and longitudinal primary suspension (PS) displacements is shown in Figure 2-20. The measurements of the stereo vision camera are shown by the cyan and magenta lines. Figure 2-20 shows that both measurement techniques produce similar measured results. The stereo vision results are noisier since the camera box was rigidly connected to the wagon body. This induces unwanted relative movement of the primary suspension relative to the mounting of the camera. Figure 2-20 shows that the simulated lateral displacements of the primary suspension closely represent the measurements. The longitudinal displacements show larger discrepancies. This is mainly due to a restriction in the measurement setup. The measurement setup was not constructed to measure the longitudinal displacement at the side frame and sub-frame where the primary suspension attaches, but rather between the centre of the side frame and the centre of the sub-frame (Figure 2-8). Rotations between the side frame and sub-frame may influence this measurement.

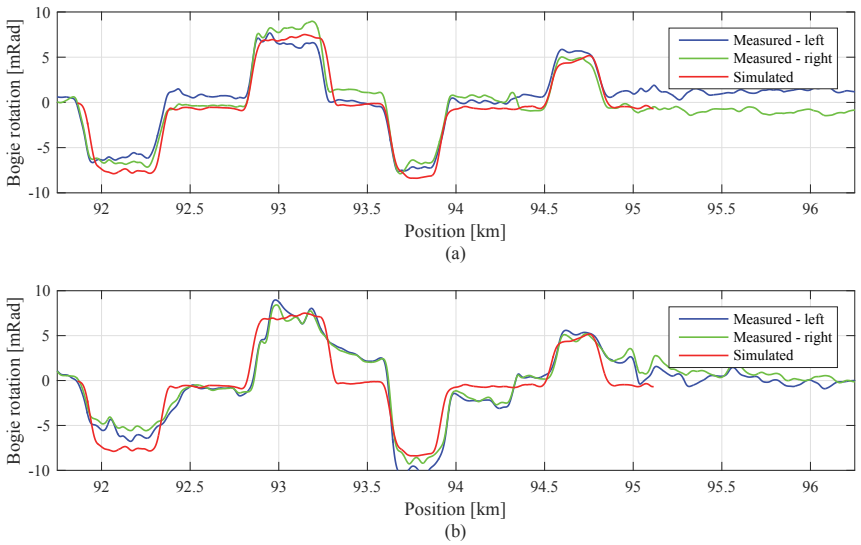

Figure 2-19: Comparison of the bogie rotation results with (a) the laser transducers and (b) the rope displacement transducers

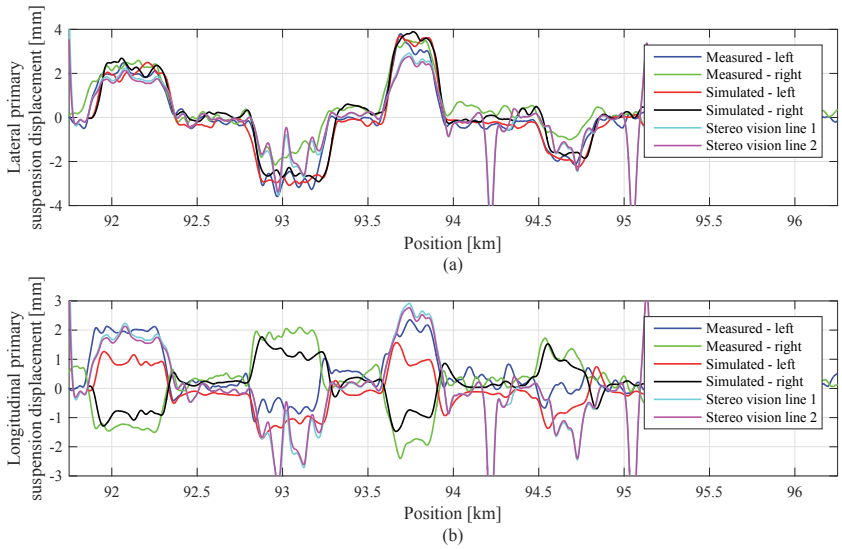

Figure 2-20: Comparison of (a) the lateral and (b) the longitudinal primary suspension displacements

The measured and simulated displacements of the secondary suspension and side bearers are compared in Figure 2-21. The simulation results do not fit the secondary suspension displacement well. The sensitivity of using rope displacement transducers to measure such small displacement is limited since these small displacements are measured with a transducer that has a large measurement range. In addition to the measurement sensitivity, it should be noted that the wagon was brand new, but was stationed at the Koedoespoort workshop for two years without being used. The components may have rusted and may therefore have increased the friction coefficient at the friction wedges. The increase in friction coefficient was not considered in the model.

The magnitude of the side bearer displacement is slightly overestimated. This can again be attributed to the measurement sensitivity of the lasers, which have a full-scale measurement range of 300 mm, and again only 6 mm of this measurement range was used. The comparison of the body roll of Figure 2-22 shows very good correlation. The measured and simulated body roll are similar and thus this body roll should cause similar displacements at the side bearer. This provides confidence that the side bearer displacement is correctly estimated by the simulation.

The measured coupler force and velocity profiles are shown in Figure 2-23. The coupler force was not modelled, since the application of the coupler force will have three components in the longitudinal, lateral and vertical direction. The coupler force in these three directions was not measured and could therefore not be applied accurately. It may have a small effect on the force measurements or displacements, although the correlations discussed thus far are of acceptable quality. The velocity controller used during the simulation matched the measured velocity profile well, as seen in Figure 2-23(b).

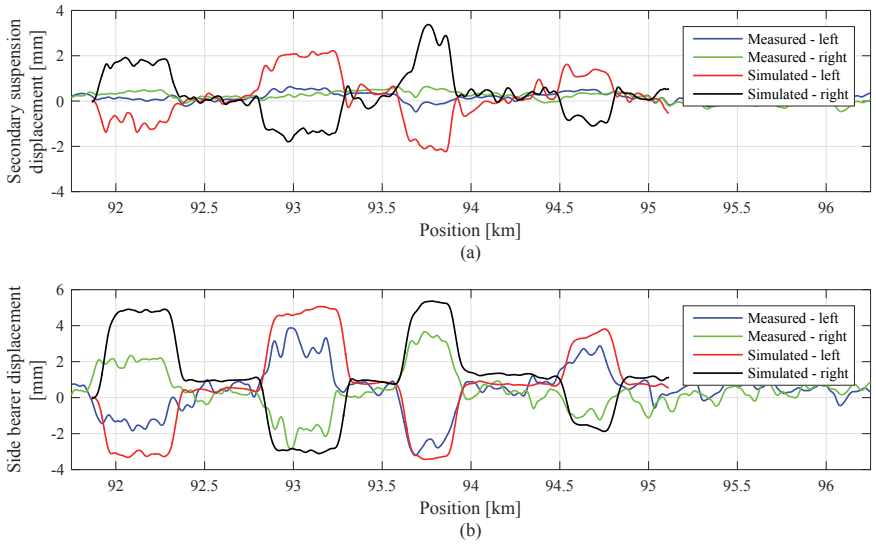

Figure 2-21: Comparison of measured and simulated (a) secondary suspension and (b) side bearer displacements

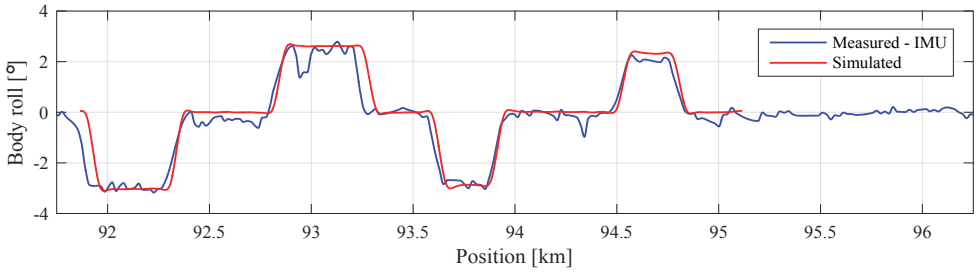

Figure 2-22: Comparison of body roll

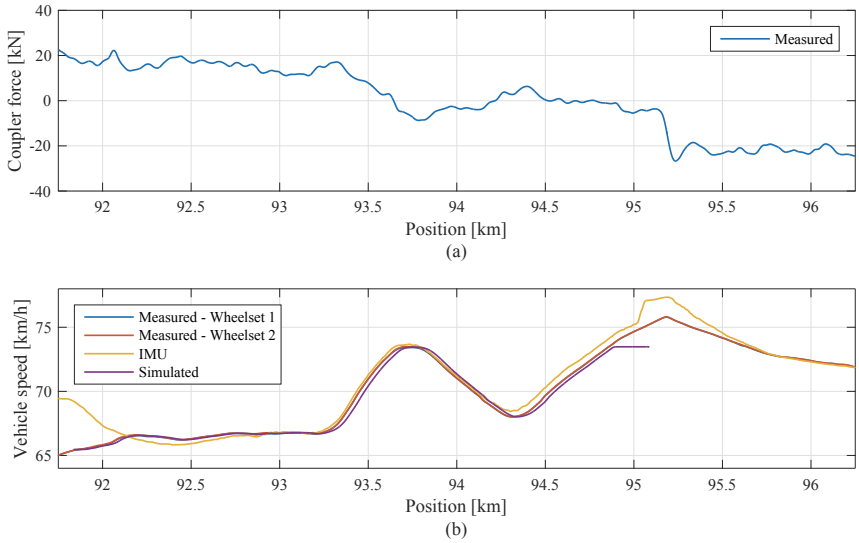

Figure 2-23: (a) Measured coupler force and (b) comparison of measured and simulated velocity profiles

2.5.2 Load-measuring wheelset data

The longitudinal and lateral wheelset forces of the leading wheelset are compared in Figure 2-24. It is clear from Figure 2-24 that the longitudinal wheelset forces correlate well for all the curves. The simulated lateral forces on the other hand show similar trends to the measured lateral forces, but there are larger discrepancies in the magnitudes. Relatively small lateral force values are present at the leading wheelset. The sensitivity and accuracy of the measurement technique, as well as the unknown friction coefficients, may explain these larger discrepancies.

The results of the longitudinal and lateral wheelset forces of the trailing wheelset are compared in Figure 2-25. The longitudinal and lateral forces of the first and third curve match considerably better than those forces measured at the second and fourth curve. The changing coefficient of friction may account for the differences between curves. Relatively low longitudinal forces are present at the trailing wheelset when compared with those of the leading wheelset. The sensitivity of the longitudinal measurement at the trailing wheelset may account for some of the magnitude differences.

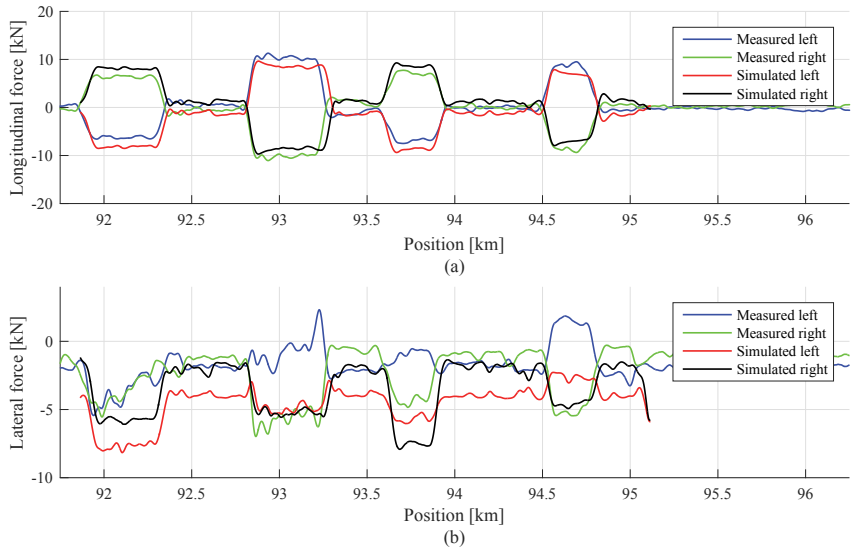

Figure 2-24: Comparison of (a) longitudinal and (b) lateral wheelset forces of the leading wheelset

The discrepancies in the measured longitudinal and lateral forces are challenging to explain, especially when the contact position on the wheels are compared (Figure 2-26). The contact positions match closely and provide confidence in the simulation model in the sense that the wheelset displacements are predicted accurately. It is generally very difficult to match force measurements. The fact that the wheelset displacements and contact positions are estimated well provides confidence in the simulation model. Any correlation in the forces provides even more confidence in the model.

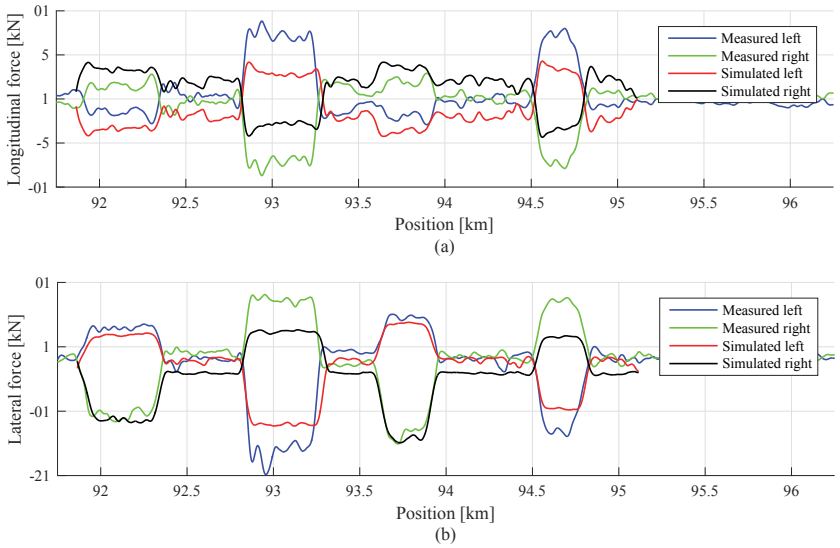

Figure 2-25: Comparison of (a) longitudinal and lateral wheelset forces of the trailing wheelset

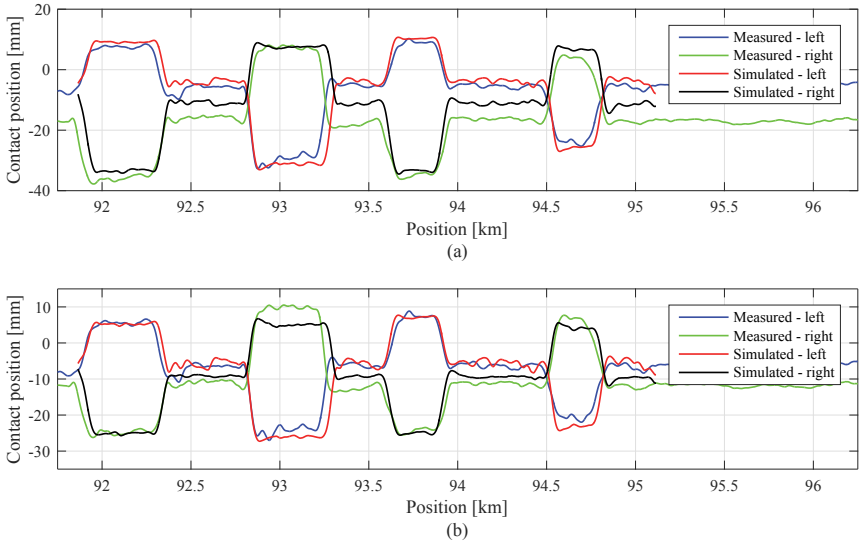

Figure 2-26: Comparison of the contact positions at (a) the leading and (b) the trailing wheelsets

The measured and simulated vertical forces are compared in Figure 2-27. The load-measuring wheelset forces differ significantly between the three 400 m curves. One would expect these forces to be of similar magnitude since the conditions in these curves are expected to be similar, as seen from the simulation results. The measured and simulated vertical forces match well at the first and third curves when compared to the other curves. This can explain the differences in longitudinal and lateral forces at the second and fourth curves of both the leading and trailing wheelsets. Different tangential wheelset forces are generated since the vertical load present at these curves are different. The difference in vertical force is much harder to explain but may have to do with the weight shift due to the body pitching (Figure 2-28), prevailing longitudinal gradient in the curve and coupler forces exerted on the wagon body at these curves. Even with

discrepancies present, the simulated vertical force values are within a 10 kN or 10 % of the measured values.

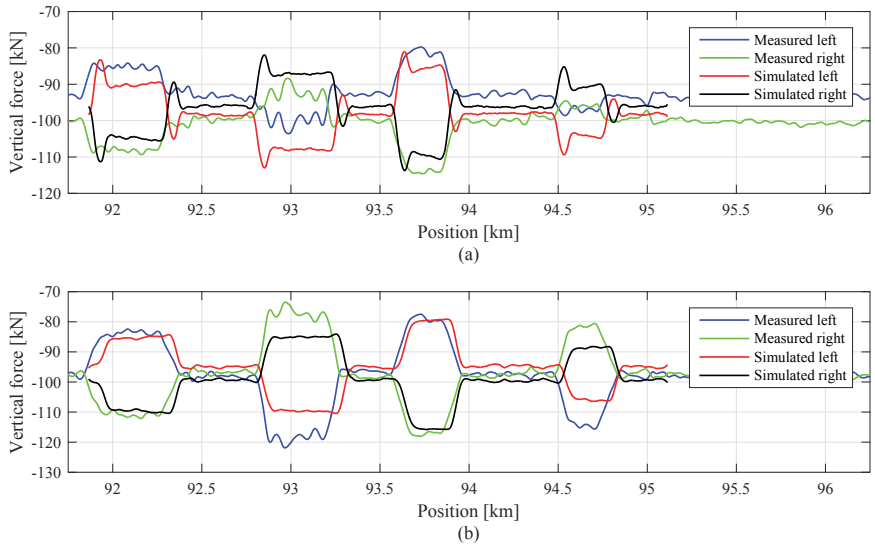

Figure 2-27: Comparison of the vertical forces measured at (a) the leading and (b) the trailing wheelsets

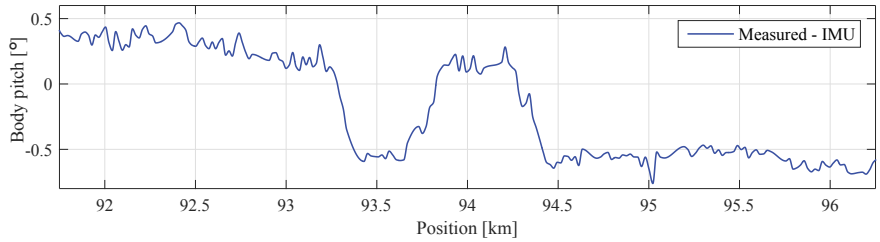

Figure 2-28: Measured body pitching

Cole (1998) suggested the use of correlation coefficient to compare measured and simulated results. The correlation coefficients were calculated with the cross correlation function in MATLAB (2015). The correlation coefficients were calculated for the various results that have been discussed and are summarised in Table 2-2. The correlation coefficients are close to, or above 90 %, except where discrepancies were noted in the preceding discussion.

2.6 Conclusion of numerical model validation results

A detailed numerical wagon model created in VI-Rail (2014) was validated against on-track tests. The results were compared visually and statistically using the correlation coefficient as suggested by Cole (1998). The results of both the visual and statistical comparison showed an acceptable degree of correlation, with the correlation coefficients close to, or above 90 %. No vehicle is manufactured and assembled perfectly and this may account for some of the discrepancies. The numerical model has been validated

against on-track measurements within curves. The numerical model can thus be applied with confidence to study the response of the MkV self-steering bogie and CR-13 wagon for similar running conditions. The vehicle model has not been validated against other dynamic phenomena such as the critical hunting speed. The validity of the model will have to be proven in the study of such phenomena. The vehicle dynamics and wear simulations that follow were carried out with this validated model in VI-Rail (2014).

Table 2-2: Correlation coefficients of matching responses

Result	**Correlation coefficients**	
	Leading wheelset or vehicle responses	**Trailing wheelset**
	%	%
Longitudinal force – Left wheel	97	93
Longitudinal force – Right wheel	97	93
Lateral force – Left wheel	56	96
Lateral force – Right wheel	77	98
Vertical force – Left wheel	91	94
Vertical force – Right wheel	92	94
Wheel contact position– Left wheel	97	97
Wheel contact position– Right wheel	97	96
Wagon body roll	97	
Bogie rotation – Left	97	
Bogie rotation – Right	98	
Side bearer clearance – Left	92	
Side bearer clearance – Right	90	
Secondary suspension displacement – Left	82	
Secondary suspension displacement – Right	35	
Lateral PS displacement – Left	97	
Lateral PS displacement – Right	94	
Longitudinal PS displacement – Left	87	
Longitudinal PS displacement – Right	93	

Chapter 3: Influence of wheel and rail profile shape on the initiation of rolling contact fatigue cracks at high axle loads

3.1 Introduction

Heavy haul railways allow cost-effective operations when the system is performing harmoniously. The system has many factors that determine the cost of operation. Some of the largest costs are associated with maintenance and/or replacement of wheels and rails. Two damage mechanisms driving the maintenance and replacement of wheels and rails are wear and rolling contact fatigue (RCF). Excessive wear and surface-initiated RCF may result when the wheel-rail interface is not properly managed or maintained.

Scheffel (1974) designed a self-steering, high-stability freight bogie to reduce wheel flange wear. This type of freight bogie has been used on Transnet Freight Rail's iron ore export line since April 1976 (Scheffel, 1978). Following the introduction of the self-steering bogie, together with straighter track and tight gauge control, concentrated hollow wheel wear started occurring with the characteristic gauge side and field side false flanges. These hollow-worn wheel profiles caused surface-initiated RCF damage on the gauge side of high rails and field side of low rails because of the adverse contact conditions (Figure 3-1). Consequently, a hollow wear limit of 2 mm was introduced. Strict adherence to this limit brought about a reduction in the occurrence of RCF (Tournay and Mulder, 1996). Surface-initiated RCF on the gauge corner of the high rail and field side of the low rail re-emerged after the iron ore export line was upgraded from an axle load of 26 tons to an axle load of 30 tons in 2001.

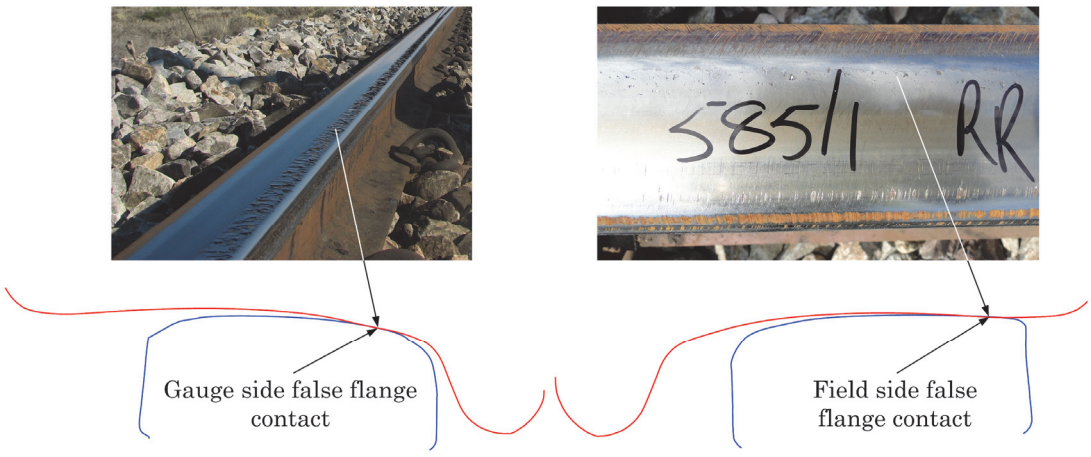

Figure 3-1: RCF damage on the high rail and low rail due to false flange contact

Fröhling et al. (2008) examined the risk of hollow-worn wheel profiles initiating surface RCF at the rail gauge corner. The high contact pressures and tangential forces arising from hollow wheel contact showed a high propensity towards RCF development. Fröhling et al. (2008) suggested that the impact of false flange contact could be restricted by means of limiting the wheels' hollow wear. The effect of the hollow-worn wheel profile shape on the initiation of RCF was further investigated by Fröhling et al. (2012) and Karttunen et al. (2014b). Wu et al. (2010) noted that high energy in the wheel-rail contact patch leading to RCF initiation or wear is generally caused by poor vehicle curving performance and poor wheel-rail contact conditions.

Visual inspections of the iron ore export line were carried out before the start of every grinding cycle since April 2010. The RCF damage was classified according to Transnet Freight Rail's internal classification chart (Fröhling et al., 2005). The RCF on the gauge corner (head checks) was classified from class 1 to 5 ranging from none, light, moderate, heavy to severe damage, respectively. These inspections have shown that some rails experience more damage than others. Although track quality, curve radii and super-elevation play a significant role in the initiation of RCF (see Karttunen et al., 2014a and Tunna and Urban, 2009), it was observed that measured rail profiles with gauge corners lower than the target rail profile were more prone to severe RCF damage. Distributions of RCF class versus rail gauge corner deviation at -15° as measured from April 2010 to January 2015 support this observation (Figure 3-2). The term rail gauge corner deviation is used to describe the distance from the target rail profile to the measured rail profile at a given tangent angle. Thus, the amount the measured profile deviates from the target profile. A negative deviation indicates that the measured rail profile is higher than the target profile and a positive deviation indicates the opposite.

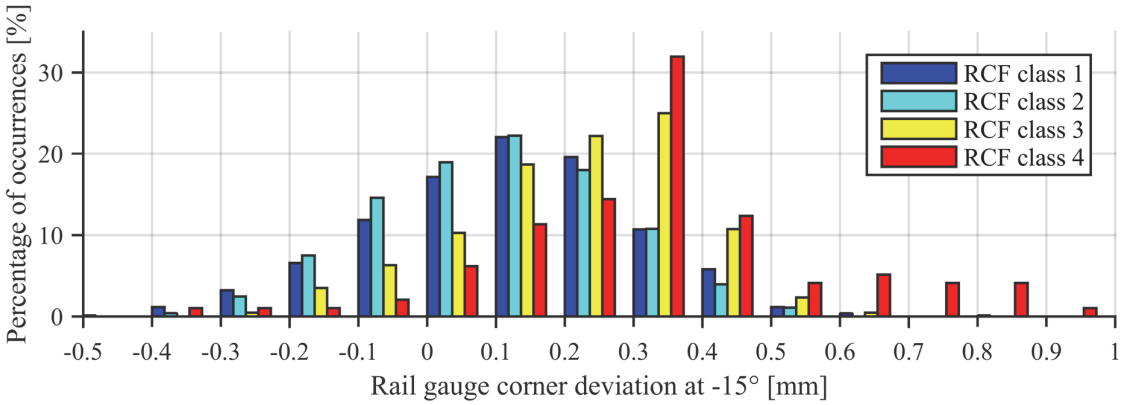

Figure 3-2: RCF class distribution versus rail gauge corner deviation at -15°

The shapes of worn wheels and rails influence the initiation and growth of surface RCF cracks. Features defining the worn shape of wheels and rails are investigated to understand how these profile shapes contribute to the initiation and growth of RCF cracks.

3.2 Vehicle dynamics

The study of the wheel and rail profile shape features that contributes to RCF damage is performed through multibody vehicle dynamics simulations. Measured worn wheel and rail profiles are used during simulations and the results are post-processed to calculate RCF damage parameters. These RCF damage parameters are analysed together with the profile features to find those features that cause the highest and most occurrences of RCF damage.

Multibody vehicle dynamics simulations were carried out to calculate the wheel-rail contact parameters required to calculate the damage parameter values. The vehicle model described in chapter 2 was used during the investigation. A single wagon was simulated running over seven different track sections in both the forward and reverse directions.

In-service wheel profiles were measured during May 2011 on 44 different CR-13 wagons, totalling 352 wheel profiles. The wagon was simulated to have measured wheel profiles in the same position as measured on the wagon. Different profiles on left and right wheels as well as between the various axles were used. The spectrum of worn wheels that were considered during the analysis is comparable to the spectrum of the entire fleet as shown in Figure 3-3(a).

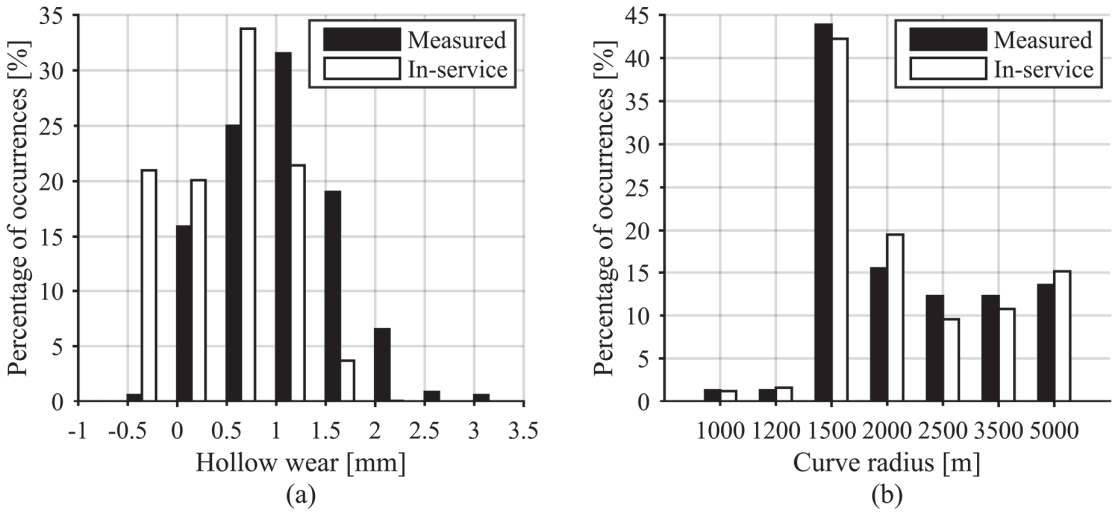

Figure 3-3: Hollow wheel wear (a) and curve radius (b) distributions used in simulations

The seven different tracks were modelled as constant radius curves varying from 1000 to 5000 m. The track gauge was kept constant at 1065 mm and the super-elevation (cant) was assumed constant within a curve. The relevant super-elevation was selected from Transnet Freight Rail's maintenance manual (Marutla et al., 2012). The wagon was simulated to run at a constant speed of 60 km/h which is representative of the average operating speed of the production trains. The speed and chosen super-elevation resulted in the 1000 and 1500 m curves having 0 cant deficiency, the 1200, 2000, 3500 and 5000 m curves having a 5 mm cant deficiency and the 2500 m curves a 2 mm cant

deficiency. The cant deficiency is relatively small and therefore cant deficiency or excess should have little effect on the initiation of RCF. The wheel and rail profile features are the main subject of interest and therefore track irregularities were not included in the track definition to limit the number of variables considered to initiate RCF cracks. The maximum coefficient of friction allowed between wheel and rail was set to 0.4.

The rail profiles used for this analysis were measured at 2 km intervals through the total length of all curves on the iron ore line. In total 155 rail profiles were measured on UIC60 CrMn rails during April 2011. The curve distribution is shown in Figure 3-3(b). These rail profiles were used to simulate wheel-rail contact conditions as a function of the measured rail profiles within a particular curve radius. Rail profiles within a particular curve were changed every 100 m to allow the vehicle to reach a steady state condition before entering the next 100 m rail section. The resulting wheel-rail combinations that were simulated equalled 54 560.

3.3 Processing of simulation results

3.3.1 Shakedown values and wear number extraction

The shakedown values and wear numbers were calculated directly from the simulation results at each contact patch on the high rail. The shakedown values were determined using equation (1-6) divided by k_e giving the normalised vertical load and equation (1-7) as presented by Ekberg et al. (2002). The minimum of the material's shear yield strength of 553 MPa (Table 3-1) was used during the calculation of the normalised vertical load. The wear number was calculated using equation (1-14) (Burstow, 2003).

Table 3-1: UIC60 CrMn rail strength parameters (Fröhling et al., 2012)

Rail strength parameter	Value
	MPa
Tensile yield strength	590
Ultimate tensile strength	1080
Yield strength in shear	553-621

The shakedown values and wear numbers were averaged over 30 m of track ending 10 m before the rail profile was changed. The shakedown values and wear numbers were only considered when the contact position on the rail was more than 8.75 mm from the rail profile centre towards the gauge corner. Any contact positions closer to the rail profile centre were deemed not to contribute to gauge side RCF damage in the area of interest as confirmed by field observations. An example of this averaging is shown for a single wheelset of a vehicle as it ran over a section of track in Figure 3-4.

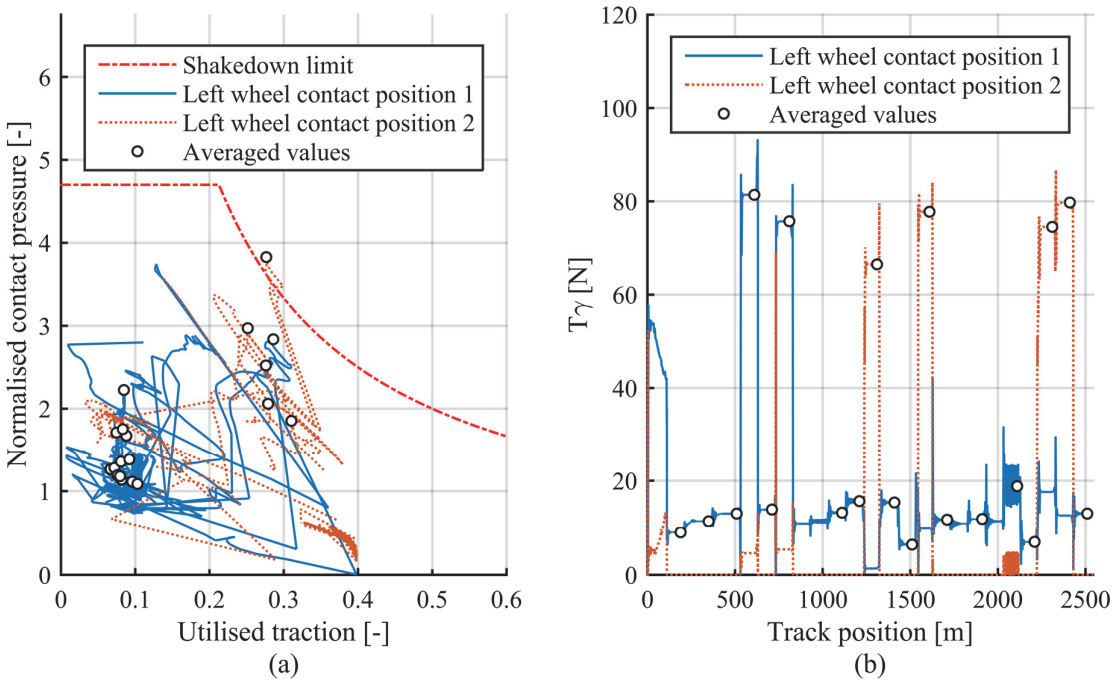

Figure 3-4: Illustration of (a) shakedown value and (b) wear number extraction

3.3.2 RCF modelling

RCF failure is usually confined to the gauge corner of the high rail or the field side of the low rail in curves. RCF cracks may grow, unite or branch across the railhead causing spalling of the rail surface or a complete fracture of the rail (Johnson, 1989). Plastic deformation and crack initiation are predominantly caused by high contact stresses and tractive steering forces. Ekberg and Kabo (2002) and Tunna et al. (2007) review the mechanisms of wear and RCF.

Predictive models that are currently applied in literature are focussed either on the shakedown map as developed by Johnson (1989) or on the energy dissipated in the contact patch (Burstow, 2003). Both these models have been shown to predict the initiation of RCF cracks, although there are differences between the models and their assumptions.

The results obtained from the above-mentioned vehicle dynamics simulations were post-processed to calculate both the surface fatigue index Ekberg et al. (2002) and the damage index (Burstow, 2003). All creep forces, lateral and longitudinal, were considered to contribute to RCF initiation. The surface fatigue index (FI_{Surf}) was calculated as the shortest distance from the working point on the shakedown diagram to the shakedown limit. The true distance was calculated to avoid the limitation of the horizontal projection surface fatigue index, which becomes inaccurate at very high utilised traction values and low normalised vertical loads (Ekberg et al., 2002). RCF initiation is predicted when the FI_{Surf} value exceeds zero. The damage index (DI) was calculated from the wear number ($T\gamma$) and the damage function shown in Figure 3-5. The FI_{Surf} values and DI values

greater than zero were finally summed per wheel or rail profile to indicate the total RCF damage that the profile will cause or undergo.

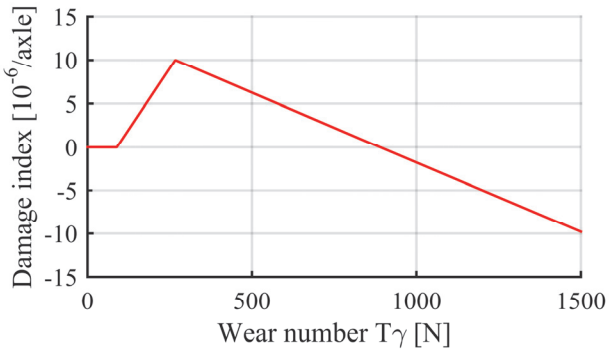

Figure 3-5: Rolling contact fatigue damage function

The turning points of the damage function in Figure 3-5 were calculated using equation (3-1) as proposed by (Burstow, 2004).

$$T\gamma_{TP} = \frac{1}{2\sqrt{3}}(\sigma_y + \sigma_{ut})A\gamma_{TP} \quad \textbf{(3-1)}$$

The median of the contact areas calculated during the various simulations was 183mm^2 and was used in equation (3-1). The three turning points were calculated at creepages of 0.1 %, 0.3 % and 1 %, with a peak damage of 10×10^{-6}/axle at 0.3 % creepage. The locations of the turning points were calculated at 89, 267 and 890 N (see Figure 3-5) from the rail strength values listed in Table 3-1.

3.3.3 Comparison of damage parameters with and without track irregularities

The simulations did not include the effects of track geometry or irregularities to reduce simulation time and reduce the number of factors influencing RCF development. However, it is well known that track irregularities have a significant influence on RCF damage Karttunen et al. (2014a). The number of external factors such as macro geometry and super-elevation was minimised to facilitate the evaluation of RCF damage as a function of the wheel and rail profile shape.

To quantify the exclusion of track irregularities, the peak-valley surface fatigue index (FI_{Surf}) values are compared with the averaged values over the same section for a simulation including track irregularities in Figure 3-6(a). The peak-valley values appeared to lie on a line with a constant FI_{Surf} value. It therefore appears that irregularities do not significantly influence the averaged FI_{Surf} values. The averaged FI_{Surf} values from simulations with and without the inclusion of track irregularities are shown in Figure 3-6(b). The averaged values are similar and the values extracted from simulations without irregularities provide a good estimation of the fatigue damage

caused by real track including irregularities for the current simulation conditions and data processing technique. The wear number extraction with and without track irregularities showed similar results.

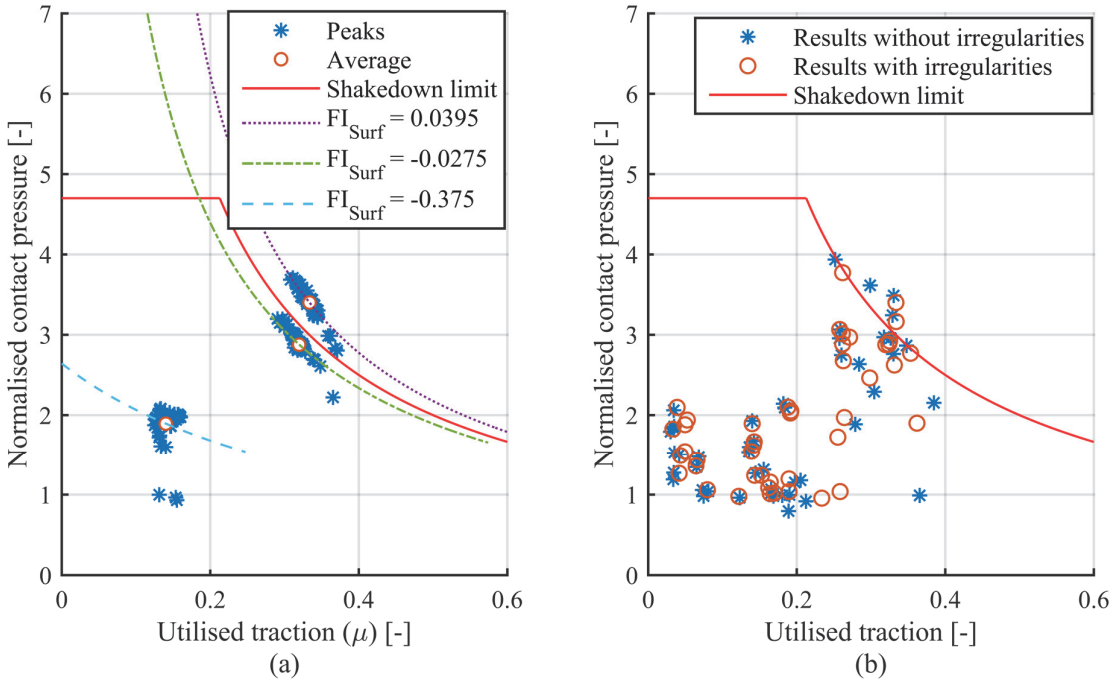

Figure 3-6: Comparison of (a) peak-valley and averaged shakedown values and (b) shakedown values with and without the inclusion of track irregularities

The influence of irregularities may cause a local over prediction of fatigue damage by a wheel-rail combination. The influence of the wheel and rail profile shape on RCF development might become inaccurately assessed when the results are skewed by too many external factors. Track irregularities were therefore excluded from the current analysis, since the results with and without its inclusion are similar; the simulation time is significantly reduced and the number of external factors possibly influencing the results is reduced.

3.3.4 Wheel and rail profile shape features

All the calculated FI_{Surf} values are plotted as a function of the contact positions on the rail and wheel (Figure 3-7). Figure 3-7 shows that the largest collection of wheel-rail contact points occurs between -0.00875 and -0.020 m on the rail profile and between -0.030 and -0.0175 mm on the wheel profile. The contact is mainly towards the wheel taping line and centre of the rail. The formation of hollow wear and associated false flanges can be linked to these concentrated contact points. As the contact position moves closer to the either the rail gauge corner or the wheel flange, the probability of a wheel-rail combination producing a high FI_{Surf} value increases. The rail and wheel profile shapes thus have a definite influence on the contact position and predicted fatigue damage. Most of the FI_{Surf} values greater than zero occur close to the gauge corner or

the wheel flange. The selected wheel-rail contact area, excluding rail contact positions greater than -0.00875 mm, focuses on this area of predicted RCF initiation.

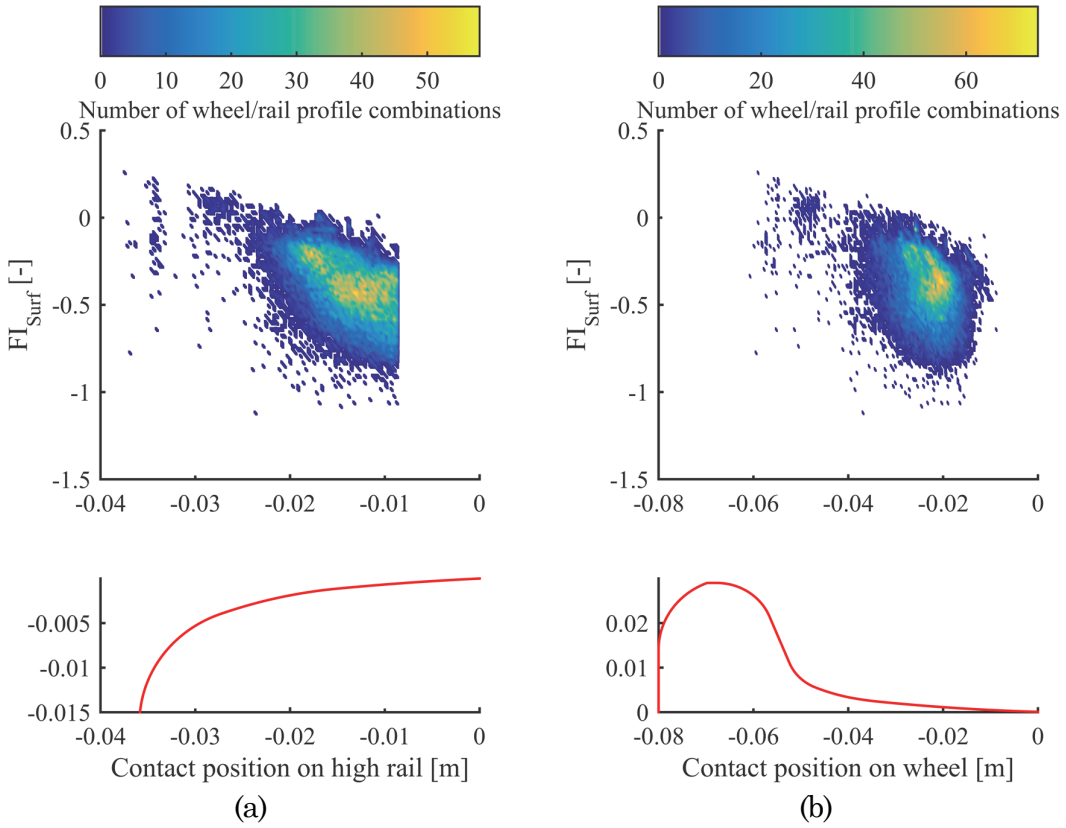

Figure 3-7: FI_{Surf} as a function of the contact position on (a) the rail and (b) the wheel

The features used to describe the worn wheel and rail profile shape included hollow wear, gauge side false flange height, gauge side false flange gradient, hollow wear position relative to the taping line and the rail gauge corner deviation at -15° (Figure 3-8). These features are consistent with those defined by Fröhling et al. (2012), except for the maximum hollow wear position. When a bogie is well aligned and runs true, with only small differences in wheel diameters, it will result in a maximum hollow wear position close to the taping line. The maximum hollow wear position is considered since it indicates the health of a bogie and its tracking. The gauge side false flange height and gradient are calculated as the largest difference in height or gradient between a new and worn wheel profile between 35 and 60 mm from the back of the wheel flange.

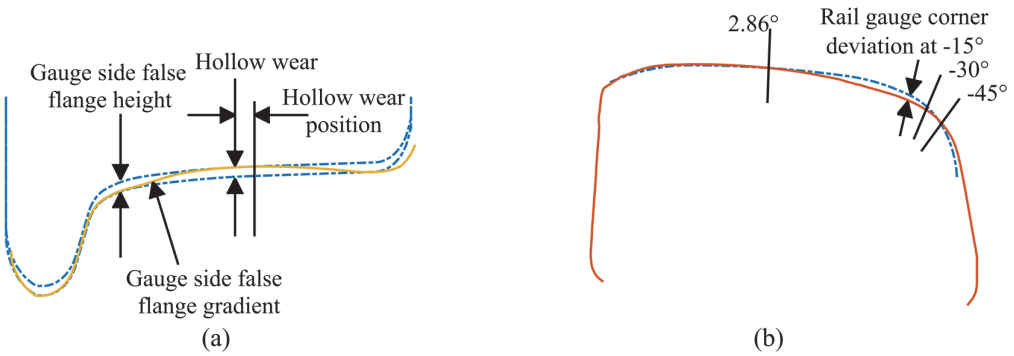

Figure 3-8: Graphic representation of (a) wheel and (b) rail features

3.4 Sensitivity of RCF damage parameters to profile shape features

The cumulative RCF damage parameters ($\sum DI$ and $\sum FI_{Surf}$) calculated from the simulation results were used to examine the potential of the profile shape features to promote the initiation of surface RCF. Box plots were used to examine the damage parameters' sensitivities to the observed head check classes (Figure 3-9). The bottom, centre and top lines of the boxplot correspond to the 25th, 50th (median) and 75th percentile values. The whiskers correspond to ±2.7 times the standard deviation providing a 99.3 % coverage of the data, assuming it as normally distributed. Values beyond the whiskers are included as crosses.

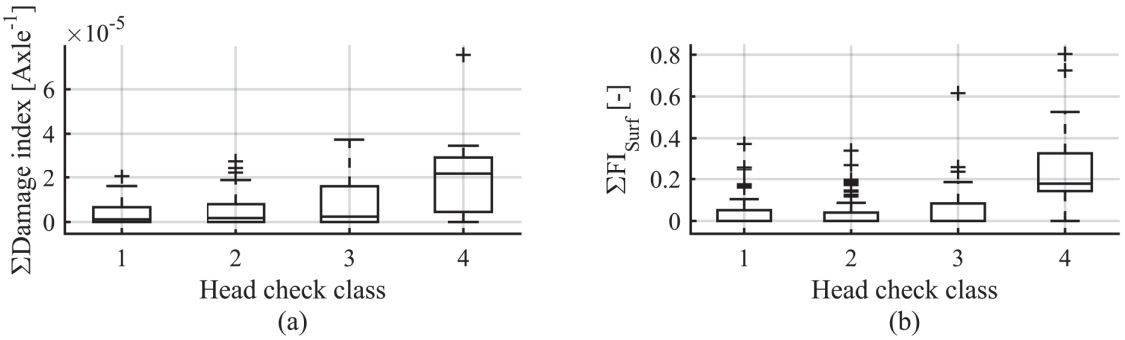

Figure 3-9: In-field observed RCF class and its correlation to (a) the damage index and (b) the surface fatigue index

The medians, 75th percentiles and outer whiskers increase as the observed RCF damage increases. Both damage parameters show that the rails that were visually classified with more fatigue damage show higher predicted RCF damage.

3.4.1 Wheel features

It is known from (Tournay and Mulder, 1996, Fröhling et al., 2008 and Fröhling et al., 2012) that hollow wear is an effective feature to monitor and limit the initiation and growth of RCF cracks. The hollow wear is compared to the DI and FI_{Surf} values in

Figure 3-10. Figure 3-10 clearly shows that both damage parameters are sensitive to hollow wear. Wheel profiles with more hollow wear causes more RCF damage in general.

Fröhling et al. (2012) suggested that RCF initiation might be more sensitive to the gauge side false flange gradient than the hollow wear. From Figure 3-11 it can be seen that both damage parameters show sensitivity to the gauge side false flange height and gradient. These features prove that the hollow wear shape has an influence on RCF initiation.

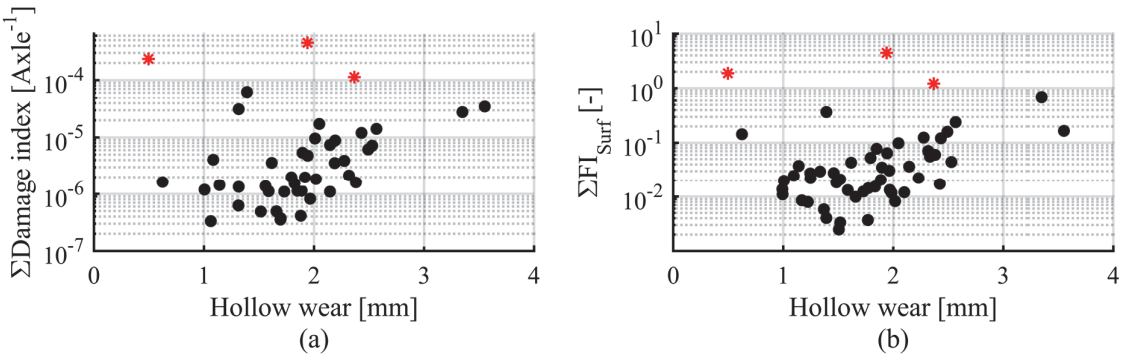

Figure 3-10: The influence of hollow wear on (a) the damage index and (b) the surface fatigue index (outliers shown with *)

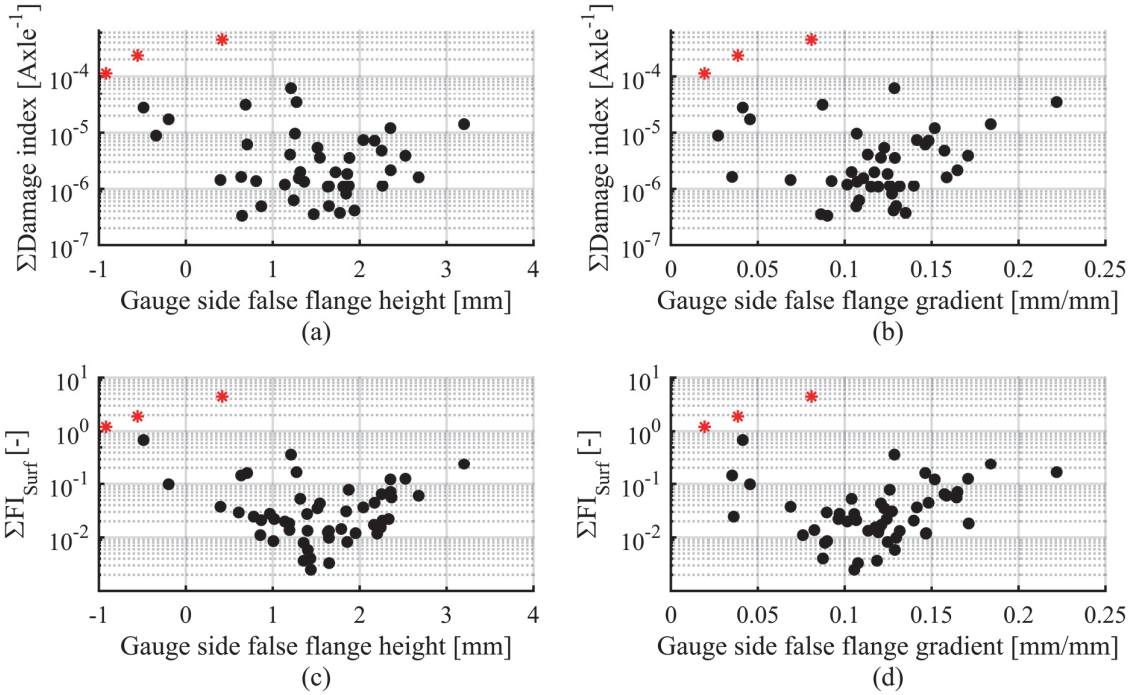

Figure 3-11: The influence of the gauge side false flange height and gradient on (a), (b) the damage index and (c), (d) the surface fatigue index (outliers shown with *)

There are however, outliers to these relationships, of which three are indicated by stars in Figure 3-10 to Figure 3-12. The profiles of these three outliers showed distinctive signs of skew running bogies. The wheel profiles do not show significantly high false flange

heights, gradients or even hollow wear, but these profiles produce contact conditions promoting fatigue damage on many rail profiles. The outliers prove the reality of in-service wheel profiles that react outside the norm. There are wheel profiles that are flagged by the limits imposed on them, that is, limiting hollow wear to 2 mm reduces the fatigue impact of these wheel profiles. However, there are underperforming wheel profiles that cannot accurately be identified by the wheel features of Figure 3-10 and Figure 3-11.

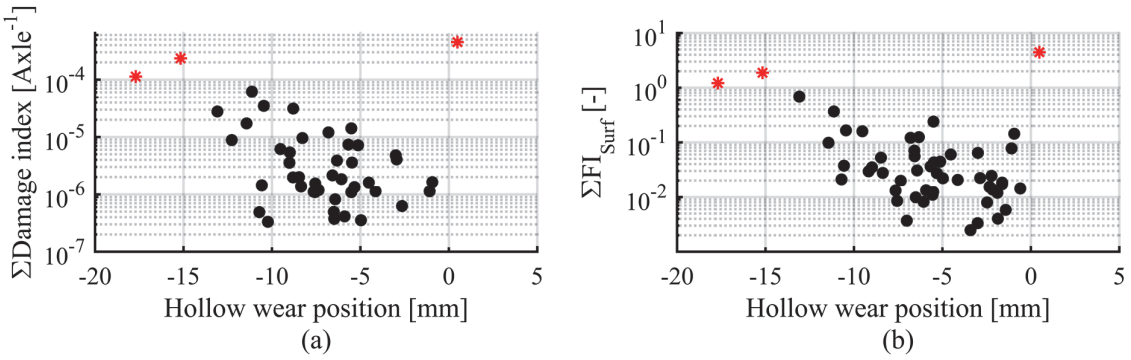

Figure 3-12: The influence of hollow wear position on (a) the damage index and (b) the surface fatigue index (outliers shown with *)

The hollow wear position shown in Figure 3-12 was investigated to be able to segregate the outliers. From Figure 3-12 it can be seen that both the damage parameters are the most sensitive to the hollow wear position. The hollow wear position shows the best correlation compared with the other wheel features. As the hollow wear position becomes increasingly negative and thus moves closer to the wheel flange, the probability of severe RCF increases. The importance of good vehicle tracking is thus highlighted. Bogies running true with low wheelset diameter differences will yield hollow wear positions closer to the taping line. The fatigue impact of wheels can thus be limited by reducing skew running bogies.

It should be noted that the y-axes of Figure 3-10 to Figure 3-12 are shown as a non-linear log scales. Any linear relationship on this log scale will produce a non-linear increase on a linear scale. The four wheel features show that an increase in their values produce a non-linear increase in the predicted damage. By limiting any of these features, it is possible to limit damage produced at their extreme values.

3.4.2 Rail features

Visual inspections and in-field observations have shown that rail profiles with lower than target gauge corners are more prone to severe RCF damage (see Figure 3-2). Although Fröhling et al. (2012) were unable to prove any relationship between the gauge corner deviation and the amount of RCF damage, the gauge corner deviation at -15° was once again studied to determine its potential contribution to RCF initiation and crack growth.

DI and FI_{Surf} values are compared with the gauge corner deviation at -15° in Figure 3-13(a) and (b), respectively. The damage parameters show an increase as the gauge

corners become increasingly lower than the target rail profile. This indicates that rail profiles with low gauge corners are more prone to RCF damage. These rail profiles do not have sufficient material to establish the required rolling radius difference and promote wheelset steering. Higher tangential curving forces are generated during inadequate steering. The as-ground shape of the rail should therefore be tightly controlled to reduce the fatigue impact of the rail profile shape. The limit imposed by Transnet Freight Rail is a maximum deviation of ±0.3 mm. The rail profiles contributing the most to RCF damage lie beyond 0.3 mm and therefore RCF damage can be limited by adhering to this limit.

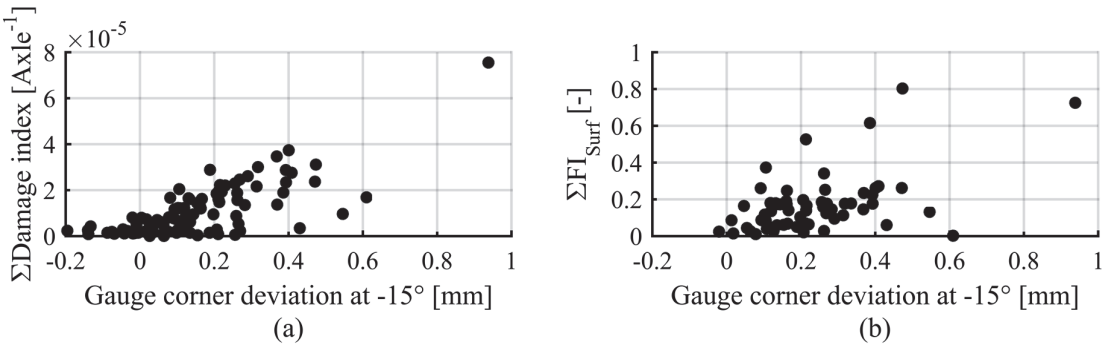

Figure 3-13: The influence of the gauge corner deviation at -15° on (a) the damage index and (b) the surface fatigue index

3.4.3 Reduction in rail RCF damage by eliminating damaging features

The analysis of the different wheel and rail profile shape features proved that the RCF on the high rails is caused by its profile deviation as well as underperforming wheel profiles. If the wheel features that proved to contribute to RCF initiation are eliminated, the damage caused to the high rails should reduce. The effect of applying various feature limits to the wheel profiles can be evaluated based on the total damage caused to the rails. This evaluation is performed by summing all the damage parameter values for all the rails after applying a limit to the wheels and dividing it by the total original accumulated damage. This provides a percentage value of the total amount of damage remaining once the limit has been applied. The significance of applying limits to each wheel feature can then be assessed. The various limits were chosen to eliminate the same number of wheel profiles as a 2 mm hollow wear limit would. The same wheels are not necessarily flagged by the different limits, although there may be some repeating wheels. The results as well as the various limits are shown in Table 3-2.

Table 3-2: Remaining damage after the application of wheel feature limits

Feature to limit	Limiting value	Remaining damage based on DI	Remaining damage based on FI_{Surf}	Number of wheels eliminated	Percentage of total wheel population
		%	%		%
Hollow wear	2mm	75.00	70.60	28	7.95
Gauge side false flange height	1.85mm	94.40	90.60	28	7.95
Gauge side false flange gradient	0.129mm/mm	91.10	88.50	28	7.95
Hollow wear position	-8.1mm	48.40	55.20	28	7.95
All wheel features	All limits	42.80	45.40	64	18.18

By applying these limits independently, each feature effectively removes 8 % of wheels from the total wheel population. Therefore, by removing a small number of wheels it is possible to achieve a great reduction in RCF damage. By placing a limit on the hollow wear position, the highest amount of damage is removed and approximately 50 % of the initial damage remains. This result stresses the importance of good vehicle tracking. By reducing skew running bogies, the hollow wear position can be limited to the taping line and the initiation of RCF can be reduced.

The limit that provides the second best performance is the hollow wear limit, followed by the gauge side false flange gradient and finally the gauge side false flange height. When all the limits are applied in combination 64 wheels are removed, which is equivalent to 20 % of the total wheel population. The reduction in damage parameter values due to the application of all the limits are shown as a comparison in Figure 3-14. However, this results in only removing some of the damage. The remaining wheels contribute 45 % of the initial RCF damage. This is not a significant improvement over the hollow wear position limit and requires many wheels to be removed. The hollow wear position appears to provide the best feature to limit and monitor.

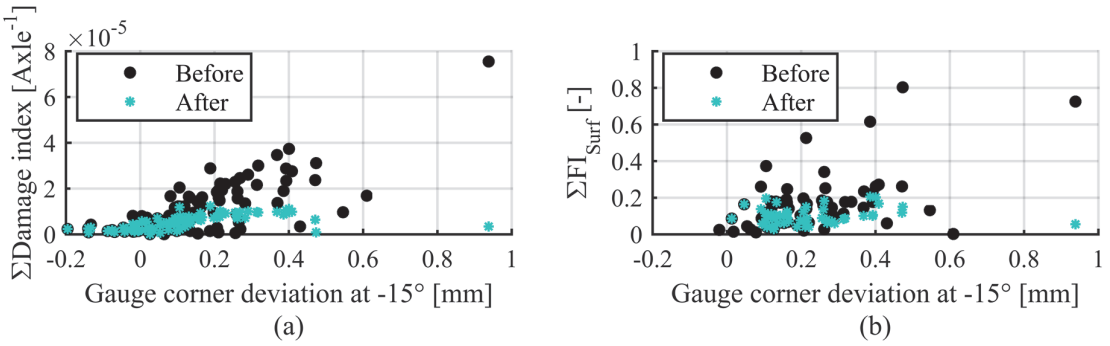

Figure 3-14: Comparison of damage index values before and after application of all the wheel feature limits

In this chapter the influence of wheel and rail profile shape features on the initiation of RCF cracks was evaluated using multibody vehicle dynamics simulations. The damage

index and surface fatigue index were used to assess the influence of the different features.

The purpose of this study was not intended to establish new limits to wheel and rail profile shapes, but rather to understand the influence of the various shapes on RCF initiation. Should the most damaging shapes be avoided or eliminated through maintenance and/or through an improvement in the system, it will result in a reduction of RCF damage.

The features that were studied prove that wheel profiles with concentrated hollow wear resulting in gauge and field side false flanges are prone to initiate RCF damage. The damage parameters showed sensitivity to all the wheel features. The hollow wear position proved to be the most sensitive wheel feature. However, measuring and controlling hollow wear depth remains the most practical method to control RCF initiation. Rail profiles with their gauge corners lower than target afford the underperforming wheels the opportunity to contact the gauge corner and promote RCF initiation. These features should be reduced or eliminated through better designs and maintenance. Such designs could spread the wear across the wheel tread, reducing the formation of concentrated hollow wear. Grinding maintenance of rails should be aimed at improving the rail profile's compliance to the specified target rail profile.

However, the biggest improvement related to RCF initiation could come from improving bogie tracking. The bogie tracking and subsequently the position of the hollow wear is greatly influenced by bogie maintenance and diametrical equivalence of wheelsets. Should the bogie tracking be improved, the position of the hollow wear can be constrained to the wheel taping line and the probability of RCF initiation will be greatly reduced.

According to Ekberg et al. (2014) RCF can be limited if the wheel-rail system as a whole is maintained to suppress the worst operating conditions. Only some of the operating conditions were considered in this study and other contributing factors such as track irregularities should receive attention in an effort to reduce RCF initiation.

Chapter 4: The success of rolling contact fatigue mitigation measures on wheel wear and rail fatigue

4.1 Introduction

The development of RCF has been attributed to contact between the so-called false flanges of the wheels and the gauge corner and field side of the rails (see Fröhling et al., 2008 and Spangenberg et al., 2016). The adverse contact conditions resulting from the false flanges are shown in Figure 1-9.

The use of head-hardened rails to reduce rail wear has become more common on heavy haul railway lines and has exacerbated the effect of RCF in rails. Dikshit et al. (1991) suggested that the higher wear resistance of head-hardened rails causes rails to retain their shape much longer prolonging adverse worn wheel contact with as-ground rail profiles. This wear resistance results in an increase in surface-initiated RCF, because the adverse contact conditions are sustained and the RCF cracks are not naturally worn away. The progression from the wear regime, where rail side wear and wheel flange wear is dominant, to the stress regime, where RCF is dominant, has been discussed by Tournay and Mulder (1996).

Both wear and RCF drive the cost of wheel and rail replacement and maintenance. By using Scheffel's self-steering bogies rail maintenance has shifted its focus from wear to a strategy of balancing wear and RCF. Grinding of rails is thus used to maintain the rail shape and to control surface-initiated RCF. Grinding can however be a costly exercise and excessive grinding will lead to reduced rail life (Evans and Iwnicki, 2002). Rail maintenance costs could thus be lowered by reducing the initiation of RCF and thus increasing the rail grinding interval and ultimately reducing rail replacement costs. A strategy to reduce the occurrence and severity of surface-initiated RCF is therefore sought. This chapter evaluates the effectiveness of two potential RCF mitigation measures: suspension changes that spread wheel wear across the tread and the use of gauge corner relief rail profiles. Multibody dynamics simulations together with a wear prediction algorithm are used to investigate the effectiveness of the mitigation measures, as they pertain to the South African iron ore export line.

4.2 Factors that influence rolling contact fatigue development

Hollow wear of wheels, here defined as is the vertical distance from the worn profile to the original wheel profile at 82.5 mm from the back of the wheel flange, and the subsequent development of false flanges, play a significant role in rail RCF initiation.

The relationship between hollow wear and surface-initiated RCF on rails has been discussed by Tournay and Mulder (1996). A 2 mm hollow wear limit was proposed to reduce contact stresses as well as tangential steering forces. According to the shakedown diagram of Johnson (1989) this will result in a reduction of RCF initiation. This relationship was further investigated by Fröhling et al. (2008), Fröhling et al. (2012) and Karttunen et al. (2014b). These authors highlighted the strong relationship between hollow wear and surface-initiated RCF. Tournay and Mulder (1996) argued that hollow-worn wheels cause contact beyond the hollow wear band increasing the risk of RCF initiation. The severity of RCF damage caused by hollow wear can be linked to the hollow-worn wheel shape (see Fröhling et al., 2012 and Spangenberg et al., 2016). It is therefore important to spread the wear across the wheel tread to maintain its original shape as far as possible and limit false flange formation on worn wheels.

Various bogie and wheel designs have been proposed to spread wear across the wheel tread. Scheffel (1976) argued that the hunting stability could be maintained for longer distances if the wheel profile is not changed much by wear. The original shape of the wheel could potentially be maintained longer by spreading the wear across the wheel tread through bogie and wheel design. Wheel designs capable of spreading wheel wear have been investigated by Shevtsov (2008) and Polach (2011). A change in the transverse stiffness of the primary suspension will be investigated as one of the ways of spreading the wheel wear across the tread and reducing RCF initiation. This is the first method evaluated to reduce RCF initiation.

Anti-head check wheel and/or rail profile designs is a second method used to limit the initiation of RCF. The anti-head check profiles aim at eliminating contact at the locations where RCF cracks are generally observed by removing material at these locations. If there is no material to make contact, there should be no RCF initiation and growth. This school of thought was mentioned by Stow et al. (2011) in the design of the P12 wheel profile and has been applied to wheel profile designs made by Shevtsov (2008) and Shevtsov et al. (2008). Schöch (2011) discusses the application of anti-head check rail profiles in Europe. Anti-head check wheel and rail profiles have been used in Sweden (Persson et al., 2010) and the United Kingdom (Evan and Iwnicki, 2002, Stow et al., 2011 and Iwnicki, 2009). The anti-head check rail profiles have a gauge corner relief up to 0.6 mm (Evan and Iwnicki, 2002 and Schöch, 2011). Evans and Iwnicki (2002) even suggested a larger rail inclination to get more gauge corner relief. Stow et al. (2011) argue that an anti-head check wheel profile, such as the P12 wheel profile, could be applied in addition to anti-head check rail profiles to increase the gap between the wheel and the rail gauge corner. These studies showed that anti-head check profiles could potentially reduce RCF initiation and growth. Two rail profiles with gauge corner relief will be investigated as a second method to reduce RCF initiation. This is the second method evaluated to reduce RCF initiation.

4.2.1 Increasing the transverse primary suspension stiffness

It is well known that RCF initiation is related to curve radius Evans and Iwnicki (2002), Fröhling (2002), Tunna and Urban (2009), Dirks and Enblom (2011) and Karttunen et al.

(2014a), because higher steering forces arise in sharper curves. Scheffel's self-steering bogie design provides a flexible yaw constraint to the wheelset, which allows the wheelset to approach a pure rolling position in curved tracks. This flexible yaw constraint is provided by the primary suspension of the bogie. The self-steering bogie design was proven to have a superior curving ability with reduced flange forces and energy dissipated by slip or creep Scheffel (1978).

Spreading the wheel wear across the tread is one way in which RCF, initiated by concentrated hollow-worn wheels, could be reduced. In principle, the wheel wear can be spread across the tread by reducing the steering ability of the self-steering bogies.

Simulations with increasing suspension stiffness were performed, because the effect of suspension stiffness changes on wear and RCF is unknown. The primary suspension stiffness was increased by a factor of one and a half, two and five, respectively. A stiffness increase by a factor of five approaches the stiffness of a conventional three-piece bogie design.

4.2.2 Wheel and rail profiles

A single wheel profile design and three rail profile designs were used during the simulations. The wheel profile design was a Number 21 wheel profile, which was developed in South Africa to suite the prevailing conditions. The development of this profile is broadly described by Fröhling (2003). The wheel profile is shown and compared to the S1002 wheel profile in Figure 4-1.

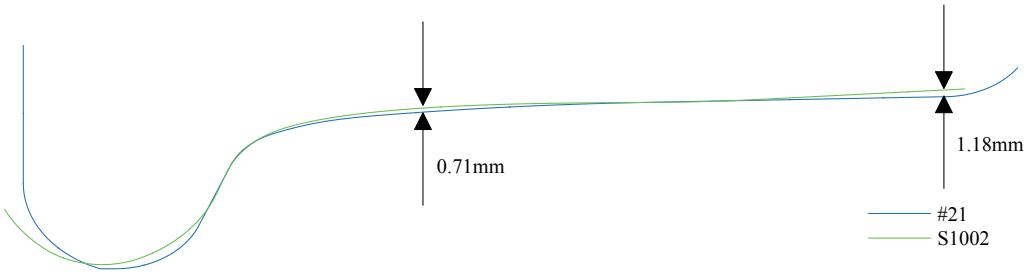

Figure 4-1: Comparison of the Number 21 and S1002 profiles

The three rail profiles included the iron ore line target profile, a knife-edge profile and an anti-head check profile. The iron ore line target profile has a similar shape to the UIC60E1 rail profile inclined at 1:20. However, it has a lower field side than the UIC60E1 rail profile.

The grinding tolerances required on this line are similar to international standards requiring a class Q (European Committee for Standardisation, 2012) reprofiling. The tolerance applied on this line is ±0.3 mm. The way grinding maintenance is performed together with the required grinding tolerance often results in a so-called knife-edge profile. The knife-edge profiles usually comply with the grinding tolerance requirement, but are near the limit. For this investigation, a theoretical knife-edge profile was generated which is close to the target profile's reprofiling limit.

The anti-head check rail profile was based on the UIC60E1 1:20 anti-head check SNCF profile described by Schöch (2011). The profile was generated from the iron ore line target profile by removing 0.6 mm from the profile at -13.4°. The profiles are compared to one another in Figure 3. The profiles were aligned at -2.86° and -45°.

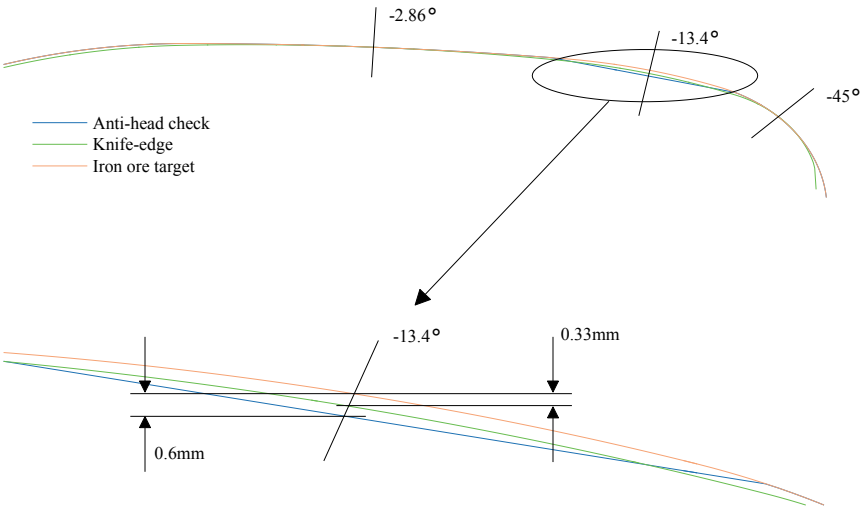

Figure 4-2: Iron ore line target compared to the knife-edge and anti-head check rail profiles

Three different virtual tracks were created for the investigation. One track was created with the iron ore line target applied along the full track length. This track was used for the investigation of the effect of increasing the transverse primary suspension stiffness. Another two tracks were created for the investigation of the gauge corner relief rail profile designs. The first of these tracks had the knife-edge profile applied along the full track length. The second track contained both the iron ore line target profile and the anti-head check rail profile. The anti-head check rail profile was only applied as the high leg profile in curves. The iron ore line target profile was used as the tangent and low leg rail profile.

4.3 Wheel-rail interface damage

Maintenance and replacement costs of wheels and rails are largely determined by wear and RCF. Kimura et al. (2002) analyse and discuss the elemental process that affects wear and RCF. It is noted that the elemental process is similar. Essentially, if wear dominates, RCF is usually reduced and vice versa.

The long-term behaviour of profiles must be evaluated to ensure that a low wear rate and reduced risk of RCF initiation is maintained as suggested by Nia et al. (2015). It has therefore become essential to predict wear and RCF to understand the long-term behaviour of wheel and rail profiles with respect to wear rates and risk of initiating RCF.

4.3.1 Modelling wear damage

VI-Rail's wear toolkit (2014) was used to predict wheel and rail wear. This algorithm is based on the proportionality between the worn material and the energy dissipated during contact. Details of the wear algorithm can be found in paragraph 1.2.3.3. The uncertainty related to the wear coefficient is discussed in paragraph 1.2.3.1.3.

In the following analysis, the wear toolkit within VI-Rail (2014) together with the load collective definition allows the prediction of wheel wear for a CR-13 wagon. Although there are some uncertainties regarding the wear coefficients, a relative or quantitative comparison of wear can be made successfully.

The baseline running distance was defined by the distance that the baseline arrangement (discussed later in Table 4-1) required to reach 2 mm hollow wear. The wear and RCF simulations of the two mitigation measures were repeated until this baseline running distance was achieved. The running distances of the various simulation scenarios were normalised with respect to the baseline running distance as discussed below.

4.3.2 Modelling RCF damage

RCF observed on the iron ore line is confined to the gauge corner of the high rail and field side of the low rail. RCF cracks may grow to such an extent that they may unite, branching across the railhead causing spalling of the rail surface or resulting in a complete fracture of the rail (Johnson, 1989). The greatest concern is the severe RCF damage observed on the high rail of curves on the iron ore export line.

The prediction of surface-initiated RCF cracks was performed by post-processing the dynamic simulation results. The surface fatigue index, as proposed by Ekberg, et al. (2002), was applied to predict the initiation of RCF. The surface fatigue index (FI_{Surf}) is based on the shakedown map as developed by Johnson (1989). The shakedown map consists of the normalised vertical load (ν) on the y-axis and the utilised traction coefficient (μ) on the x-axis. The calculation of the working point on the shakedown map is determined from the normalised pressure and utilised traction coefficient (equation (1-7)). The calculation of the contact pressure is given in equation (1-6) and is normalised by the material's yield strength in cyclic shear (k_e).

The rail material properties used during RCF modelling was that of UIC60 CrMn rails (see Table 3-1). The minimum of the shear yield strength of 553 MPa was used in normalising equation (1-6). All creep forces, lateral and longitudinal, were considered to contribute to RCF initiation. The surface fatigue index was calculated as the shortest distance between the working point on the shakedown map and the shakedown limit. The true distance was calculated to avoid the limitation of the horizontal projection surface fatigue index, which becomes inaccurate at very high utilised traction values and low normalised vertical loads (Ekberg et al., 2002). The initiation of RCF is predicted when the FI_{Surf} value exceeds zero.

4.4 Methods

The two RCF mitigation measures together with their subcases that are evaluated to reduce RCF initiation are summarised in Table 4-1. The study of the two RCF mitigation measures is performed through multibody vehicle dynamics simulations. Wheel wear is predicted from these simulations to study the effects each of these measures have on the worn profile shape, the wear rate and RCF initiation.

Table 4-1: Summary of the baseline and two RCF mitigation measures

RCF mitigation measure	Subcase	Rail profile	Wheel profile
Baseline	Baseline	Iron ore target	#21
1. Increase transverse primary suspension stiffness	Stiffness x1.5	Iron ore target	#21
	Stiffness x2	Iron ore target	#21
	Stiffness x5	Iron ore target	#21
2. Gauge corner relief rail profile design	Knife-edge	Knife-edge design	#21
	Anti-head check	Anti-head check design	#21

4.4.1 Vehicle dynamics analyses

A vehicle model of a CR-13 type iron ore wagon was used to predict both wear and RCF during the wear life of the wheel. This vehicle model is described in chapter 2 and was used during the investigation. A fully loaded wagon was considered during the analysis. The analysis process started with a dynamic analysis being performed during which the wheel profile wear was calculated and the profile updated. The first dynamic analysis constituted the wear simulation. The wheel profiles therefore regularly changed during this dynamic analysis and subsequently influenced the vehicle's dynamic behaviour and contacting forces. The wear simulation was followed by a second dynamic analysis that used the wheel profiles generated during the wear simulation. The results from the second dynamic analysis were used to predict RCF initiation. This second dynamic analysis constituted the RCF simulation and the analysis process ended with the RCF prediction. Once the wear and RCF simulations were completed, the analysis process would be repeated until a predetermined travelling distance was reached. The predetermined travelling distance was taken as the distance the baseline arrangement would need to reach the 2 mm hollow wear limit.

4.4.2 Load collective design

Fröhling (2002) and Jendel (2002) discussed the importance and definition of a representative load collective for wheel wear predictions. The load collective generally includes a representation of the track layout, traffic conditions, wheel-rail profiles, coefficient of friction, track irregularities as well as vehicle braking and traction. There are many simplifying assumptions that can be made during the load collective design to ensure faster solution times while maintaining accurate wear predictions. The assumptions made by Fröhling (2002), Enblom and Berg (2005), Jendel (2002) and Jendel and Berg (2002) were considered when the load collective was designed.

Track layout: A single representative track of the iron ore line was built and all the simulations were performed on this virtual track. The total track length was 8 696 m with a 40 m run-in and 320 m run-out section at the start and end of the track, respectively. The curves had a 60 m long transition curve. A representation of the virtual track layout is shown in Figure 4-3(a).

Super-elevation: The super-elevation or cant was assumed to be constant within a curve and is shown in Figure 4-3(b). The relevant super-elevation was selected from Transnet Freight Rail's rail maintenance manual (Marutla et al., 2012).

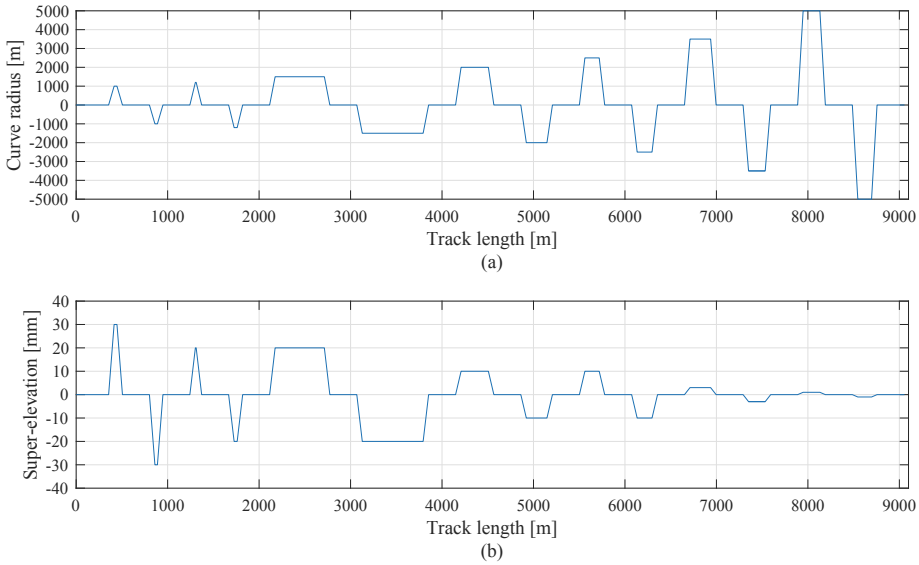

Figure 4-3: Representative (a) track layout and (b) super-elevation of the iron ore line

Track Gauge: The track gauge on the iron ore line is nominally 1065 mm. The track gauge is widened by 5 mm in curves and in 30 % of the tangent track it is widened by 10 mm to apply pummeling as described by Magel and Kalousek (2002).

Traffic conditions: The CR-13 type wagons run solely on this line. The wagons are periodically turned around and track symmetry can be assumed (see Fröhling, 2002 and Nia et al., 2015). Based on the assumption of symmetry, the wear on the left and right wheels of the outer axles are expected to be similar. Similarly, the left and right wheels of the inner axles are expected to experience the same amount of wear. The wheel wear experienced by the four wheels on the outer axle and the four wheels on the inner axle was accumulated, producing two individual worn profiles. These worn profiles were used during the succeeding RCF or wear simulation.

Wheel profiles: The wheel and rail profile designs are discussed in detail in paragraph 4.2.2. The original wheel profile used during simulations was the South African Number 21 wheel profile.

Rail profiles: Rail designs included the iron ore line target rail profile, a pronounced crown or "knife-edged" profile and an anti-head check profile.

Coefficient of friction: A constant coefficient of friction of 0.4 was used and lubrication was not considered.

Track irregularities: Measured track irregularities of a single representative section of the iron ore line track was used during all the simulations.

Vehicle speed and braking: A constant vehicle speed of 60 km/h was maintained during the simulations. The effect of braking was not considered.

Contact algorithm: The FASTSIM contact algorithm was applied during the dynamic simulations.

Wear data sampling: The wear algorithm sampled data every metre.

4.5 Results of wear and RCF damage prediction

The two RCF mitigation measures were evaluated and compared to the baseline arrangement. The wear rates and potential to initiate RCF were examined to evaluate the success of the RCF mitigation measures while maintaining a low wear rate. The wear results shown in the discussions on wear are associated with the wear of the outer axles. The results for the inner axles are not shown, but illustrated similar wear behaviour.

4.5.1 Wear algorithm verification

The wear algorithm of VI-Rail (2014) was verified by comparing the predicted worn profile of the baseline simulation displaying approximately 2 mm hollow wear with measured wheel profiles (Figure 4-4(a)). The wagon numbers and wheel numbers of the measured wheels are indicated in the legend. The running distances of the wheels were not compared, since the wear coefficients were not tuned for the wheel and rail materials and simulation conditions. The profile wear is compared quantitatively in Figure 4-4(b). It shows that the simulated and measured profiles are similar between -25 and 10 mm. The biggest differences in profiles occur at the gauge side and field side false flanges, respectively at -38 and 20 mm. The difference at the gauge side false flange can be attributed to the exclusion of worn rail profiles during the wear simulations. The same argument can be made regarding the field side false flange. The exclusion of switches and crossings in the load collective has been discussed by Nia et al. (2015). This exclusion, could partially account for the limited field side wear and large differences between the simulated and measured profiles at the field side false flange.

A second verification was performed with a similar load collective design as described for the iron ore export line, but the track layout was changed to that of the South African coal export line. The predicted worn profile with approximately 1.5 mm hollow wear is compared to a measured wheel profile with 2 mm hollow-worn wheels in Figure 4-5(a). The worn wheel profile comparison in Figure 4-5(b) shows a constant offset of 0.5 mm. Similar differences to the wheel profile worn by the iron ore target profile are noticeable at the gauge and field side false flanges, respectively at -44 and 25 mm. The difference at

the false flanges can be attributed to the exclusion of worn rail profiles as well as switches and crossings. The similarities in wear amounts across the hollow wear band in both cases show that the wear algorithm performs reasonably well.

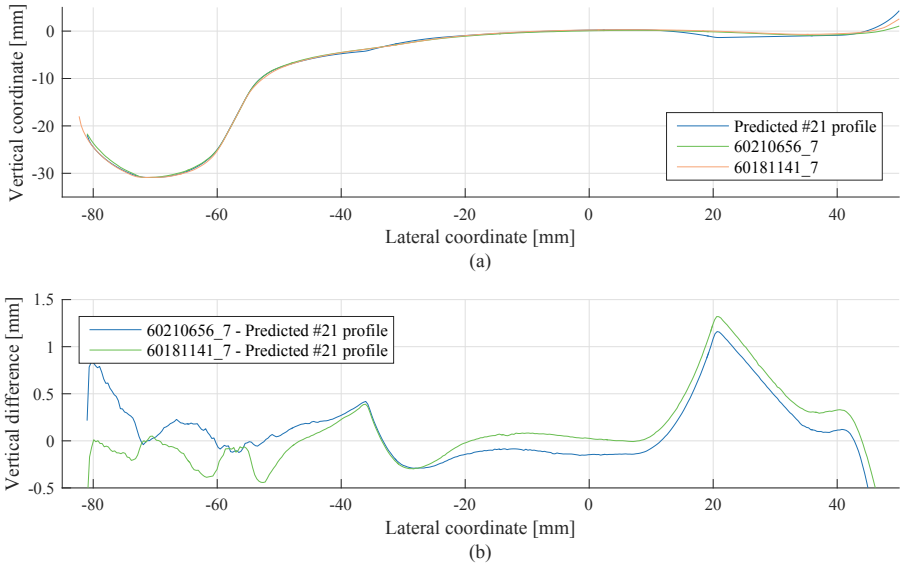

Figure 4-4: Comparison of wheel wear of a Number 21 wheel profile and measurements (a) profiles and (b) vertical differences

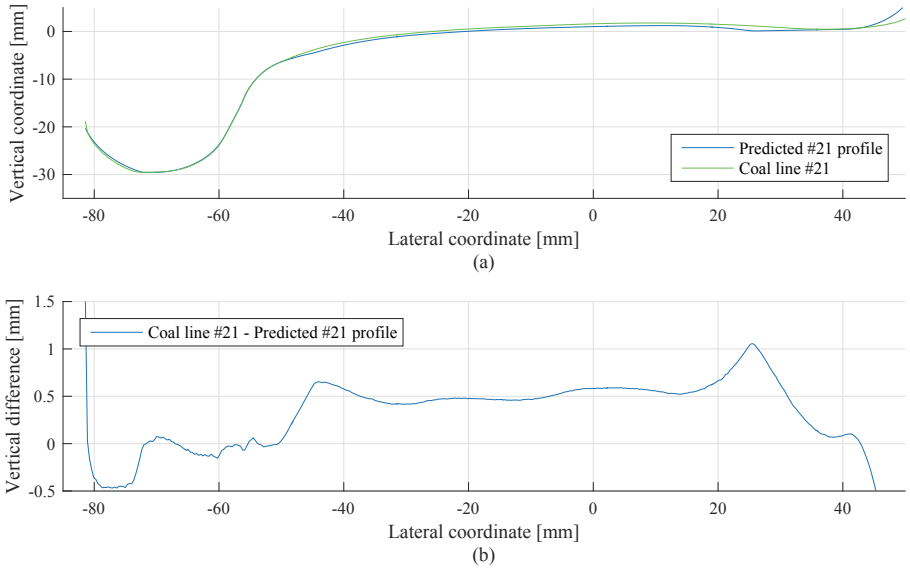

Figure 4-5: Comparison of wheel wear of a Number 21 wheel profile and coal line measurement (a) profiles and (b) vertical differences

4.5.2 Wear as a result of suspension stiffness changes

The influence of an increase in the transverse stiffness of the primary suspension has on the wheel wear was investigated by increasing the stiffness by a factor of one and a half, two and five. The worn wheel profiles that were predicted for these suspension changes are shown in Figure 4-6(a).

The constant vertical difference in the hollow wear bands indicate that the hollow-worn shapes in the centre of the wheel tread are all similar (Figure 4-6(b)). There is only a slight increase in the hollow wear spread when the primary suspension stiffness is increased. Even if the primary suspension stiffness is increased to five times the baseline stiffness, the wear is only spread between -42 and 25.5 mm. This primary suspension stiffness approaches the stiffness of a conventional three-piece bogie. All the worn profiles show false flange formation. The shape of the false flanges becomes more pronounced with an increase in primary suspension stiffness.

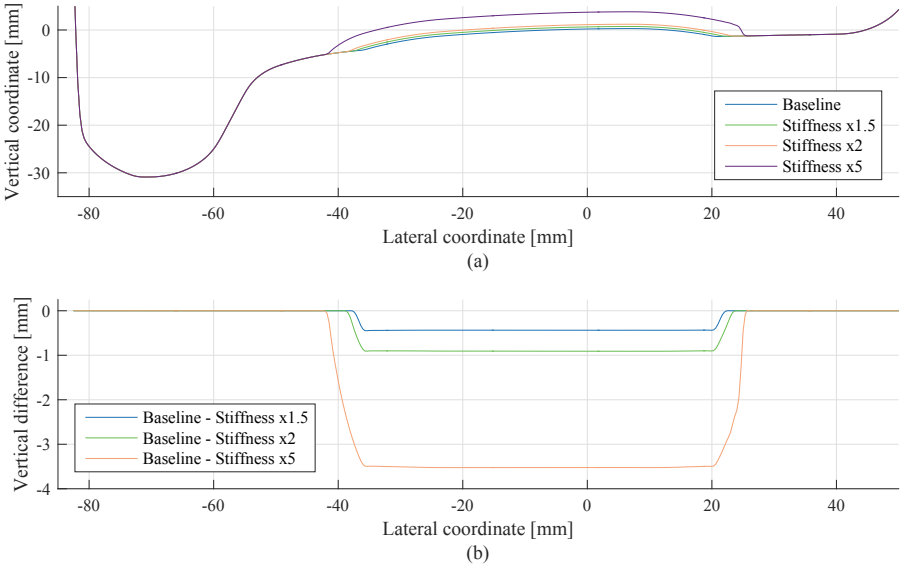

Figure 4-6: Wheel wear predictions as a function of suspension stiffness (a) profiles and (b) vertical differences

The disadvantage of increasing the primary suspension stiffness is evident from Figure 4-7 (a). As the primary suspension stiffness is increased, the area that is worn off becomes larger. This increase in worn-off area is not only due to the spread of wear across the tread, but the depth of wear also increases. This wear depth is reflected in the comparison of hollow wear depth (Figure 4-7(b)). The distance travelled to reach the 2 mm hollow wear limit is progressively reduced. The distances travelled to reach this limit are equal to 79 %, 67 % and 37 % of the baseline distance for increasing suspension stiffness by a factor of one and a half, two and five respectively. Therefore, any change in primary suspension stiffness will cause not only a spread in wear, but also an increase in the hollow wear rate. The wear life of the wheel profiles is reduced by increasing the primary suspension stiffness. This in turn will result in increased wheelset reprofiling

and replacement costs. This increase in hollow wear rate is thus unwanted. The low wear rate of the baseline suspension stiffness emphasises the use of Scheffel's original self-steering design instead of a conventional three-piece bogie design.

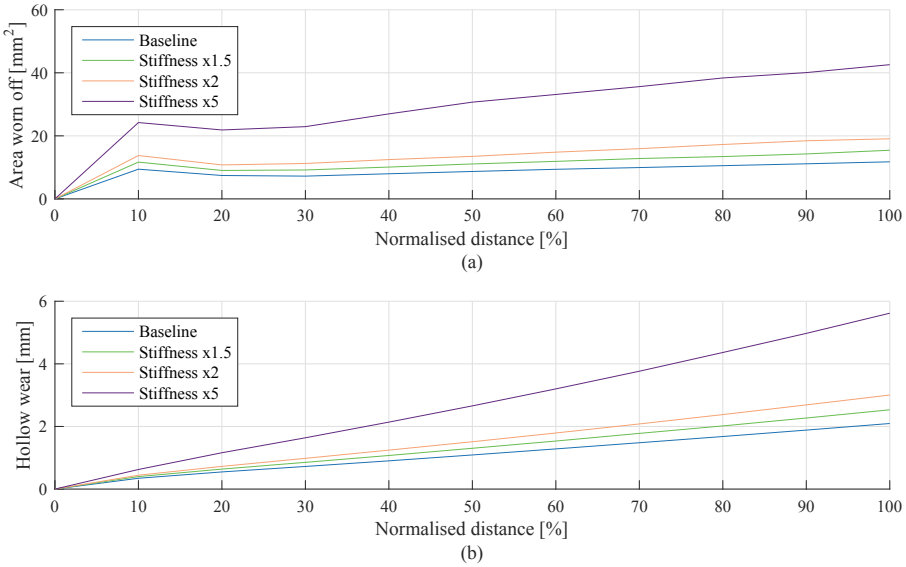

Figure 4-7: Suspension stiffness induced wear progression with (a) area worn off and (b) hollow wear

4.5.3 Wheel wear caused by rail profiles with gauge corner relief

The influences of rail profile changes on the worn wheel profile shapes were analysed using the iron ore line target, the knife-edge and the anti-head check rail profiles. The worn wheel profiles that were predicted for these rail profile changes are shown in Figure 4-8(a). Note that the worn wheel profile caused by the anti-head check rail profile is shown after 80 % of the baseline distance. This profile could not reach the full baseline distance, because the worn off area became too severe (Figure 4-9(a)).

The hollow-worn shapes of the wheel profile produced by the baseline and knife-edge profile differ significantly at the centre of the wheel tread (Figure 4-8(b)). The hollow wear is more pronounced with the knife-edge profile.

The worn wheel profiles produced by the baseline and anti-head check profiles are similar at the centre of the tread. This can be attributed to the fact that the tangent rail profile remained the same for the baseline and anti-head check wear simulations. The only difference was at the high leg of the curves and even then, the gross part of the profiles was similar with only the gauge corner being lowered. The influence of the gauge corner relief is evident from the large variations at the false flanges located at -36 and 20 mm.

For the knife-edge profile the same wear pattern of worn wheel profiles is observed as those produced by the anti-head check profiles at the false flanges. This can mainly be

attributed to the relief at the gauge corner of both rail profiles as it will require larger lateral displacement of the wheelset to steer around the curves. The wheel will have more contact at the false flanges, wearing the false flanges away. This will effectively smoothen out the shape of the pronounced false flanges. The findings of chapter 3, Spangenberg et al. (2016) and Fröhling et al. (2012) suggest that the worn wheel shape produced by the knife-edge and anti-head check rail profiles may thus be less conducive to RCF initiation. This could explain why maintenance personnel prefer the use of rail profiles with relief at the gauge corners.

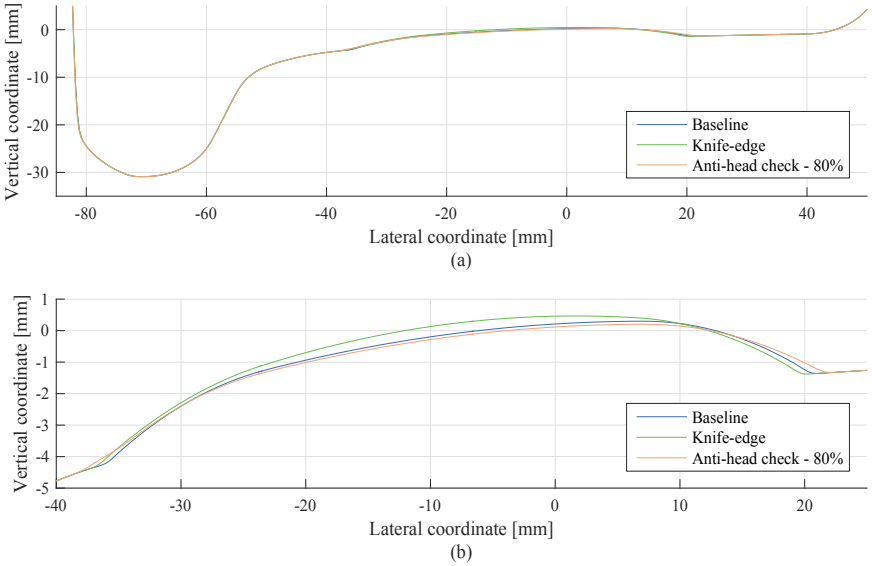

Figure 4-8: Wheel wear predictions as a function of rail profile changes, (a) profiles and (b) zoomed hollow wear band

The wear performances of the wheels caused by the different rail profiles are shown in Figure 4-9. The wheel wear rates produced by the knife-edge and anti-head check rail profiles are on average higher than the baseline. This will have a significant influence on the hollow wear rate as shown in Figure 4-9(b). The knife-edge and anti-head check profiles reach the hollow wear limit at 86.8 % and 80 % of the baseline distance respectively. If these rail profiles are used, the wear life of the wheel profiles will therefore be reduced, increasing the wheelset reprofiling and replacement costs.

The wheel profile wear caused by the anti-head check rail profile increased dramatically beyond 80 % of the baseline distance (see Figure 4-9(a)). The anti-head check wheel profile results at 80 and 90 % of the baseline distance are compared in Figure 4-10. It can be seen that the false flanges have been worn off, indicating that the wheel had to run on the false flanges during the wear simulation. When running on the false flanges the normal contact pressure will increase because of the reduced contact area and higher longitudinal creep forces are generated due to a larger rolling radius differential. According to the shakedown map an increase in the normal contact pressure and increased longitudinal creep forces will result in more severe rail RCF.

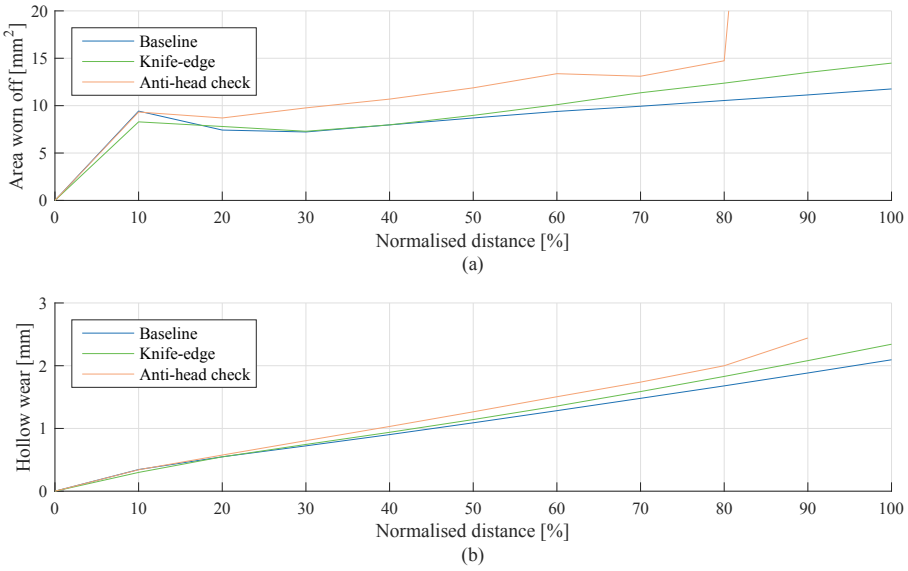

Figure 4-9: Rail profile induced wear progression with (a) area worn off and (b) hollow wear

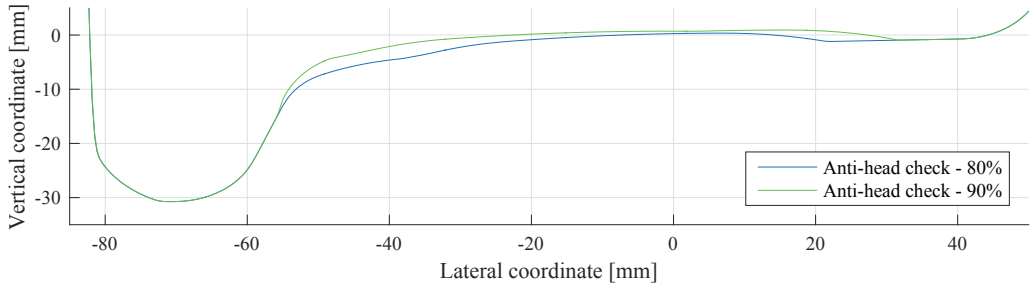

Figure 4-10: Wheel wear predictions of the anti-head check rail profile at 80 and 90 % of the baseline distance

Pearce and Sherratt (1991) showed the importance of wheel wear calculations to understand the evolution of the equivalent conicity. The dramatic increase in tread wear can be explained when evaluating the rolling radius difference and equivalent conicity of the worn wheel profiles that are produced by the anti-head check rail profiles at various stages of wear (see Figure 4-11). The rolling radius difference and the equivalent conicities of the worn wheel profiles produced by the anti-head check rail profiles were calculated with the ore line target as the low rail profile and the anti-head check rail profile as the high rail profile. A positive lateral displacement indicates that the wheel flange moved closer to the gauge corner of the high rail. A discontinuity in the rolling radius difference graph becomes more severe with an increase in wheel wear (Figure 4-11(a)). The equivalent conicity graph of Figure 4-11(b) shows that the wheelset is unstable at a lateral amplitude of 0 mm, becoming more stable at 3 mm. The discontinuity in the rolling radius difference causes an increase in the equivalent conicity between 3 and 5 mm.

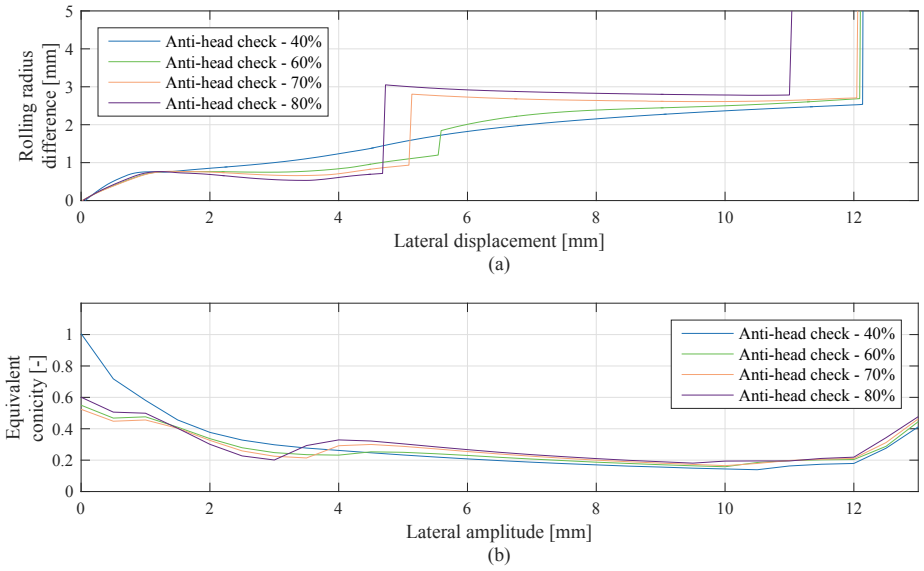

Figure 4-11: Comparison of the anti-head check wheel profiles' (a) rolling radius differences and (b) equivalent conicities as a function of travelling distance

The simulations have shown that the MkV self-steering freight bogies require approximately a rolling radius difference of 1.1 mm to steer around a 1 000 m radius curve. The profile at 80 % of the baseline distance would not allow the wheel and rail profiles to achieve this rolling radius in a 1 000 m radius curve at a lateral displacement before the discontinuity. The wheel will thus attempt to reach this required rolling radius by displacing laterally beyond the discontinuity. However, due to the sharp increase in the rolling radius and equivalent conicity, it will steer away from this discontinuity, reducing its lateral displacement. It will keep oscillating on this rolling radius discontinuity to traverse the 1 000 m radius curve. Due to the large longitudinal and lateral steering forces generated during these oscillations the wheel wear will increase, wearing the false flanges away. This will result in a sharp increase in the wear rate. This type of oscillation together with large steering forces and contact at the false flanges are observed in-field as oscillating RCF cracks on the high rail as shown in Figure 4-12.

The false flange wheel wear will cause a decrease in the equivalent conicity. The decrease in the wheel's equivalent conicity, together with the equivalent conicity decrease enforced by the anti-head check rail profile (Stow et al., 2011), cause the wheel to contact over a wider area. Wear will be spread across a wider band during further curve negotiations. This is evident from the initiation of flange wear of the wheel profile at 90 % of the baseline distance (Figure 4-10). In-service rail profiles do not show such severe gauge corner relief as that of the anti-head check rail profile and thus such severe wheel wear is not observed on in-service wheels. However, such a severe increase in wheel wear after a certain distance could be a major disadvantage of the anti-head check rail profiles.

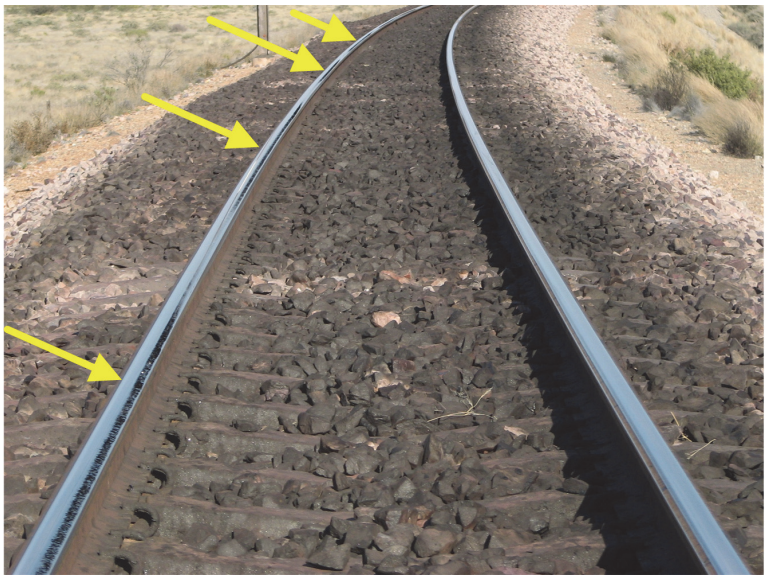

Figure 4-12: Oscillation of RCF observed in-field

4.5.4 Evaluation of RCF mitigation measures with worn wheels

The long-term RCF performance of the two RCF mitigation measures needs to be evaluated to ensure that the probability of RCF initiation is reduced. The potential to initiate surface RCF is evaluated from the dynamic simulations of the worn wheels at different stages of wear while travelling the equivalent of the baseline distance. The probability of initiating RCF was only evaluated on the high rail in curves. Since the left and the right wheel on the same axle experienced the same amount of wear, the RCF data is reported per axle. The long-term RCF performance is evaluated from the cumulative distribution function (CDF) of the FI_{Surf} values as shown in Figure 4-13. It should be noted that the rail profiles used during the RCF study are unworn. Figure 4-13 and Figure 4-14 include the dynamic simulation results of the wheel profiles produced by the anti-head check rail profile up to 80 % of the baseline distance, since the wear and worn shape changed significantly after this distance.

The baseline arrangement shows the lowest FI_{Surf} values over its running distance. The worn wheel profiles produced by the anti-head check rail profiles have the worst RCF performance on all the axles. This confirms the finding of Stow et al. (2011) that RCF damage returned to sites with anti-head check rail profiles after a moderate amount of tonnage, since the worn wheel profiles could contact the anti-head check rail profile. When the anti-head check results are ignored, it can be seen that contact conditions produced by the wheel profiles worn by the knife-edge rail profiles are much worse than the contact condition produced by the worn wheel profiles produced by the baseline and the change in suspension stiffness by a factor of two. This can be attributed mainly to the rail profile being more pronounced, which reduces the size of the contact patches relative to those of the ore line target profile. The knife-edge wheel profile is less suitable to reduce RCF initiation than the baseline arrangement.

The wheel profile resulting from a stiffness change by a factor of two performs similar to the baseline arrangement. Once the CDF of Figure 4-13 is zoomed in the vicinity where RCF initiation is predicted, it is revealed that the wheel profile produced by the anti-head check rail profile exceeded the threshold at axles one and three (Figure 4-14). This shows that the wheel profile produced by the anti-head check rail profile will produce RCF initiation with unworn rail profiles. This analysis shows that the RCF performance of the wheel profiles produced by the baseline and a factor of two increase in suspension stiffness, are desired.

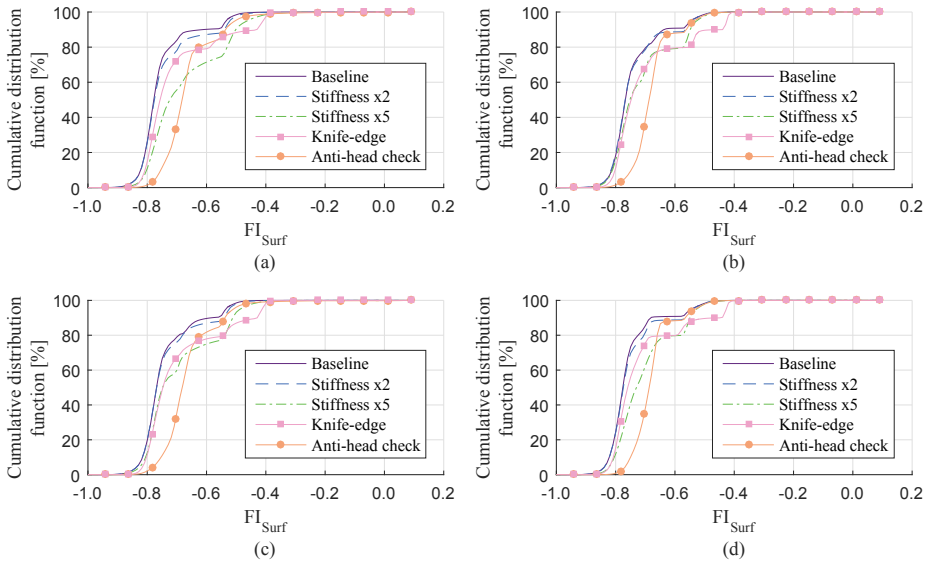

Figure 4-13: Cumulative distribution functions showing long-term RCF performance of RCF mitigation measures on (a) axle one, (b) axle two, (c) axle three and (d) axle four

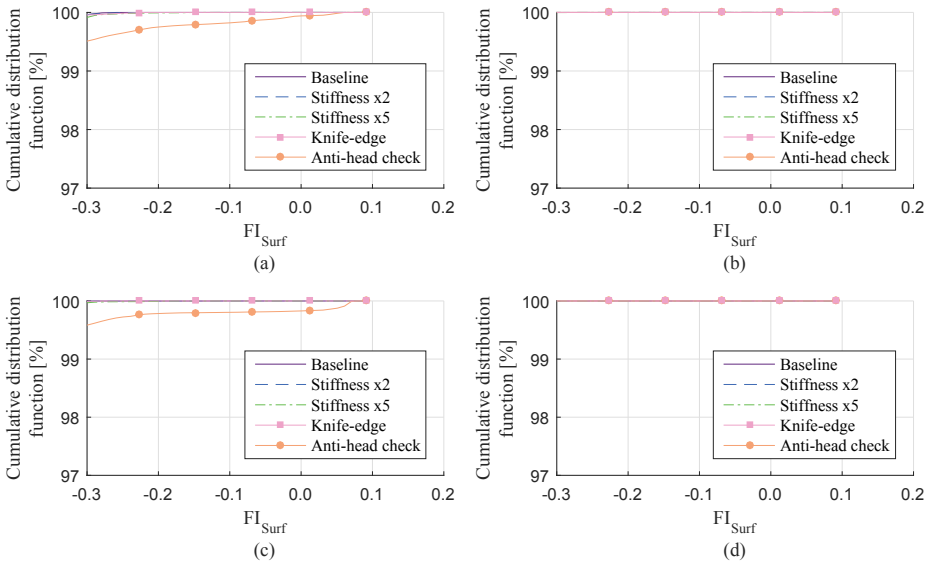

Figure 4-14: Zoomed cumulative distribution functions showing long-term RCF performance of RCF mitigation measures on (a) axle one, (b) axle two, (c) axle three and (d) axle four

4.6 Conclusion

The wear and RCF performances of wheel profiles produced when applying two RCF mitigation measures have been studied. The worn wheel profiles produced by the RCF mitigation measures all resulted in a concentrated hollow-worn shape. None of these mitigation measures resulted in the wear being spread more evenly across the tread, reducing the prevalence of false flanges. The wear and RCF performance of two RCF mitigation measures are summarised in Table 4-2.

Table 4-2: Wear and RCF performance of RCF mitigation measures compared with the baseline arrangement

RCF mitigation measure	Subcase	Wear performance	RCF performance
1. Increase transverse primary suspension stiffness	1.1. Stiffness x1.5	Increased wear rate	-
	1.2. Stiffness x2	More severe wear rate	Similar
	1.3. Stiffness x5	Most severe wear rate	Worse
2. Gauge corner relief rail profile design	2.1. Knife-edge	Increased wear rate	Worse
	2.2. Anti-head check	Increased wear rate	Significantly worse

If the stiffness of the primary suspension is increased, the wheel wear will be spread slightly more across the tread. However, the reduction in the wheel's wear life resulting from these suspension changes, is unwanted. Suspension stiffness changes up to a factor of two showed similar RCF behaviour compared with the baseline arrangement. Once the suspension stiffness was increased by a factor of five, approaching that of a conventional three-piece bogie, the RCF performance worsened significantly. The change in suspension stiffness is therefore ruled out as a RCF mitigation measure.

The two rail profiles of the gauge corner relief rail profile designs proposed as a mitigation measure, both showed a reduced wheel wear life. This reduction in wheel wear life is unwanted, since the aim is to maintain the baseline's wheel wear life, while reducing RCF initiation. The RCF performance of these two subcases did not present an improvement over the baseline arrangement. In fact, the wheel profile produced by an anti-head check rail profile had the worst RCF performance.

Both RCF mitigation measures are ineffective at spreading the wheel wear and reducing RCF initiation. Subsequently maintenance costs of wheels and rails will not be reduced by any of these RCF mitigation measures. The baseline arrangement showed that the current operating conditions on the iron ore line are better in terms of its wear and RCF performance compared with the two RCF mitigation measures. However, this baseline condition is still far from the optimum when RCF is concerned, since RCF is widespread on this line.

4.7 Recommendations

To reduce the occurrence and propagation of RCF cracks, more conformal wheel and rail profiles are required that would spread the wheel wear across its tread, reducing the adverse false flange contact conditions. However, since changes to the rail profile are expensive to implement, it is recommended that a conformal wheel profile should be

developed. An increase in the suspension stiffness should not be considered, as it will reduce the wheel's wear life.

Chapter 5: Long-term wear and rolling contact fatigue behaviour of a conformal wheel profile designed for large radius curves

5.1 Introduction

A redesign or optimisation of the wheel-rail interface is one of the ways in which a reduction in wear and RCF initiation can be achieved (Lundén and Paulsson, 2009 and Grassie, 2009). An investigation into the primary drivers of RCF on the iron ore line was performed in chapter 3, by Fröhling et al. (2012) and Spangenberg et al. (2016). These studies together with the study by Karttunen et al. (2014) found that surface-initiated RCF is sensitive to the hollow-worn shape of the wheel and the position of hollow wear relative to the taping line of the wheel.

Based on the findings of chapter 3 and 4 the control of the worn shape of the wheel is paramount. The current chapter evaluates the long-term effectiveness of a conformal wheel profile design in maintaining a more favourable worn shape and reducing the initiation of RCF cracks.

5.2 Wheel profile design considerations

5.2.1 Two-point vs. conformal contact

When wheel and rail profiles are designed or maintained to reduce RCF initiation, there are generally two schools of thought. The first aims at eliminating contact at the locations where RCF is generally observed by removing material from the wheel and/or rail at these locations. This concept is based on the assumption that should there be no material to contact, then there should be no RCF initiation. The second school of thought relies on the fact that single point conformal contact could be used to increase the steering ability of the wheelset, thus lowering lateral wheel-rail interaction forces, lower curving resistance and increase wheel-rail contact areas to reduce contact stresses (Wu, 2006).

5.2.1.1 Anti-head check profile designs

The use of anti-head check profiles is mentioned by Stow et al. (2011) in the design of the P12 wheel profile. The anti-head check design intent is applied by Shevtsov (2008) and Shevtsov et al. (2008) to design a wheel profile capable of reducing RCF. Anti-head check rail and/or wheel profiles have also been used in Sweden (Persson et al., 2010) and the

United Kingdom (Evans and Iwnicki, 2002; Iwnicki, 2009; Stow et al., 2011). These studies have shown that anti-head check profiles can effectively reduce RCF initiation and growth. However, these anti-head check profiles cause a reduction in conicity and impede wheelset steering. This leads to the wheelset steering with two-point flange contact. Consequently, lubrication has to be applied to reduce rail side wear and wheel flange wear (Stow et al., 2011; Evans and Iwnicki, 2002).

A wheel subjected to a large amount of flange wear requires more material removal to restore its profile (Figure 1-5(a)). Wheels that are only exposed to tread wear require less material removal to restore the design profile (Figure 1-5(b)). Flange wear caused using anti-head check profiles is thus one of the main drawbacks.

5.2.1.2 Conformal profile designs

Wheel profile designs promoting single point conformal contact have thus been proposed to increase the steering ability of wheelsets leading to a reduction in wheel flange wear. The advantages of using wheel and rail profiles promoting conformal contact is mentioned by several authors including Tournay (2001), Fröhling (2002), Kalousek (2005), Zarembski (2005) and Wu (2006). These advantages include better steering of wheelsets, reducing lateral track forces, lowering rolling resistance, increasing the spread of contact points across the wheel tread, lowering contact stresses, reducing the spread of rolling radius differences across the wheel fleet and reducing the rate of rail profile change caused by wear. Enblom (2009) argued that conformal contact reduces the risk of RCF initiation similar to works of Fröhling (2003) and Wu (2006).

Scheffel (1974) and Kalousek (2005) discussed the concept of perfect curving of a bogie. Here the bogie exploits the steering ability of the wheelset to reduce wheel flange wear and rail side wear. Under perfect curving conditions the steering forces are minimised since the wheelset is allowed to approach its pure rolling position with low steering forces. Scheffel (1974, 1976) recognised the advantages of conformal wheel profiles and developed a self-steering bogie that is capable of stable running with such profiles. Accordingly, self-steering bogies running with conformal wheel profiles will allow the worn shape of the wheelset and equivalent conicity to be maintained over longer distances due to the reduction in both wheel tread and flange wear.

Conformal wheel-rail profile designs offer more advantages compared with anti-head check profile designs. The main advantages include the reduction of flange wear and increased steering ability. The net effect of these advantages may ultimately result in a reduction of RCF initiation.

5.2.2 Wheel-rail kinematics

The minimum curve radius that a vehicle can negotiate without making flange contact is determined by its suspension design and the prevailing rolling radius differentials which are related to the equivalent conicity. Higher equivalent conicities allow the navigation of smaller radii curves without flange contact. The trade-off between curving performance and stability should be considered carefully when designing wheel and/or rail profiles

(Bruni and Braghin, 2009). Pearce (1996) has shown that wear, concentrated in the centre of the profile, leads to high conicities. When the wear is spread across the profile it results in more stable conicities. Thus, not only should the equivalent conicity of the unworn profiles be considered to provide steering without flange contact, but the equivalent conicity that may result due to wear also needs consideration. The study of the wheel and rail kinematic response is therefore invaluable during the redesign of such contacting profiles. In the current study the wheelset's kinematic response and contact parameters are calculated with the code RSGeo (2011).

5.2.3 Optimisation of wheel-rail profile designs

There are many reasons that drive railways to optimise the wheel-rail interface through redesign or maintenance. Some of the main reasons are maintaining a low to medium equivalent conicity through the lifetime of the wheel, increasing safety against derailment, minimising wear and RCF initiation on either wheel or rail or both (Grassie, 2009). Magel and Kalousek (2002) described that this can be achieved by sustaining low contact stresses, avoiding closely conformal profiles, providing a rolling radius difference appropriate to the track's curve distribution, ensuring that the equivalent conicity is within the stable envelope of the bogie and distributing the contact positions across the wheel tread.

Many authors have applied numerical optimisation to the wheel profile design process (Smallwood et al., 1991; Shevtsov et al., 2005; Shevtsov et al., 2008; Persson et al., 2010). Though experience is also being applied in the development of new wheel profile designs (Fröhling, 2003; Kalousek, 2005). Various other experience based design methodologies have been developed to reduce the time spent designing new profiles. Leary et al. (1991) designed wheel profiles based on two different approaches. Firstly, by averaging worn profiles and secondly, through expansion of the rail profile. Zobory (1997) derived a formulation that could be used to optimise wheel profiles. Shevtsov (2008) described an optimisation method that can be applied to design new wheel and/or rail profiles using the rolling radius difference (RRD) function. Polach (2011) developed a wheel profile design procedure intended to spread wheel tread wear. Dede et al. (2015) describe an optimal wheel profile design procedure that produces conformal wheel profiles with a rolling radius function suited to the track's layout while producing minimal wear.

Mathematical optimisation presents an attractive alternative to the experience based design of new profiles, though it requires a comprehensive definition of the cost function and constraint boundaries to arrive at a meaningful result. Therefore, engineering experience is considered in this investigation.

The redesign of the wheel profile was chosen to achieve conformal contact, since the wheel profile can be controlled accurately during machining, wheels are reprofiled more often than rails (Shevtsov, 2008) and a sudden change in rail profile may lead to unacceptably high contact stresses.

5.3 Wheel-rail interface damage

5.3.1 Modelling wear damage

VI-Rail's wear toolkit (2014) was used to predict wheel and rail wear. This algorithm is based on the proportionality between the worn material and the energy dissipated during contact. Details of the wear algorithm can be found in paragraph 1.2.3.3. The uncertainty related to the wear coefficient is discussed in paragraph 1.2.3.1.3.

In the following analysis, the wear toolkit within VI-Rail (2014) together with the load collective definition allows the prediction of wheel wear for a CR-13 wagon. Although there are some uncertainties regarding the wear coefficients, a relative or quantitative comparison of wear can be made successfully.

5.3.2 Modelling RCF damage

RCF observed on the iron ore line is confined to the gauge corner of the high rail and field side of the low rail. The greatest concern is gauge corner RCF cracks on the high rail, since RCF cracks may grow, unite and branch across the railhead leading to spalling of the rail surface or even result in a rail break (Johnson, 1989).

In this study the prediction of surface-initiated RCF cracks is performed by post-processing the dynamic simulation results. The results within the curves are extracted and used in the RCF prediction. The shakedown diagram, as developed by Johnson (1989), is used to predict RCF initiation. The calculation of the working point on the shakedown map is determined from the normalised pressure and utilised traction coefficient (equation (1-7)). The calculation of the contact pressure is given in equation (1-6) and is normalised by the material's yield strength in cyclic shear. The rail material properties used during RCF modelling was that of UIC60 CrMn rails (see Table 3-1). The minimum of the shear yield strength of 553 MPa was used in normalising equation (1-6). All creep forces, lateral and longitudinal, were considered to contribute to RCF initiation. The surface fatigue index (FI_{Surf}) proposed by Ekberg et al. (2002) is based on the shakedown limit line. Shakedown maps together with lines of constant FI_{Surf} values are used during the RCF performance evaluation.

5.4 Method

5.4.1 Wheel profile design

The iron ore line is relatively straight with approximately 67 % tangent track and a minimum curve radius of 1 000 m. Concentrated hollow wheel wear is caused by the combination of the topography of this line and the self-steering bogies together with the wheel-rail profiles. The current Number 21 wheel profile used on this line is broadly described by Fröhling (2003). The target rail profile design used on the iron ore line has a

similar shape to the UIC60E1 rail profile inclined at 1:20, although it has a lower field side than the UIC60E1 rail profile. The current wheel and rail profile designs are not conformal.

Vehicle dynamics simulations have shown that the self-steering bogie requires a rolling radius difference of approximately 1.1 mm to negotiate a 1 000 m radius curve. The rolling radius difference of the current design is not adequate and thus the wheelset requires 9 mm lateral movement to achieve steering without flanging (as shown in Figure 5-4(a)). The contact positions are not spread across the tread when only displaced laterally by 9 mm laterally, increasing the concentration of hollow wear (see Figure 5-1).

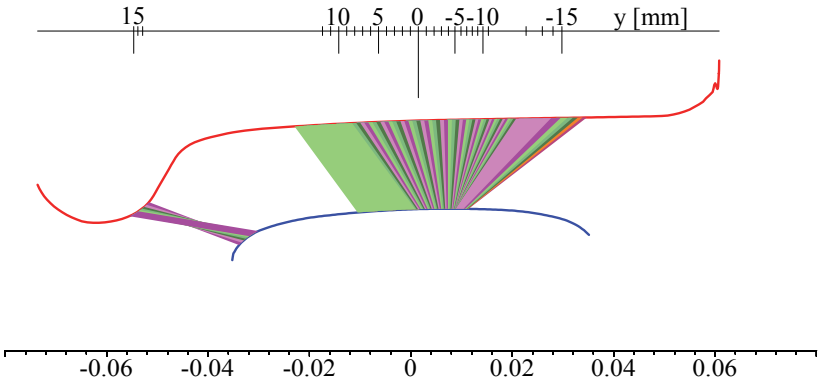

Figure 5-1: Contact distribution of Number 21 wheel profile and ore line target profile

The full potential of a conformal wheel-rail combination that spreads wear across the tread together with the low steering forces of the self-steering bogie can currently not be realised on the iron ore line, since the main wear mode is concentrated hollow wear. The effect which a conformal wheel-rail pair combined with a self-steering bogie has on the wear life of the wheel and initiation of rail RCF thus needs to be evaluated.

The conformal wheel profile design is based on the method proposed by Polach (2011). A conical profile section with a 1:100 inclination was added from the taping line to the field side. The field side radii and flange section of the Number 21 wheel profile was retained in the new design. This design methodology led to a profile with a steep rolling radius difference function. This initial profile design was then refined to lower the rolling radius difference function but still achieve the required 1.1 mm rolling radius difference when the wheel is laterally displaced by approximately 8 mm. Mathematical optimisation was used to increase the contacting areas while maintaining the rolling radius difference of the refined design. The resulting profile is compared with the Number 21 wheel profile currently used on the iron ore line and the S1002 wheel profile (see Figure 5-2).

The improved spread in the contact areas across the wheel tread is evident from Figure 5-3. The rolling radius difference and equivalent conicity of the Number 21 wheel profile and newly developed wheel profile are compared with one another in Figure 5-4(a) and (b), respectively. It is clear that the Number 21 wheel profile shows a linearly increasing rolling radius difference until it reaches two-point flange contact at approximately 12 mm. The equivalent conicity of the Number 21 wheel profile shows a constant value

until flange contact due to this linear rolling radius difference. The wheelset will thus run into flange contact with no increasing tendency to steer. The newly designed wheel profile on the other hand shows a non-linear increasing rolling radius difference with a smooth transition into flange contact. The equivalent conicity shows an increased tendency to steer as the wheel displaces laterally. The contact distribution, rolling radius difference and equivalent conicity illustrate the benefits of the conformal wheel design. The contact locations are spread widely across the wheel tread with increased steering ability that should reduce flange contact.

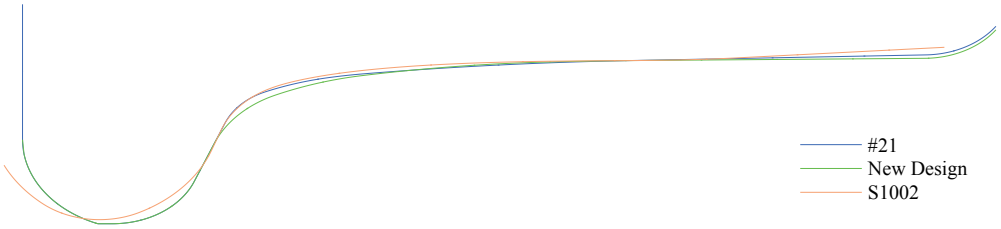

Figure 5-2: Comparison of the newly developed wheel profile with the Number 21 and S1002 wheel profiles

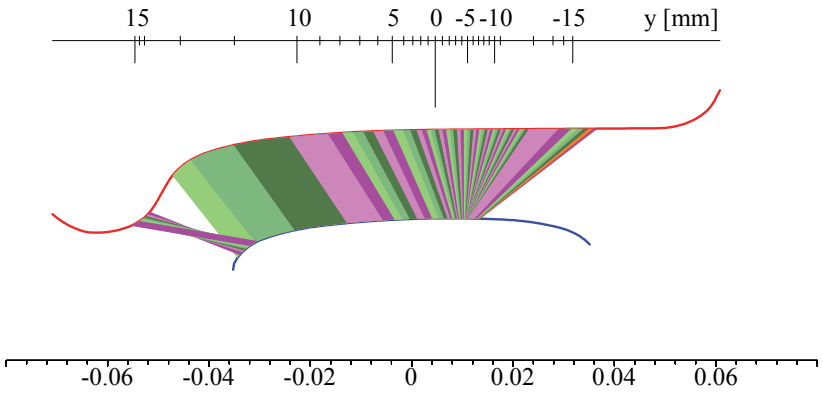

Figure 5-3: Contact distribution of newly designed wheel profile and ore line target profile

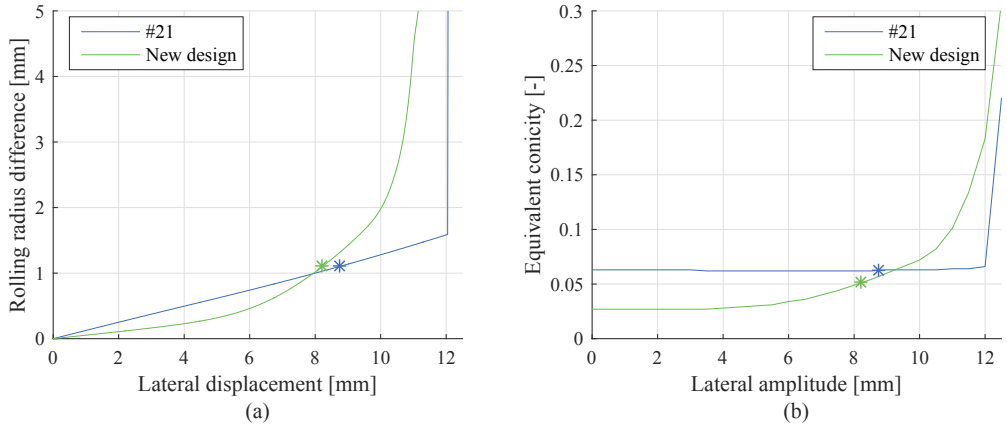

Figure 5-4: Comparison of (a) rolling radius difference and (b) equivalent conicity of the Number 21 and newly developed wheel profiles (values associated with 1.1 mm rolling radius difference indicated by a *)

5.4.2 Vehicle dynamics analyses

The CR-13 wagon is the main wagon type used on the iron ore line. The vehicle model described in chapter 2 was used during the investigation. A fully loaded wagon was considered during the analysis. The vehicle model was used to predict both wheel wear and rail RCF. Two separate vehicle dynamics analyses were performed to calculate wheel wear and rail RCF at discrete travelling distances. Wheel profile wear was calculated and the wheel profiles updated during the first analysis. During this wear simulation, the wheel profiles changed regularly and subsequently influenced the vehicle's dynamic behaviour and contacting forces. The wear simulation was followed by a RCF simulation. The RCF simulation used the results from a dynamic analysis including the worn wheel profiles generated during the preceding wear simulation to predict RCF initiation. Once the wear and RCF simulations were completed, the analysis process would be repeated until a predetermined travelling distance was reached. The predetermined travelling distance was defined by the distance that the CR-13 wagon, with a Number 21 wheel profile, required to reach 2 mm hollow wear. The travelling distance of the new design wheel profile simulations were normalised with respect to this travelling distance.

5.4.2.1 Load collective design

The load collective generally includes a representation of the track layout, traffic conditions, wheel-rail profiles, coefficient of friction, track irregularities as well as vehicle braking and traction. There are many simplifying assumptions that can be made during the load collective design to ensure faster solution times while maintaining accurate wear predictions. The load collective used to evaluate the performance of the conformal wheel design is the same load collective defined in paragraph 4.4.2. The current load collective definition, however, considers both the Number 21 and newly designed wheel profiles together with worn rail profiles. The iron ore line target rail profile was used for the first tangent section of the track. Thereafter different measured worn rail profiles were used for each curve or tangent section. These worn rail profiles are representative of the worn state of rail profiles found at the relevant curve radius or at various tangent sections on the iron ore line. In total 56 worn rail profiles were used.

5.5 Wear and RCF damage prediction results

5.5.1 Wear algorithm verification

A verification of VI-Rail's (2014) wear algorithm is presented in 4.5.1. Discrepancies were noted at the gauge side and field side false flanges. These discrepancies were attributed to the fact that only a single rail profile was considered during the simulations. With the inclusion of more worn rail profiles these discrepancies should reduce. Measured worn wheel profiles are compared with the predicted wear on the Number 21 wheel profile in Figure 5-5. The vehicle numbers and wheel numbers are given in the legend. The worn profile predicted by the wear algorithm with the current load collective is similar to the measured worn wheel profiles. The difference at the gauge side and field side false

flanges are relatively small although they are still present. This can be attributed to the fact that only 56 worn rail profiles were included in the load collective design. This limitation will have to be considered when evaluating the performance of both wheel profile designs.

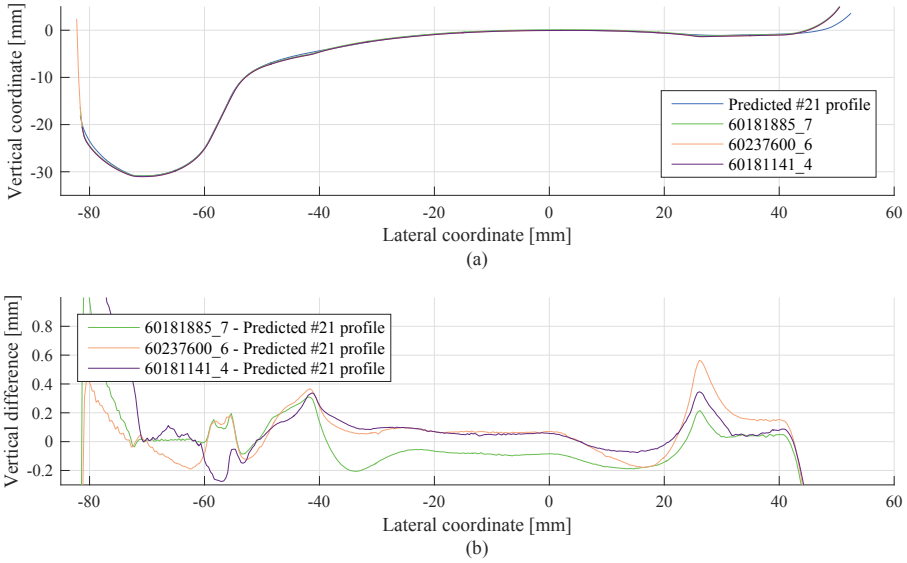

Figure 5-5: Comparison of measured and predicted wear of Number 21 (a) wheel profiles and (b) vertical differences

5.5.2 Performance evaluation of wheel profiles

5.5.2.1 Wear results

The wear performance of the two wheel profiles was evaluated based on the area worn off and hollow wear progression as shown in Figure 5-6. The predicted areas worn off are similar between the two profiles (Figure 5-6(a)). The amount of hollow wear and subsequently the hollow wear rate of the newly designed conformal wheel profile is reduced, since the contact locations are spread across the tread (Figure 5-6(b)). This indicates a distinct advantage of the conformal wheel design over the Number 21 wheel profile.

The wheel profile wear progression and worn profile gradient progression of the Number 21 wheel profile is shown in Figure 5-7. The concentration of the hollow wear is evident from Figure 5-7(a) and no flange wear is predicted. The gradient progression shows that from the start of the wear process a jagged transition is present at both the gauge side and field side false flanges (Figure 5-7(b)). This means that the hollow wear band stops abruptly as it joins the unworn section of the wheel profile. Based on the findings of chapter 3, Fröhling et al. (2012) and Spangenberg et al. (2016), this worn shape of the wheel profile is unwanted, since the contact stresses increase and larger longitudinal forces are caused when the wheel contacts the rail at these false flanges. An increase in both the contact stresses and longitudinal forces according to the shakedown diagram, increase the tendency to initiate surface RCF.

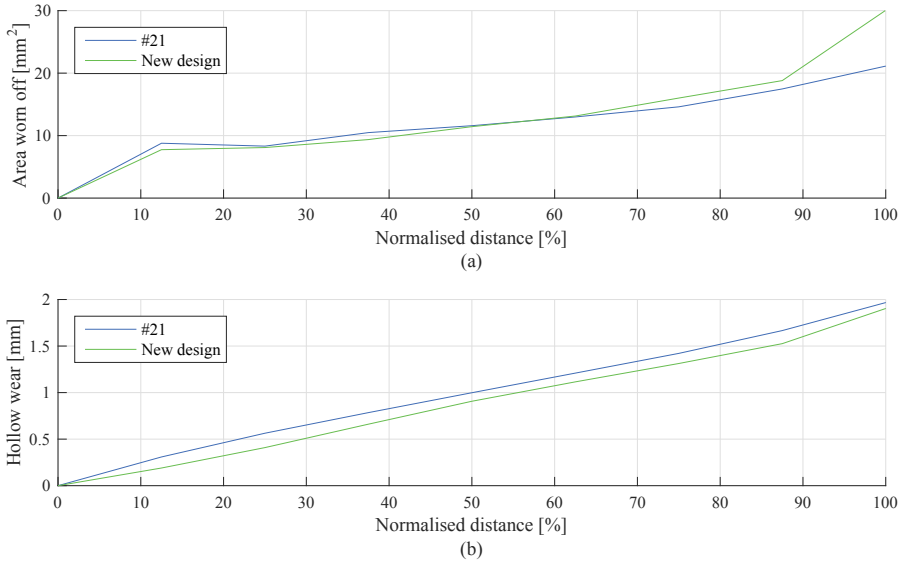

Figure 5-6: Comparison of the Number 21 and newly designed wheel profiles (a) area worn off and (b) hollow wear progression with travelling distance

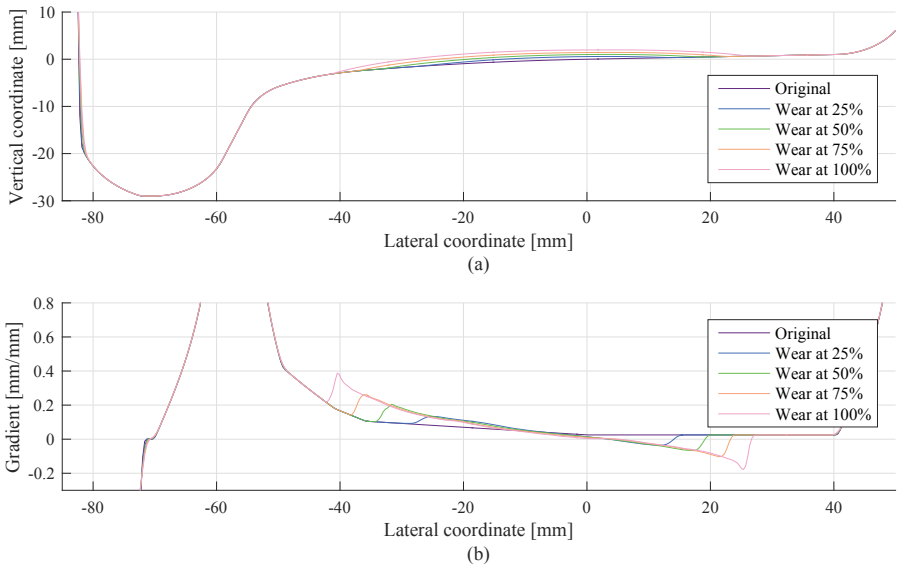

Figure 5-7: Progression of the Number 21 (a) wheel profile wear and (b) associated profile gradients with percentage of running distance

The wear progression and the worn profile gradient progression of the newly designed conformal profile are shown in Figure 5-8. The worn shape at 100 % of the running distance shows a worn shape with gauge side and field side false flanges (Figure 5-8(a)), although the wear has been spread across the wheel tread compared with the Number 21 wheel profile. No flange wear is predicted. The gradient progression of Figure 5-8(b) shows that worn wheel shapes, up to 50 % of the running distance, have a smoother transition from the gauge side false flange section to the original profile. Thus, the worn profiles up to 50 % of the running distance will be less inclined to initiate RCF, since the

worn shape is more favourable. This smoother transition shows an improvement over the original Number 21 wheel profile design.

It was noted in paragraph 5.5.1 that the gauge and field side false flanges are more pronounced with the analytical wear prediction than with in-service wheel profiles. These differences indicate that the in-service wheel profiles contact at the false flanges. Should the newly designed wheel profile be implemented in service, the false flanges might be worn away. However, this is one of the potential disadvantages of both profiles, since contact at the false flanges lead to RCF initiation.

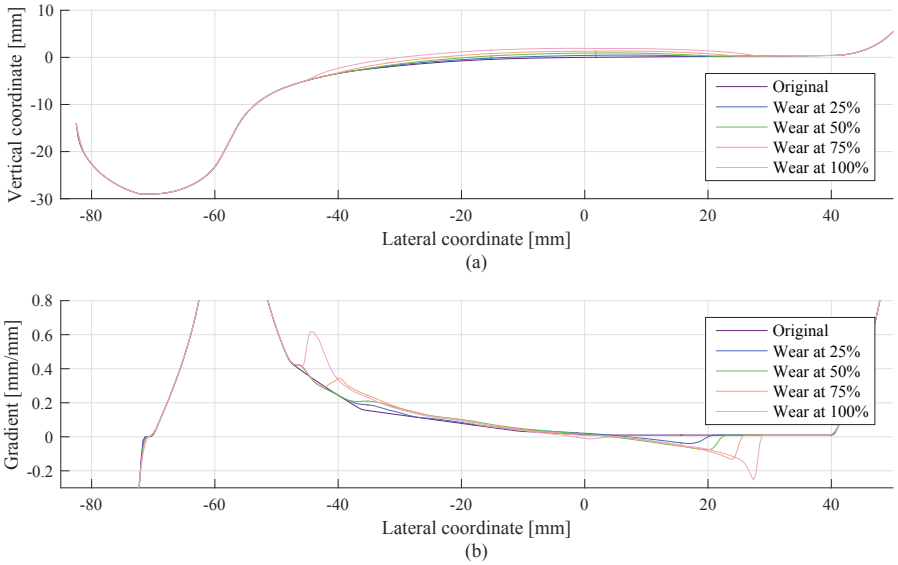

Figure 5-8: Progression of the new conformal design (a) wheel profile wear and (b) associated profile gradients with percentage of running distance

According to Kalousek (2005), a conformal wheel profile should be designed in such a manner that it results in a semi-concave wear pattern. Here the wheel wear is spread across the tread with no false flanges present. The worn shape of the new design wheel profile does not result in this ideal semi-concave wear pattern. This is mainly due to two limitations. Firstly, to obtain conformal contact between the wheel and rail profile at the wheel's flange throat, the contacting profiles' geometries and rolling radius difference need to be considered. The rolling radius difference of conformal profiles increases non-linearly. The design of a wheel profile with a non-linear increasing rolling radius difference that allows 1.1 mm difference at flange throat contact is constrained by the geometry of the contacting profiles. Secondly, flange wear will occur when a wheelset, designed for flange throat contact, displaces laterally too far towards the wheel flange. The new wheel profile had been designed considering these two limitations, in so realising the best compromise.

5.5.2.2 Worn wheelset kinematics

The wheelset kinematics is evaluated from the equivalent conicity plots in Figure 5-9. It is evident that large conicity changes occur with the Number 21 wheel profile during its

wear life. The equivalent conicity at the lateral amplitude required for steering without flanging through a curve radius of 1 000 m, increases significantly before reducing later during the wear life of the wheel (Figure 5-9(a)). The lateral amplitude required for steering without flange contact moves closer towards zero before increasing again. When the equivalent conicity of the newly designed wheel profile in Figure 5-9(b) is considered, it is clear that the equivalent conicity at the lateral amplitude required for steering without flanging does not increase as significantly as that of the Number 21 wheel profile. The conicity range over which the lateral amplitude required for steering without flanging (the stars in Figure 5-9) of the Number 21 wheel operates during its wear life is relatively large compared with that of the new design wheel profile. Changes in the lateral amplitude required for steering also changes less significantly during the life of the newly designed wheel profile. This result together with the observation from the wear results of the preceding paragraph illustrates the advantage of conformal contacting profiles and confirms Scheffel's (1974) assumption that a self-steering bogie fitted with conformal wheel profiles will allow the worn shape of the wheel and its equivalent conicity to be maintained over longer distances.

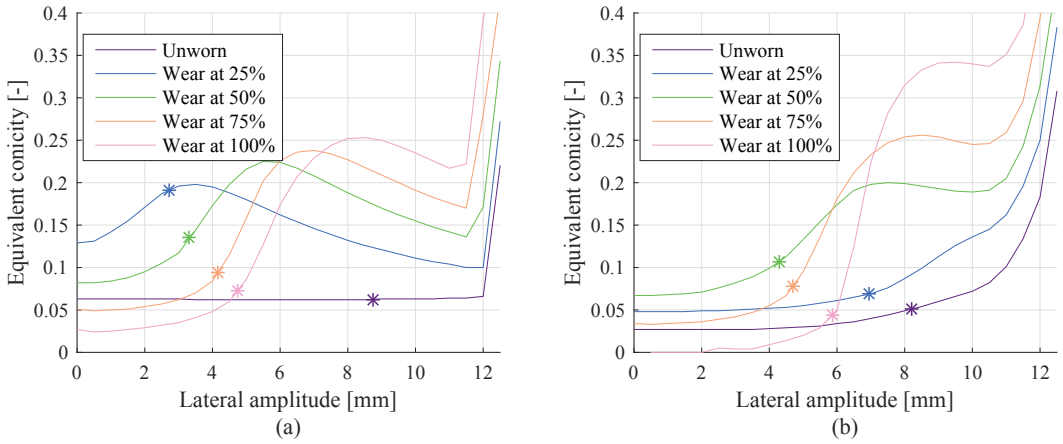

Figure 5-9: Equivalent conicity of (a) the Number 21 and (b) the newly developed worn wheel profiles as a function of travelling distance (values associated with 1.1 mm rolling radius difference indicated by a *)

5.5.2.3 RCF results

The RCF performance of the two wheel profiles over their wear life is evaluated based on their working points on the shakedown diagram as shown in Figure 5-10. The bulk of the contact conditions result in similar working points for both profiles. The shakedown map in Figure 5-10(a) shows that the Number 21 wheel profile will not result in RCF initiation. The new design wheel profile, though, will cause RCF initiation, since some of the working points exceed the shakedown limit (Figure 5-10(b)). It was found that when two-point contact occurred it often resulted in these shakedown limit exceedances. The first contact point was closer to the tread centre while the second contact point was at or close to the gauge side false flange. Rail profiles that do not allow the wheelsets to steer before the contact point reaches the false flange will therefore result in two-point contact and RCF initiation. Such rail profiles have gauge corners lower than that of the target rail profile and are at the limit of the grinding tolerance. This result confirms the

conclusion of chapter 3 and Spangenberg et al. (2016) that showed that rail profiles with their gauge corners lower than the target rail profile have an increased tendency to initiate RCF. This contact condition can be avoided if the in-service rail profiles in curves have their gauge corners compliant to the target rail profile. The increased material available for contact will allow the wheelset to steer before two-point contact occurs, ultimately reducing RCF initiation.

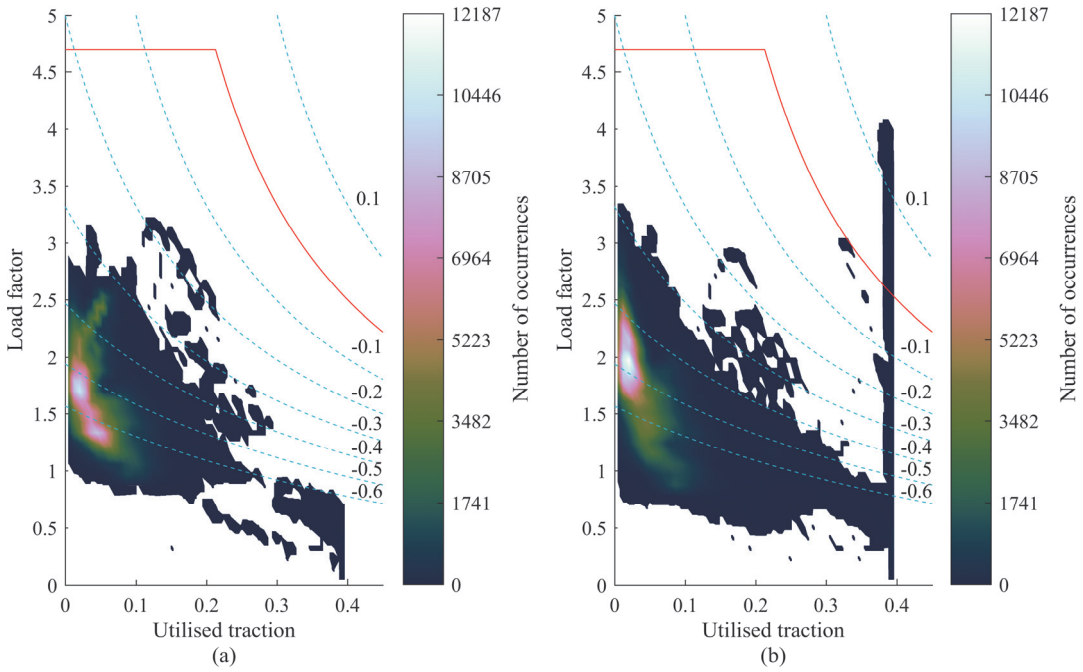

Figure 5-10: Shakedown map of working points for worn profiles over the total travelling distance for (a) the Number 21 and (b) the newly designed profiles (- shakedown limit, - - constant FI_{Surf} lines)

Both profiles do not result in RCF initiation when the worn profile reaches 100 % of the normalised distance, or in other words the worn profiles with 2 mm of hollow wear, are excluded (see Figure 5-11). This shows the sensitivity of the 2 mm hollow wear limit together with the compliance of in-service rail profiles to the target rail profile. When in-service rail profiles are ground approaching the grinding tolerance and wheel profiles are at or beyond the hollow wear limit, the potential to produce two-point contact and initiate RCF is increased.

Conformal wheel and rail profiles are not the decisive solution to reduce RCF initiation. Otherwise there would be no RCF damage once conformal profiles had been introduced. Rail profiles with gauge corners much closer to the rail target or higher than target may be required in curves to reduce RCF initiation. Such rail profiles will allow the wheel to reach the required rolling radius difference earlier, steering away from two-point contact with the gauge side false flange. Lower than target gauge corner rail profiles can be used in tangents together with narrower gauge as suggested by Magel and Kalousek (2002) to force contact at the false flanges, wearing them down and producing more favourable wheel profile shapes. The steering forces in tangents are lower than in curves and thus the potential to initiate RCF in tangents should be reduced during false flange contact.

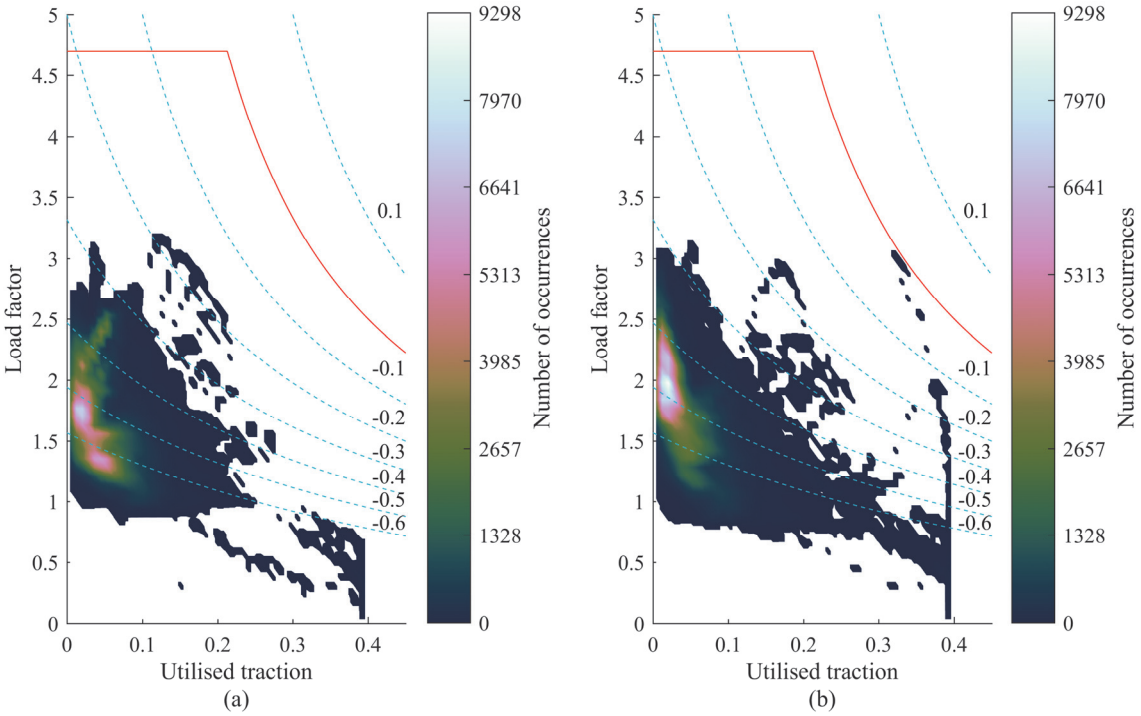

Figure 5-11: Shakedown map of working points for worn profiles over 87.5 % of the travelling distance for (a) the Number 21 and (b) the newly designed profiles (- shakedown limit, - - constant FI_{Surf} lines)

5.6 Conclusion

The study of vehicle dynamics together with algorithms facilitating the prediction of wear evolution and RCF initiation allows a rapid evaluation of a new wheel design and its long-term performance. The evaluation is, however, based on algorithms that only allow a quantitative comparison of the performance of two wheel profile designs. A wear and RCF performance evaluation of a new conformal wheel design was made and compared to the currently employed Number 21 wheel profile.

The advantages of the conformal wheel profile were illustrated by evaluating the worn shape and the resulting kinematics. A more favourable wheel shape is maintained by the conformal design up to at least 50 % of the travelling distance, since the false flange shape transitions smoothly into the original profile as opposed to that of the Number 21 wheel profile. The equivalent conicity progression and conicity range of the conformal design is smaller than that of the Number 21 wheel profile. Thus, more stable conicities are produced over the wear life of the conformal wheel profile.

The RCF performance of the conformal wheel profile seemed worse than that of the Number 21 wheel profile. However, the sensitivity of the hollow wear limit and the compliance of in-service rail profiles to the target rail profile were proven. At 2 mm hollow wear the RCF performance of the conformal wheel design is sensitive to rail profiles with their gauge corners lower than target rail profile. This sensitivity is due to

the reduced steering ability imposed by such rail profiles resulting in two-point contact at the gauge side false flanges and increased probability of RCF initiation.

A conformal wheel profile design has many associated benefits over the current Number 21 wheel profile design. Implementation of such a conformal wheel profile design has to be accompanied by improved rail grinding maintenance to ensure rail profile compliance.

Chapter 6: Conclusion

The aim of the study is to develop an approach to reduce rail RCF on South Africa's iron ore export line by managing the worn wheel shape. This approach is developed by evaluating wheel and rail profile shapes that contribute the most to RCF initiation, studying the influence of a suspension stiffness and rail profile changes as well as a redesign of the wheel profile used on this line. This study was performed numerically with a validated multibody dynamics model of a CR-13 wagon.

The influence of wheel and rail profile shape features on the initiation of RCF cracks was evaluated to determine those features that contribute the most to RCF initiation. These features included the hollow wear, gauge side false flange height, gauge side false flange gradient, hollow wear position relative to the taping line and the rail gauge corner deviation at -15°. The hollow wear position proved to be the most sensitive wheel feature. It was also shown that the probability of RCF increases as the hollow-worn of the wheel exceeds the 2 mm hollow wear limit and the rail gauge corner at -15° drops below that of the target rail profile.

The suspension stiffness and rail profile changes were studied as two potential RCF mitigation measures. The wear and RCF performances of wheel profiles produced when applying these two RCF mitigation measures were studied. The worn wheel profiles produced by the RCF mitigation measures all resulted in a concentrated hollow-worn wheel shape. None of these mitigation measures resulted in the wear being spread more evenly across the tread, reducing the prevalence of false flanges.

It was determined that the current operating conditions on the iron ore line are better in terms of its wear and RCF performance than the performance of the two RCF mitigation measures. However, this baseline condition is still far from the optimum when RCF is concerned, since RCF is widespread on this line.

The results of these studies indicated that a redesign of the contacting wheel and rail profiles are required to spread the wheel wear across the tread and produce more favourable worn wheel profiles. A wear and RCF performance evaluation of a new conformal wheel design was made and compared to the currently employed Number 21 wheel profile. The advantages of the conformal wheel profile were illustrated by evaluating the worn shape and the resulting kinematics. The worn wheel shape of the new conformal wheel design appeared to be more favourable and stable than that of the Number 21 wheel profile.

The most damaging wheel and rail shapes need to be minimised or eliminated. The most damaging wheel shapes cannot be eliminated through a change in suspension or by changing the rail profile to a knife-edged or anti-head check rail profile. It was shown that the worn shape of a wheel profile promoting conformal contact with the current ore line target rail profile may offer advantages over the current wheel profile design. It is

therefore suggested that an in-service trial of the conformal wheel profile design should be made to evaluate its actual wear and RCF performance. However, the implementation of such a conformal wheel profile design must be accompanied by improved rail grinding maintenance to ensure rail profile compliance to the target rail profile.

Based on these findings an approach is proposed where the conformal wheel profile design together with improved compliance of the in-service rail profiles to the target rail profile are implemented. This has the potential to reduce RCF initiation on South Africa's iron ore export line.

References

Berggren, E.G., Li, M.X.D. & Spännar, J. (2008). A new approach to the analysis and presentation of vertical track geometry quality and rail roughness. *Wear*, 265: 1488-1496.

Bevan, A., Molyneux-Berry, P., Eickhoff, B. & Burstow, M. (2013). Development and validation of a wheel wear and rolling contact fatigue damage model. *Wear*, 307:100-111.

Bower, A.F. & Johnson, K.L. (1991). Plastic flow and shakedown of the rail surface in repeated wheel-rail contact. *Wear*, 114: 1-18.

Braghin, F., Bruni, S. & Lewis, R. (2009). Chapter 6: Railway wheel wear. In *Wheel-rail interface handbook*. Edited by Lewis, R. and Olofsson, U. Cambridge: Woodhead Publishing Ltd., pages 172-210.

Bruni, S. & Braghin, F. (2009). Chapter 15: Effect of damage on vehicle dynamics. In *Wheel-rail interface handbook*. Edited by Lewis, R. and Olofsson, U. Cambridge: Woodhead Publishing Ltd., pages 456-476.

Burstow, M.C. (2003). *Whole Life Rail Model Application and Development for RSSB: Development of an RCF Damage Parameter*. Derby: Rail Safety & Standards Board.

Burstow, M.C. (2004). *Whole Life Rail Model Application and Development for RSSB (T115) - Continued Development of and RCF Damage Parameter*. Derby: Rail Safety & Standards Board.

Chang, C., Wang, C. & Li, L. (2010). A study of a numerical analysis method for the wheel-rail wear of a heavy-haul train. *Proceedings of the Institute of Mechanical Engineers Part F: Journal of Rail and Rapid Transit*, 224: 473-482.

Chudzikiewicz, A., Kik, W., Moelle, D. & Piotrowski, J. (1998). *A survey of wear theories for wheel and rail*, Internal paper ArgeCare, Berlin: ArgeCare.

Cole, C. (1998). *How Accurate is Your Train Simulator? A Discussion of Simulation and Validation Techniques*. In: Oghanna, Wardina (Editor). Conference on Railway Engineering Proceedings: Engineering Innovation for a Competitive Edge. Rockhampton, Qld: Central Queensland University, 1998: 167-171.

Dede, J., Reimann, U. & Reimann, M.A. (2015). The Wheel/Rail Interface Study. *European Railway Review*, 22(5):41-46.

Dikshit, V., Clayton, P. & Christensen, D. (1991). Investigation of rolling contact fatigue in a head-hardened rail. *Wear*, 144: 89-102.

References

Dirks, B. & Enblom, R. (2011). Prediction model for wheel profile wear and rolling contact fatigue. *Wear*, 271: 210-217.

Ekberg, A. & Kabo, E. (2002). *Rolling contact fatigue of railway wheels and rails - an overview*. Proceedings of Rolling Contact Fatigue: Applications and Development, Brescia, Italy, pp 5-26.

Ekberg, A., Kabo, E. & Andersson, H. (2002). An engineering model for prediction of rolling contact fatigue of railway wheels. *Fatigue & Fracture of Engineering Materials & Structures*, 25: 899-909.

Ekberg (2009). Chapter 7: Fatigue of railway wheels. In *Wheel-rail interface handbook*. Edited by Lewis, R. and Olofsson, U. Cambridge: Woodhead Publishing Ltd., pages 211-244.

Ekberg, A., Åkkesson, B. & Kabo, E. (2014). Wheel/rail rolling contact fatigue - Probe, predict, prevent. *Wear*, 314: 2-12.

Enblom, R. (2009). Deterioration mechanisms in the wheel-rail interface with focus on wear prediction: a literature review. *Vehicle System Dynamics: International Journal of Vehicle Mechanics and Mobility*, 47(6): 661-700.

Enblom, R. & Berg, M. (2005). Simulation of railway wheel profile development due to wear - influence of disc braking and contact environment. *Wear*, 258:1055-1063.

European Committee for Standardisation (2012). *EN 13231-3:2012: Railway applications – Track – Acceptance of works – Part 3: Acceptance of reprofiling rails in track*. Brussels: European Committee for Standardisation (CEN).

Evans, J. & Iwnicki, S.D. (2002). *Vehicle Dynamics and the Wheel-Rail Interface*. IMechE Seminar – Wheels on Rails – An update, Understanding and managing the Wheel/Rail Interface. London: IMechE. Available from: http://e-space.mmu.ac.uk/e-space/bitstream/2173/11370/1/vehicle%20dynamics%20wheel%20rail%20interface.pdf (Accessed: 1 July 2015).

Fletcher, D.I., Franklin, F.J. & Kapoor, A. (2009). Chapter 9: Fatigue of railway wheels. In *Wheel-rail interface handbook*. Edited by Lewis, R. and Olofsson, U. Cambridge: Woodhead Publishing Ltd., pages 280-310.

Fröhling, R.D. (2002). Strategies to Control Wheel Profile Wear. *Vehicle System Dynamics Supplement*, 37:490-501.

Fröhling, R.D. (2003). Vehicle/track interaction optimisation within Spoornet. In: *System Dynamics and Long-Term Behaviour of Railway Vehicles, Track and Subgrade*. Edited by Popp, K. and Schiehlen, W. Berlin: Springer, pages 17–34.

References

Fröhling, R.D., Mistry, K.C. & Maree, H. (2005). *BBB8324 – Rail Surface Fatigue Classification Chart (Head Checks and Field Side Surface Cracks)*. Pretoria: Transnet Freight Rail.

Fröhling, R.D., Ekberg, A. & Kabo, E. (2008). The detrimental effects of hollow wear -- field experiences and numerical simulations. *Wear*, 265: 1283-1291.

Fröhling, R.D., Spangenberg, U. & Hettasch, G. (2012). Wheel/rail contact geometry assessment to limit rolling contact fatigue initiation at high axle loads. *Vehicle System Dynamics: International Journal of Vehicle Mechanics and Mobility*, 50 (Suppl. 1): 319-334.

Garcia, J.F., Olaizola, X., Martin, L.M. & Gimenez, J.G (2000). Theoretical Comparison Between Different Configuration of Radial and Conventional Bogies. *Vehicle System Dynamics: International Journal of Vehicle Mechanics and Mobility*, 33:233-259.

Garg, V.K. & Dukkipati, R.V. (1984). *Dynamics of Railway Vehicle Systems*. Don Mills: Academic Press Canada.

Grassie, S.L. (2009). Chapter 20: Maintenance of the wheel-rail interface. In *Wheel-rail interface handbook*. Edited by Lewis, R. and Olofsson, U. Cambridge: Woodhead Publishing Ltd., pages 576-607.

Grassie, S.L. (2015). Traction, curving and surface damage of rails, Part 2: Rail damage. *Proceedings of the Institute of Mechanical Engineers, Part F: Journal of Rail and Rapid Transit*, 229(3):330-339.

Ignesti, M., Malvezzi, M., Marini, L., Meli, E. & Rindi, A. (2012). Development of a wear model for the prediction of wheel and rail profile evolution in railway systems. *Wear*, 284-285: 1-17.

International Heavy Haul Association (IHHA). (2001). *Guidelines To Best Practices For Heavy Haul Railway Operations: Wheel and Rail Interface Issues*. Virginia Beach: International Heavy Haul Association.

International Union of Railways (2004). *UIC code 519: Method for determining the equivalent conicity*, 1st edition. Paris: International Union of Railways.

Iwnicki, S.D. (Editor). (1999). *The Manchester Benchmarks for Rail Vehicle Simulation*. Lisse: Swets & Zeitlinger.

Iwnicki, S.D. (Editor). (2006). *Handbook of Railway Vehicle Dynamics*. Boca Raton: Taylor & Francis Group.

Iwnicki, S.D. (2009). The Effect of Profiles on Wheel and Rail Damage. *International Journal of Vehicle Structures and Systems*, 1(4): 99-104.

References

Jendel, T. (2002). Prediction of wheel profile wear – comparisons with field measurements. *Wear*, 253:89-99.

Jendel, T. & Berg, M. (2002). Prediction of Wheel Profile Wear, *Vehicle System Dynamics*, 37: 502-513.

Johansson, A. & Andersson, C. (2005). Out-of-round railway wheels - a study of wheel polygonalization through simulation of three-dimensional wheel–rail interaction and wear. *Vehicle System Dynamics*, 43(8):539-559.

Johnson, K.L. (1985). *Contact Mechanics*. Cambridge: Cambridge University Press.

Johnson, K.L. (1987). *Plastic flow, residual stress and shakedown in rolling contact*. Proc. Int. Symp. on Contact Mechanics and Wear of Rail/Wheel Systems II, Kingston, RI. University of Waterloo Press: Waterloo, Ontario, pp. 83-97.

Johnson, K.L. (1989). The strength of surfaces in rolling contact. *Journal of Mechanical Engineering Science*, 203: 151-163.

Kalker (1990). *Three-Dimensional Elastic Bodies in Rolling Contact*. Dordrecht: Kluwer Academic Publishers.

Kalker, J.J. (1991). Simulation of the development of a railway wheel profile through wear. *Wear*, 150: 355-365.

Kalousek, J. (2005). Wheel-rail damage and its relationship to track curvature. *Wear*, 258:1330-1335.

Karttunen, K., Kabo, E. & Ekberg, A. (2014a). The influence of track geometry irregularities on rolling contact fatigue. *Wear*, 314: 78-86.

Karttunen, K., Kabo, E. & Ekberg, A. (2014b). Numerical Assessment of the influence of worn wheel tread geometry on rail and wheel deterioration. *Wear*, 317: 77-91

Kimura, Y., Sekizawa, M. & Nitanai, A. (2002). Wear and fatigue in rolling contact. *Wear*, 253: 9-16.

Leary, J.F., Handal, S.N. & Rajkumar, B. (1991). Development of freight car wheel profiles - a case study. *Wear*, 144: 353-362.

Lewis, R. & Olofsson, U. (2009). Chapter 2: Basic tribology of the wheel-rail contact. In *Wheel-rail interface handbook*. Edited by Lewis, R. and Olofsson, U. Cambridge: Woodhead Publishing Ltd., pages 34-57.

Lundén, R. & Paulsson, B. (2009). Chapter 1: Introduction to wheel-rail interface research. In *Wheel-rail interface handbook*. Edited by Lewis, R. and Olofsson, U. Cambridge: Woodhead Publishing Ltd., pages 3-33.

References

MATLAB version 8.6.0.267246 (R2015b) (1984-2015). (Computer software). Massachusetts: The MathWorks, Inc.

Magel, E. & Kalousek, J. (2002). The application of contact mechanics to rail profile design and rail grinding. *Wear*, 253: 308-316.

Marutla, M.A., Mistry, K., Van Aardt, J.H.P. & Mtetwa, C.Q. (2012). *BBB0481 ver. 2 – Manual for track maintenance*. Johannesburg: Transnet Freight Rail.

Nia, S.H., Casanueva, C. & Stichel, S. (2015). Prediction of RCF and wear evolution of iron-ore locomotive wheels. *Wear*, 338-339: 62-72.

Olofsson, U., Zhu, Y., Abbasi, S., Lewis, R. & Lewis, S. (2013). Tribology of wheel-rail contact - aspects of wear, particle emissions and adhesion. *Vehicle System Dynamics*, 51(7): 1091-1120.

Pearce, T.G. (1996). Wheelset guidance - conicity, wheel wear and safety. *Proceedings of the Institute of Mechanical Engineers, Part F: Journal of Rail and Rapid Transit*, 210: 1-9.

Pearce, T.G. & Sherratt, N.D. (1991). Prediction of wheel profile wear. *Wear*, 144: 343-351.

Persson, I., Nilsson, R., Bik, U., Lundgren, M. & Iwnicki, S.D. (2010). Use of a genetic algorithm to improve the rail profile on Stockholm Underground. *Vehicle system dynamics*, 48 (Supplement 1): 89-104.

Polach, O. (2011). Wheel profile design for target conicity and wide tread wear spreading. *Wear*, 271: 195-202.

Pombo, J., Ambrósio, J., Pereira, M., Lewis, R., Dwyer-Joyce, R., Ariaudo, C. & Kuka, N. (2011). Development of a wear prediction tool for steel railway wheels using three alternative wear functions. *Wear*, 271: 238-245.

Ramalho, A. (2015). Wear modelling in rail–wheel contact. *Wear*, 330-331: 524-532.

RSGeo version 3.03 in ACRadSchiene version 4.6 (2011). (Computer software). Berlin: ArgCare.

Sawley, K., Urban, C. & Walker, R. (2005). The effect of hollow-worn wheels on vehicle stability in straight track. *Wear*, 258: 1100-1108.

Scheffel, H. (1974). A new design approach for railway vehicle suspension. *Rail Int.*, 638: 638-651.

Scheffel, H. (1976). Self-steering wheelsets will reduce wear and permit higher speeds. *Railway Gazette International*, December 1976: 453-456.

References

Scheffel, H. (1978). *Experience gained by South African Railways with the diagonally stabilised (cross-anchor) bogies having self-steering wheelsets*. Heavy Haul Railways Conference, Perth, Western Australia, September 1978.

Schöch, W. (2011). Recommendations for strategic rail maintenance in Europe - The application of anti-headcheck profiles and cyclic grinding. *Rail Engineering International*, Edition 2011, Number 1: 6-10.

Shabana, A.A., Zaazaa, K.E. & Sugiyama, H. (2008). *Railroad Vehicle Dynamics: A Computational Approach*. Boca Raton: CRC Press Taylor & Francis Group.

Shevtsov, I.Y., Markine, V.L. & Esveld, C. (2005). Optimal design of wheel profile for railway vehicles. *Wear*, 258: 1022-1030.

Shevtsov, I.Y., Markine, V.L. & Esveld, C. (2008). Design of railway wheel profile taking into account rolling contact fatigue and wear. *Wear*, 265: 1273-1282.

Shevtsov, I.Y. (2008). *Wheel-Rail Interface Optimisation*. Doctoral Dissertation. Delft: Delft University of Technology.

Smallwood, R., Sinclair, J.C. & Sawley, K.J. (1991). An optimization technique to minimize rail contact stresses. *Wear*, 144: 373-384.

Spangenberg, U., Fröhling, R.D. & Els, P.S. (2016). Influence of wheel and rail profile shape on the initiation of rolling contact fatigue cracks at high axle loads. *Vehicle System Dynamics: International Journal of Vehicle Mechanics and Mobility*, 54: 638-652.

Stow, J., Bevan, A. & Burstow, M. (2011). *Developing Effective, Evidence Based Control Measures for Rolling Contact Fatigue*. Proceedings of the 9th World Congress on Railway Research. Lille: France, 22-26 May 2011.

Tournay, H.M. & Mulder, J.M. (1996). The transition from the wear to the stress regime. *Wear*, 191: 107-112.

Tournay, H. (2001). Part 2: Supporting technologies vehicle track interaction. In *Guidelines To Best Practices For Heavy Haul Operations: Wheel and Rail Interface Issues*. 1st edition. Virginia Beach: International Heavy Haul Association.

Tunna, J., Sinclair, J. & Perez, J. (2007). A review of wheel wear and rolling contact fatigue. *Proceedings of the Institute of Mechanical Engineers, Part F: Journal of Rail and Rapid Transit*, 221: 271-289.

Tunna, J. & Urban, C. (2009). A parametric study of the effects of freight vehicles on rolling contact fatigue of rail. *Proceedings of the Institution of Mechanical Engineers, Part F: Journal of Rail and Rapid Transit*, 223: 141-151.

VI-grade. (2014). *VI-Rail 16.0 Documentation*. Marburg: VI-grade GmbH.

References

VI-Rail version 16.0.23615 (2006-2014). (Computer software). Marburg: VI-grade GmbH.

Wickens, A.H. (2003). *Fundamentals of Rail Vehicle Dynamics: Guidance and Stability*. Lisse: Swets & Zeitlinger.

Wu, H. (2006). Effects of wheel and rail profiles on vehicle performance. *Vehicle System Dynamics: International Journal of Vehicle Mechanics and Mobility*, 44 (Suppl. 1): 541-550.

Wu, H., Kalay, S. & Tournay, H. (2010). Development of the wheel–rail interface management model and its applications in heavy haul operations. *Proceedings of the Institute of Mechanical Engineers Part F: Journal of Rail and Rapid transport,* 225: 38-47.

Zobory, I. (1997). Prediction of Wheel/Rail Profile Wear. *Vehicle System Dynamics*, 28: 221-259.

Zarembski, A. M. (2005). *The art and science of rail grinding*. 1st edition. Omaha: Simmons-Boardman Books, Inc.